Technical University of Denmark

Informing groundwater models with near-surface geophysical data

Daan Herckenrath

DTU Environment
Department of Environmental Engineering

PhD Thesis
March 2012

Informing groundwater models with near-surface geophysical data

Daan Herckenrath

PhD Thesis
March 2012

DTU Environment
Department of Environmental Engineering
Technical University of Denmark

Daan Herckenrath

Informing groundwater models with near-surface geophysical data

PhD Thesis, March 2012

The thesis will be available as a pdf-file for downloading from the homepage of the department: www.env.dtu.dk

Address:	DTU Environment Department of Environmental Engineering Technical University of Denmark Miljoevej, building 113 DK-2800 Kgs. Lyngby Denmark
Phone reception:	+45 4525 1600
Phone library:	+45 4525 1610
Fax:	+45 4593 2850
Homepage:	http://www.env.dtu.dk
E-mail:	reception@env.dtu.dk

Printed by:	Vester Kopi Virum, March 2012
Cover:	Torben Dolin
ISBN:	978-87-92654-53-3

Preface

The work presented in this PhD thesis, entitled "Integration of groundwater models and near-surface geophysical data", was conducted at the Department of Environmental Engineering at the Technical University of Denmark (DTU) under the supervision of Associate Professor Peter Bauer-Gottwein (DTU) and Associate Professor Esben Auken (Aarhus University). The PhD research project was conducted in the period November 2008 to November 2011 and was funded by DTU and the Danish Agency for Science and Innovation. The study included an external stay of two months at the Department of Geophysics at Stanford University under supervision of Professor Rosemary Knight and an intensive collaboration with the Geophysics Department at Aarhus University under supervision of Associate Professor Esben Auken.

This PhD thesis comprises a synopsis and three papers that were submitted to international, ISI-indexed scientific journals:

I. Herckenrath, D., Legaz-Gazoty, A., Fiandaca, G., Auken, E., Christensen, M., Balicki, M. and P. Bauer-Gottwein, Sequential and Coupled Hydrogeophysical Inversion of a Groundwater Model using Geoelectric and Transient Electromagnetic Data, *Journal of Hydrology*, submitted.

II. Herckenrath, D., Odlum, N., Nenna, V., Auken, E., and P. Bauer-Gottwein, Calibrating salt water intrusion models with Time-Domain Electromagnetic Data, *Ground Water*, submitted.

III. Herckenrath, D., Behroozmand, A., Christiansen, L., Auken, E., and P. Bauer-Gottwein, Coupled hydrogeophysical inversion using time-lapse magnetic resonance sounding and time-lapse gravity data for hydraulic aquifer testing: potential and limitations, *Water Resources Research*, in review.

Acknowledgements

Without the comforting, inspiring and refreshing presence of family, friends, supervisors and colleagues this book would probably be worse. Thanks.

Daan Herckenrath

December 2011

Summary

Over the past decade geophysical methods have gained an increased popularity due to their ability to map hydrologic properties. Such data sets can provide valuable information to improve hydrologic models. Instead of using the measured geophysical and hydrologic data simultaneously in one inversion approach, many of the previous studies apply a Sequential Hydrogeophysical Inversion (SHI) in which inverted geophysical models provide information for hydrologic models. In order to fully exploit the information contained in geophysical datasets for hydrological purposes, a coupled hydrogeophysical inversion was introduced (CHI), in which a hydrologic model is part of the geophysical inversion. Current CHI-research has been focussing on the translation of simulated state variables of hydrologic models to geophysical model parameters. We refer to this methodology as CHI-S (State). In this thesis a new CHI-approach was developed, called CHI-P (Parameter), which applies coupling constraints between the geophysical and hydrologic model parameters.

A CHI-P was used to estimate hydraulic conductivities and geological layer elevations for a synthetic groundwater model using Time-Domain Electromagnetic (TDEM) data and for a real-world groundwater model using geo-electric data. For the synthetic study, the CHI-P resulted in improved parameter estimates and a reduction in parameter uncertainty for both the hydrologic and the geophysical model, when compared with a SHI. For the real-world groundwater model, parameter uncertainty could not be reduced significantly, but the CHI-P resulted in more consistent parameter estimates between the groundwater model and the geophysical model. To our knowledge, CHI-P is the first CHI method that can be applied to inform large-scale groundwater models with near-surface geophysical data.

In another study, we successfully applied a CHI-S to estimate parameter values of a saltwater intrusion model with TDEM data. Considering the small number of estimable parameters, data fit and parameter uncertainty, the salt water intrusion model provided an excellent interpretation of the geophysical data. The CHI-S yielded a geophysical model that could never be obtained with a separate geophysical inversion. Furthermore, we applied a CHI-S to evaluate the potential for time-lapse relative gravimetry (TL-RG) and magnetic resonance sounding (TL-MRS) to improve the estimation of aquifer properties during an aquifer pumping test. This was done, taking in account a number of practical issues that might limit the sensitivity of these techniques with respect to the estimated

aquifer properties. For this purpose a virtual pumping test was used with synthetic observation data. In contrast to the prior assumptions, the conclusions suggest that both geophysical techniques have a potential to improve the estimation of aquifer properties. In the analyses, TL-MRS outperformed TL-RG data and parameter uncertainty could be reduced with ca. 30 % for most of the scenarios that were investigated.

Dansk sammenfatning

I det seneste årti har geofysiske metoders vundet stor udbredelse i kortlægning af hydrologiske egenskaber. Disse teknikker kan levere data med høj opløsning, som kan korreleres med hydrologiske egenskaber og bruges til at forbedre hydrologiske modeller. I stedet for at benytte en fælles kalibrerings-metode, hvor de geofysiske målinger og hydrologiske data er brugt samtidig, kan mange af de nuværende undersøgelser anvende en Sequential Hydrogeophysical Inversion (SHI), hvor geofysiske modeller giver information til hydrologiske modeller. For at udnytte det fulde potentiale af geofysiske datasæt med hensyn til hydrologiske formål, blev en Coupled Hydrogeophysical Inversion (CHI) indført, hvor en hydrologisk model er en del af den geofysiske inversion. Aktuel CHI-forskning har fokuseret på oversættelse af simulerede tilstandsvariable i hydrologiske modeller til geofysiske modelparametre. Vi henviser til denne metode som CHI-S (State). I denne afhandling en ny CHI-strategi blev udviklet, kaldet CHI-P (Parameter), som baserer sig på koblingsbindinger mellem geofysiske og hydrologiske modelparametre.

En CHI-P blev anvendt til at estimere hydraulisk permeabilitet og geologisk lagtykkelse for henholdsvis en syntetisk grundvandsmodel ved hjælp af Time-Domain Elektromagnetic (TDEM) data og en eksisterende grundvandsmodel ved hjælp af geo-elektriske data. I den syntetiske undersøgelse resulterede CHI-P i forbedrede parameter værdier og en reduceret parameterusikkerhed i både den hydrologiske og den geofysiske model, når man sammenligner med en SHI. For den eksisterende grundvandsmodel, kan parameterusikkerheden ikke reduceres tilsvarende, men CHI-P resulterede i mere konsekvente parameterestimater mellem grundvandsmodellen og den geofysiske model. Så vidt vides, er CHI-P den første CHI metode, der kan anvendes til at informere regionale grundvandsmodeller om geologiske egenskaber ud fra geofysiske data.

I en anden undersøgelse har vi med succes anvendt en CHI-S til at estimere parameter værdier af en saltvandsindtrængningsmodel med TDEM data. Under hensyntagen til det lille antal parametre, datafit og parameterusikkerhed, gav saltvandindtrængningsmodellen en fremragende fortolkning af de geofysiske data. CHI-S resulterede i en geofysisk model, der aldrig ville kunne opnås med en separat geofysisk inversion. Derudover har vi anvendt en CHI-S for at evaluere potentialet for time-lapse relativ gravimetri (TL-RG) og magnetisk resonans sounding (TL-MRS) for at forbedre estimater af grundvandsmagasinets egenskaber i løbet af en pumpetest. En række praktiske problemer, der kan

begrænse følsomheden af disse teknikker med hensyn til det estimerede grundvandsmagasins egenskaber blev herunder taget i regning. Til dette formål anvendte vi en virtuel pumpetest med syntetiske observationsdata. I modsætning til tidligere antagelser tyder konklusionerne på, at begge geofysiske teknikker har potentiale til at forbedre estimering af grundvandsmagasinets egenskaber. I analyserne har TL-MRS klaret sig bedre end TL-RG data, og parameterusikkerheden kunne reduceres med ca. 30 % for de fleste af de scenarier, der blev undersøgt.

Table of Contents

1 Introduction

Groundwater resources suffer from an increasing pressure due to increasing water demands for domestic, agricultural and industrial use. To develop optimal management strategies, essential background information is needed about the geology and the present hydrologic state of an area. Three core disciplines can be identified to characterize the hydrogeological properties of a region, which are geology, geophysics and hydrogeology. Typically geologists and geophysicists characterize the geological setting of an area, where geologists typically process and interpret available borehole and outcrop information, while geophysicists try to map geological structures using surface geophysical methods such as seismic, electromagnetic and geo-electric methods. Finally, hydrogeologists develop quantitative tools to describe relevant hydrologic processes and assess the impact of different groundwater management strategies.

Over the past decade geophysical methods, have gained an increased popularity because of their ability to map hydrologic properties as well. For example methods such as ground penetrating radar (GPR) and magnetic resonance sounding (MRS) are used to map moisture content [*Legchenko et al.*, 2002; *Huisman et al.*, 2003], while electromagnetic (EM) techniques are used to map salt water intrusion in coastal aquifers [M*acaulay and Mullen*, 2007]. If interpreted separately, these geophysical datasets only provide images of a certain hydrologic property in space or time. However, the methods do not provide an explanation with regards to the physical processes underlying the distribution of the mapped hydrologic property, which is essential to make predictions for the hydrologic system under different management scenarios. For this purpose hydrologic models are needed.

The emerging use of geophysical methods for hydrogeological imaging has yielded a new field of research, called hydrogeophysics. [*Rubin and Hubbard*, 1999] and [*Vereecken*, 2006] are the first books in which geophysics and hydrologic models are consistently brought together. A topic that is given specific interest is the inversion method[1] used to estimate geophysical models

[1] Inversion: Physical theories allow us to make predictions. Given a complete description of a physical system, we can predict the outcome of some measurements using a model. The inverse problem consists of using the actual measurements to estimate the values of model parameters that characterize the physical system [modified form *Tarantola*, 2005]. In the inversion process model parameter values are changed until the difference between the actual measurements and model simulations is minimal.

and parameters of hydrologic models. [*Ferré et al.*, 2009] and [*Hinnell et al*., 2010], provide an overview of inversion frameworks that can be used to inform hydrologic models with geophysical data. Two specific types of inversion frameworks are a sequential hydrogeophysical inversion approach (SHI) and a coupled hydrogeophysical inversion approach (CHI). The main difference between both methods is that a SHI does not take into account the hydrologic model when performing a geophysical inversion.

This PhD research was part of RISKPOINT, a project funded by the Danish Council for Strategic Research, which aims to create a risk assessment tool to identify and prioritize clean up and management of point sources of contamination to groundwater. To provide an indication of the magnitude of this problem, there are ca. 13000 documented sites with contamination in Denmark and an additional 14000 sites where soil contamination is suspected [*Miljøstyrelsen*, 2009]. One of the objectives of this project is to evaluate the hydrological and hydrochemical interactions between groundwater and surface water with the ultimate goal to develop optimal management strategies.

Within the overall framework of the RISKPOINT-project, this PhD research was focused on the use of SHI and CHI to constrain, calibrate and validate numerical models of water flow and solute transport. Numerical models typically suffer from the lack of accurate and sufficiently resolved input and calibration data. Geophysical methods have the potential to provide essential information for flow and transport models over a range of scales [e.g. *Kemna et al.*, 2002; *Thomsen et al.*, 2004; *Chambers et al.*, 2004].

1.1 Previous work

Numerous papers have been published about the inclusion of geophysical data for hydrogeological site characterization. Examples are the delineation of landfills [*Radulescu et al.*, 2007; *Meju*, 2000], mapping tracer concentrations [*Singha and Gorelick*, 2005 and 2006] and the estimation of the spatial correlation structure of hydraulic properties [*Hubbard et al.*, 1999, *Day-Lewis et al.*, 2005]. The main reason for the increasing interest in using geophysical methods in hydrogeological studies is that geophysics provides spatially distributed models of physical properties in regions that are difficult to sample using conventional hydrological sampling methods [*Butler*, 2005]. *Hinnell et al.* [2010] and *Ferré et al.* [2009] discuss the different types of hydrogeophysical inversion approaches that can be used and *Hinnell et al.* [2010] provide a

comprehensive list of references to case study applications using different types of coupling approaches. For example, geostatistical methods have been employed to estimate hydrologic parameter distributions based on the correlation structures found in inverted geophysical images [*Cassiani et al.*, 1998; *Hubbard et al.*, 1999; *Yeh et al.*, 2002; *Chen et al.*, 2004]. *Hyndman and Gorelick* [1996], *Chen et al.* [2006] and *Linde et al.* [2006] are examples of studies where hydrologic structures and parameter distributions are being estimated using geophysical and hydrologic data at the same time. Other studies use geo-electric [*Kemna et al.*, 2002; *Vanderborght et al.*, 2005; *Cassiani et al.*, 2006] and electromagnetic data [*Binley et al.*, 2001; *Day-Lewis et al.*, 2003; *Lambot et al.*, 2004; *Looms et al.*, 2008; *Knight*, 2001; *Huisman et al.*, 2003], e.g. GPR, to monitor temporal changes in water content or solute concentrations.

Many previous studies use a SHI in which first a geophysical model is estimated after which the hydrologic model is informed with the geophysical model. *Hinnell et al.* [2010], *Ferré et al.* [2009], *Kowalsky et al.* [2005], *Pollock and Cirpka* [2010] and *Lambot et al.* [2006, 2009], however, describe a CHI, in which a hydrological model is part of the geophysical inversion process and a single objective function is minimized which includes both a geophysical and hydrological component. In other words, both the geophysical and the hydrologic model and their associated observations are used to constrain one another.

1.2 Aim of this study

The vast majority of previous CHI-studies perform a geophysical inversion by estimating parameters of a hydrologic model in order to fit geophysical measurement data. This is done by translating simulated hydrologic state variables (moisture content, concentration) to geophysical parameter distributions to simulate a geophysical signal that can be compared with the measurement data. This is not the only way to perform a CHI. Another approach to perform a CHI would be to couple parameters of the geophysical model with parameters of the hydrologic model. A limitation of most previous studies is the small spatial scale of CHI case study applications. Moreover, the CHI frameworks by *Hinnell et al.* [2010], *Kowalsky et al.* [2005] and *Lambot et al.* [2009] do not allow for the separate estimation of geophysical model parameters which cannot be linked to the hydrologic model. This can be a significant limitation as a hydrologic model may not have a sufficiently detailed spatial resolution to represent near-surface variations in geophysical model parameters.

This research aims to develop new general CHI methods to address the previously mentioned limitations. The need for such a general framework can best be described by an example: At many sites globally large, high-resolutions airborne EM datasets have been collected to map salt water intrusion and geological properties on a regional scale [*Auken et al*., 2008; *Macaulay and Mullen*, 2007]. At the same time regional-scale groundwater models are available to establish a regional overview of the present state and future trends in the available groundwater resources and salt water intrusion [e.g. *Henriksen et al.*, 2003; *Langevin*, 2003a]. A consistent framework to integrate the potential wealth of geophysical information into these models is lacking. With this question in the back of our mind, the aim of this research is to:

- develop a new CHI-approach to estimate hydraulic properties for regional groundwater models using electromagnetic and geo-electric data
- apply a CHI to estimate parameters of salt water intrusion model based on electromagnetic data
- apply a CHI to evaluate the use of time-lapse gravity and magnetic resonance sounding data for aquifer pumping test monitoring

The latter objective pertains to a different spatial scale, but aquifer pumping tests are used to estimate typical values for the hydraulic properties of an aquifer, which are important to inform larger scale groundwater models with.

1.3 Structure of the thesis

This thesis provides a synopsis of the three papers that are found in Chapter 9. All the remaining chapters in this book have the purpose to introduce the different methods that are used in the papers and put them into a scientific and application-oriented context. Chapter 2 gives an overview of common hydrologic models that are used to simulate groundwater water flow and solute transport in the saturated zone, together with a brief summary of common geophysical techniques that are used for mapping hydrologic properties. Chapter 3 lists the properties of the two field sites that were used in our investigations, while chapter 4 provides an overview of the inversion frameworks that were developed in this research. Chapter 5 gives a short overview of results that were obtained during this PhD study. Finally, chapters 6 and 7 summarize, respectively, the main conclusions of this research and a list of future research directions based on the work that is presented in this book.

2 Hydrologic models and geophysical methods

2.1 Hydrologic models

In this research only flow and solute transport in the saturated groundwater zone will be considered. To simulate groundwater flow we start from the continuity equation

$$-\nabla \cdot (\rho(c)\theta\vec{u}) - W\rho_s = \frac{\rho(c)\theta_s}{dt} \tag{2.1}$$

where W is the external flux per unit volume [T^{-1}], θ_s is the porosity [-] which we assume to be equal to the saturated water content, where $\rho(c)$ is the density of the water [-] and where ρ_s represents the density of the water associated with the external sinks and sources [-]. $\rho(c)$ depends on the concentration of the dissolved solutes c [ML^{-3}] in the groundwater. The pore velocity u [LT^{-1}] is calculated using Darcy's law

$$\theta_s\vec{u} = -\frac{K}{g}\left(\nabla\left(\frac{h}{\rho(c)}\right) + \vec{g}\right) \tag{2.2}$$

in which h is the hydraulic pressure [$ML^{-1}T^{-2}$], K [LT^{-1}] is the hydraulic conductivity of the subsurface and g the gravitational acceleration [L^2T^{-1}]. Solute transport is commonly simulated with a convection-diffusion equation together with some basic chemical reactions like adsorption to a solid phase and a first order rate reaction. Neglecting the inclusion of adsorption and reactions the convection-diffusion equation can be written as

$$\frac{\partial c}{\partial t} = \vec{u} \cdot \nabla c + \nabla \cdot \left(\mathbf{D} \cdot \nabla c\right) + Wc_s \tag{2.3}$$

where **D** is the dispersion tensor [L^2T^{-1}], and c_s is the solute concentration associated with the sink and sources W, which represents features such as drains, wells and surface water bodies.

For regional models, Equation 2.1 and 2.3 are often solved numerically, using groundwater modeling software such as MODFLOW [*Harbaugh and McDonald*, 2000] and the solute transport module MT3DMS [*Zheng and Wang*, 1999]. The results of MODFLOW are water fluxes and water levels, while MT3DMS

calculates solute concentrations and solute fluxes. In paper **II** we simulate salt water intrusion, for which we take into account the groundwater flow component due to density differences which are caused by differences in salinity. This is done, by coupling equation 2.1 and 2.3 with an "equation of state", which provides a relationship between groundwater density and salt concentrations. This equation of state is formulated as follows

$$\rho(c) = \rho_f + 0.71c \tag{2.4}$$

where ρ_f represents the density of freshwater and c the salt concentration calculated with equation 2.3. Equation 2.4 is based on a linearized formulation derived by [*Baxter and Wallace*, 1916] which does not take into account temperature and pressure effects on the density of the water. In this research SEAWAT [*Langevin and Guo*, 2006] is used to perform simulations for variable-density groundwater flow.

In paper **III** we use an analytical hydrologic model to calculate the water table drawdown around a pumping well due to groundwater pumping. For aquifer pumping tests, the governing equations are the same as for saturated groundwater flow. Typically uniform aquifer properties and simple aquifer geometries are assumed, in order to use an analytical expression for the simulation of water table drawdown. Many studies [*Moench*, 1997; *Neuman*, 1972] have been dedicated to the derivation of the most complete analytical expression to capture all relevant hydrologic processes and pumping test design characteristics, as delayed drainage and borehole flow. Typical software packages for pumptest analysis are AQTESOLV [*Duffield*, 2007] and WTAQ [*Barlow and Moench*, 1999].

2.2 Hydrologic applications of geophysical methods

A wide variety of geophysical techniques is available. Many books provide a description of the underlying physics and applications for the various methods [e.g. *Telford et al.,* 1990]. The art of the geophysicist is to pick out a particular geophysical method that is most suitable, given its sensitivity for the property that needs be mapped, the scale that has to be represented and the environmental noise conditions that might interfere with the geophysical survey. In this paragraph we only provide a brief overview of the different techniques, after which we describe some major applications of geophysics to map hydrologic variables.

2.2.1 Basic classification of geophysical methods

Kearey et al. [2002] provide an excellent description of available geophysical methods. Table 2.1 is based on the classification used in this book and provides a basic classification of available techniques according to their underlying physics and indicates which physical property of the earth is estimated.

Table 2.1 Classification of geophysical techniques

Method	Measured data	Estimated property
Seismic	Travel time refracted/reflected seismic wave	Density and elastic moduli
Gravity	Gravitational field of the Earth in space and time	Density
Magnetic	Geo-magnetic field in space and time	Magnetic susceptibility
Nuclear magnetic resonance	Relaxation electromagnetic field	Fluid content and relaxation constants
Geo-electric	Earth resistance	Electrical resistivity
Induced polarization	Voltage decay	Electrical chargeability
Self potential	Electric potential	Electrical resistivity
Electromagnetic	Response to electromagnetic pulses	Electrical resistivity
Radar	Travel time of reflected radar	Dielectric constant

According to Table 2.1 many different physical properties of the subsurface can be estimated. In this thesis we only discuss their use with respect to hydrologic mapping. A much wider range of applications can be associated with geophysical techniques. For example, magnetic methods are used to detect iron ore bodies and seismic methods are employed to explore existing oil and gas reservoirs. Note Table 2.1 lists two properties, a measured quantity and an estimated property. For most geophysical techniques the estimated property is obtained after a geophysical inversion process in which its value is estimated based on the measured data. This is done by calculating a geophysical forward model, which simulates the data you would measure in the field or laboratory, given a certain value of the estimated property and then fitting the simulated data to the observed data.

Instead of describing the geophysical methods according Table 2.1, we discuss a number of main application areas for geophysics in hydrology [like in *Vereecken et al.*, 2007]. For this thesis we consider three of those applications areas, which are the vadose zone, landfills and contaminant transport and regional geology and coastal regions.

2.2.2 Vadose zone

The vadose zone, commonly referred to as unsaturated zone, plays an important role associated with environmental issues such as soil and groundwater

contamination, ground stability and flood control. Monitoring the spatial and temporal variability of moisture content and the freezing/thawing of the subsurface can yield valuable information regarding these environmental concerns. Applications of geophysical techniques in frozen soils can be found in [*French and Binley*, 2004], which are commonly geo-electric methods to distinguish between the frozen and unfrozen part of the subsurface. To monitor moisture content θ [-], two groups of geophysical techniques are currently employed.

The first group of geophysical techniques comprises radar and geo-electric methods based on relating the electric permittivity and electrical resistivity of the subsurface with its water content. As pointed out in the previous paragraph, these geophysical techniques do not measure electric permittivity or resistivity directly, but estimate these values based on the measured data. For radar methods as Time Domain Reflectrometry (TDR) [*Michot et al.*, 2003] and Ground Penetrating Radar (GPR) [*Knight*, 2001], measured data comprise recorded electromagnetic wave velocities which are obtained by transmitting an electromagnetic wave after which their refracted and reflected waves are recorded.

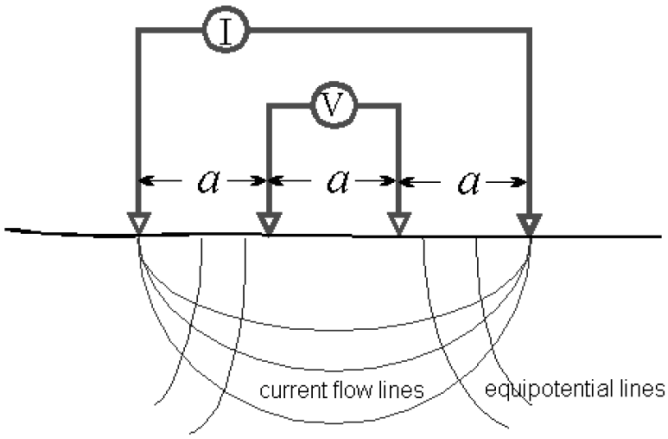

Figure 2.1 Measurement setup for Electric Resistivity Tomography [ERT]. a is the spacing between the electrodes (red arrows) where I indicates an electrical current [A] andV indicates the potential difference [V] that is measured during a survey

Figure 2.1 represents the setup of a geo-electric survey using Electric Resistivity Tomography (ERT), in which electrodes are placed in the subsurface after which potential differences (V) are measured by applying an electrical current (I) for different electrode combinations with a spacing a. Based on the potential differences [voltages] and the used electrode configuration (e.g. Wenner, Schlumberger), an apparent resistivity can be calculated. Apparent resistivities can be computed from subsurface resistivity distributions using the forward

model for DC electric surveying. Matching measured and simulated apparent resistivities results in estimated subsurface resistivity distributions.

For radar methods the estimated electrical permittivity can be related to the soil moisture content by an empirical petrophysical relationship, called the Topp-equation [*Topp*, 1980]

$$\theta = -5.3 \cdot 10^{-2} + 2.92 \cdot 10^{-2} \varepsilon_r^2 + 4.3 \cdot 10^{-6} \varepsilon_r^3 \tag{2.5}$$

where ε_r is the electrical permittivity of the subsurface normalized over the permittivity of free space, also known as the relative permitivitty or dielectric constant. Examples of studies using this approach to estimate θ can be found in *Kowalsky et al.* [2004], *Lambot et al.* [2009] and *Huisman et al.* [2003]. A more general overview of environmental applications for GPR can be found in *Knight* [2001].

When using resistivity methods, often Archie's law is used to estimate the moisture content, given by [*Looms et al.*, 2008] as

$$\theta^n = r_w \frac{\theta_s^{n-m}}{r_b} \tag{2.6}$$

where r_w indicates the electrical resistivity of water and n and m are shape factors that are soil specific [*Looms et al*., 2008]. r_b represents the resistivity of the bulk material. Note that r_b is the estimated parameter using a geo-electric method. To apply equation 2.6 for estimating moisture content a reasonable estimate is required for r_w.

The first group of techniques is not very attractive for clayey sediments, as radar methods suffer from a limited depth of penetration due to dielectric dispersion in sediments with a low electrical resistivity [*Knight*, 2001]. For geo-electric methods Archie's law does not apply anymore, as this empirical law does not include surface conductivity through the bulk material itself [*Lesmes and Friedman*, 2006]. This additional term is complicated to characterize and makes the estimation of soil moisture content less reliable.

The second group of methods does not require a relationship like Archie's law or the Topp-equation, but directly relate the measured geophysical signal with the

moisture content of the subsurface in the geophysical forward model. Two of these methods are Nuclear Magnetic Resonance (NMR) or Magnetic Resonance Sounding (MRS) [*Legchenko and Valla*, 2002] and time-lapse gravity [*Montgomery*, 1971].

With relative gravimeters, the vertical component of the gravitational acceleration is measured. This reveals spatial differences in density which can be due to ore deposits, buried paleo-channels and changing depth to bedrock [*Carmichael and Henry*, 1977; *Zawila et al.*, 1997]. Time-lapse relative gravity (TL-RG) can be applied to monitor changes in mass, which can be used to monitor natural gas extraction [*van Gelderen et al.*, 1999] and quantify changes in water storage [e.g. *Christiansen et al., 2011*].

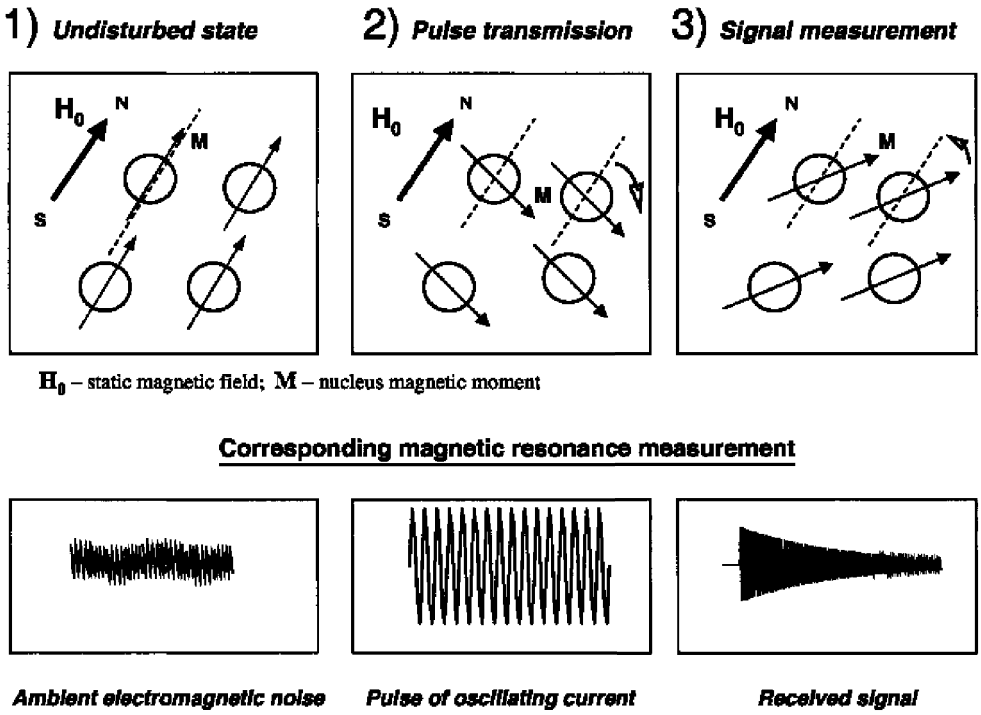

Figure 2.2 Observed data during a MRS sounding [picture from *Legchenko*, 2002]. 1) hydrogen protons in equilibrium state aligned along the Earth's magnetic field H_0, 2) hydrogen protons are excited with an external magnetic pulse and 3) hydrogen protons return to their equilibrium state yielding the received MRS signal shown on the bottom right side of the figure.

MRS is commonly known through its application in hospitals, where Magnetic Resonance Imaging (MRI) is used for imaging and diagnosis. With MRS the spins of the hydrogen protons of water molecules in the subsurface are excited with an external magnetic field, applied through a transmitter loop on the ground surface. After the external magnetic field is switched off, the spins of the

hydrogen protons return to their original state generating a new magnetic field [*Legchenko et al.*, 2002], whose magnitude is measured by a receiver on the ground. Figure 2.2 [based on *Legchenko et al.*, 2002] shows the three stages of a MRS-sounding. The bottom-right panel of this figure shows the received MRS signal, which is oscillating with exponential decreasing amplitude. Typically two properties are extracted from this signal, which are the initial amplitude of this signal, depending on soil moisture content, and an exponential decrease rate of the amplitude (relaxation constant), which correlates with the pore characteristics of the subsurface and can be used to estimate hydraulic conductivity [*Mohnke and Yarmanci*, 2008; *Vouillamoz et al.*, 2008].

2.2.3 Landfills and contaminant transport

In the past low elevation areas, such as pits and wetlands were typically used for waste deposition [*Milosevic et al.*, 2011, *Lorah et al.*, 2009]. The waste deposition at these old landfills often lacked adequate control and documentation such that the boundaries of the landfill and the type of landfill material are unknown. Some of these landfills pose a significant environmental threat in polluting groundwater and surface water [*Christensen et al.*, 2001; *Lorah et al.*, 2009]. Such landfills usually contain household-, demolition- and chemical waste, where the main impact on surrounding water bodies is associated with inorganic macro-components (chloride, sodium, ammonium), dissolved organic carbon (DOC) and several different xenobiotic organic compounds [*Bjerg et al.*, 2011; *Kjeldsen et al.*, 2002]. The heterogeneous nature of an old landfill causes high spatial variability of the leachate compounds, and a large amount of work is required to accurately delineate the landfill, and detect leachate plumes.

Meju [2000] lists the geo-electric and electromagnetic methods as most popular geophysical techniques to characterize landfills due to their ability to detect changes in electrical resistivity, which correlates with moisture content and chemical composition of the pore water, and the relative low-costs to perform such surveys. Due to the presence of saline fluids in the landfill leachate, which is a good electrical conductor, it is possible to delineate the landfill and locate a contaminant plume by employing these geophysical techniques [*Naudet et al.*, 2004, *Chambers et al.*, 2004] One major limitation of using the electrical resistivity in landfill surveys is the fact that several factors influence the electrical resistivity of the subsurface, which makes it difficult to differentiate between one another. For example, clay and saline fluids both have a small electrical resistivity.

An upcoming technique for delineating landfills and detecting solute plumes is Induced Polarization (IP), which can be performed in combination with a geo-electric survey [*Dahlin et al.*, 2002; *Sogade et al.*, 2006]. IP is based on the fact that the subsurface is able to act as an electric capacitor and store electric charge. The same measurement setup as described in Figure 2.2 can be used, but instead of measuring the potential differences when an electrical current is applied, the decay of these potential differences is measured in time after terminating the applied electrical current. The decay rate of the potential difference can then be related to the chargeability of the subsurface. The signal that is retrieved with IP is mainly the result of the local redistribution of ionic charge in the electric double layer at the mineral-fluid interface [*Slater*, 2007]. Typically, the observed IP response is fitted by an empirical relationship named the Cole-Cole model [*Pelton et al.*, 1978], which parameters (chargeability, electrical resistivity, relaxation time and shape parameter) can be correlated with hydraulic conductivity and the presence of contaminant plumes. The Cole-Cole model, however, does not provide a mechanistic understanding of the retrieved IP-signal. A physical model is still lacking to explain the IP signature of contaminant plumes. [*Vaudelet et al.*, 2011], [*Revil and Florsch*, 2010] and [*Leroy and Revil*, 2009] are examples where the development of such a physical model is investigated.

2.2.4 Regional geology and coastal regions

To characterize regional geological properties and human structures, seismic and electromagnetic methods are often employed. With seismic methods, a seismic wave is generated by an explosion or vibrator, after which the wave is reflected and refracted at geological interfaces of materials with different seismic velocities. These reflected and refracted waves are recorded by receivers, called geophones or hydrophones (off-shore applications) to obtain a seismogram. Seismic velocity depends on the density of the rock, which makes the method attractive to determine the thickness of unconsolidated sediments overlying bedrock [*Miller et al.*, 1989].

Electromagnetic surveys can be performed using ground-based and airborne instruments. In Figure 2.3 a sketch is given of the measurement setup for a ground based electromagnetic survey using a Time-Domain Electromagnetic (TDEM) sounding. In this setup a square transmitter loop is used to generate an electrical current, which is switched off to generate a magnetic field in the subsurface whose strength decreases after the electrical current is turned off. A receiver coil, placed in the middle or outside the transmitter loop, is used to

record this decrease in magnetic field strength, which can be translated to a series of apparent resistivities which, in turn, are inverted to obtain the subsurface resistivity distribution.

TDEM surveys are sensitive to estimate the depth of a layer with a low electrical resistivity, for example a clay layer or salt water saturated sediments. The depth of penetration can be up to 500 m [*Kearey et al.*, 2002], but this depends on the magnitude of the transmitted electrical pulse, the electrical resistivity of the subsurface and the frequency at which the electrical pulse is applied. In coastal regions this technique is very attractive as TDEM can potentially delineate the location of the freshwater/salt water interface, which is of major interest for supporting freshwater resources management in coastal aquifers. Examples of other applications of electromagnetic surveys are the mapping of buried channels [*Auken et al.*, 2008] and the mapping of a cave system in Mexico [*Supper et al.*, 2009].

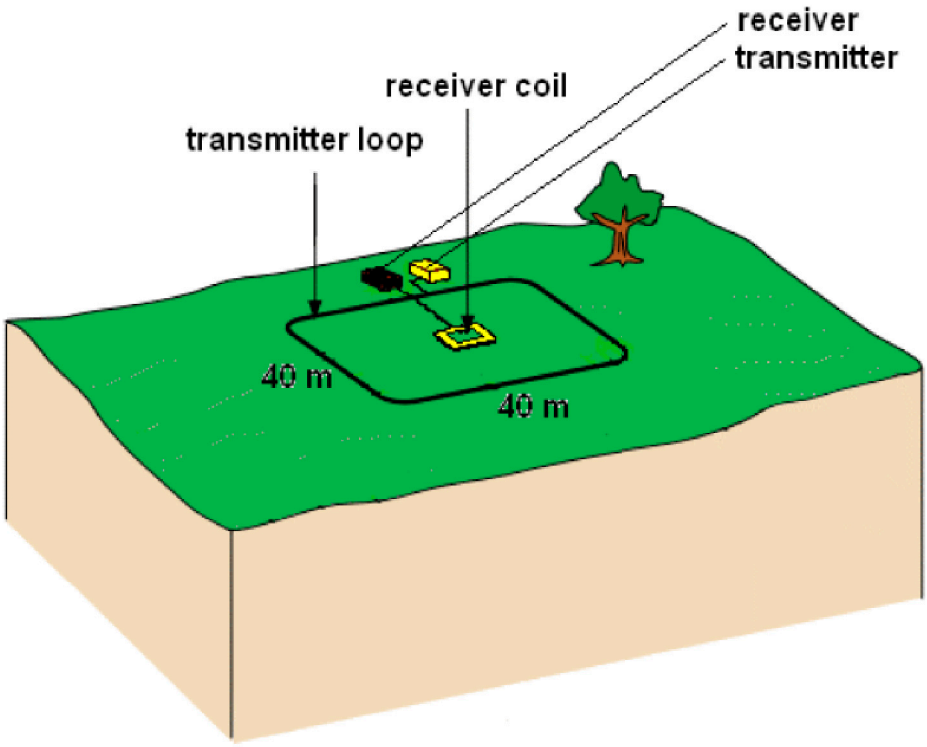

Figure 2.3 Measurement setup of a Time-Domain Electromagnetic (TDEM) sounding

Figure 3.1 Installing a benchmark point for a geodesy survey at Risby Landfill (upper left). Seepage meter measurements at Risby Landfill (upper right). Performing a Time Domain Electromagnetic (TDEM) sounding at Monterey Bay, California (bottom).

3 Field sites and data collection

3.1 Risby landfill

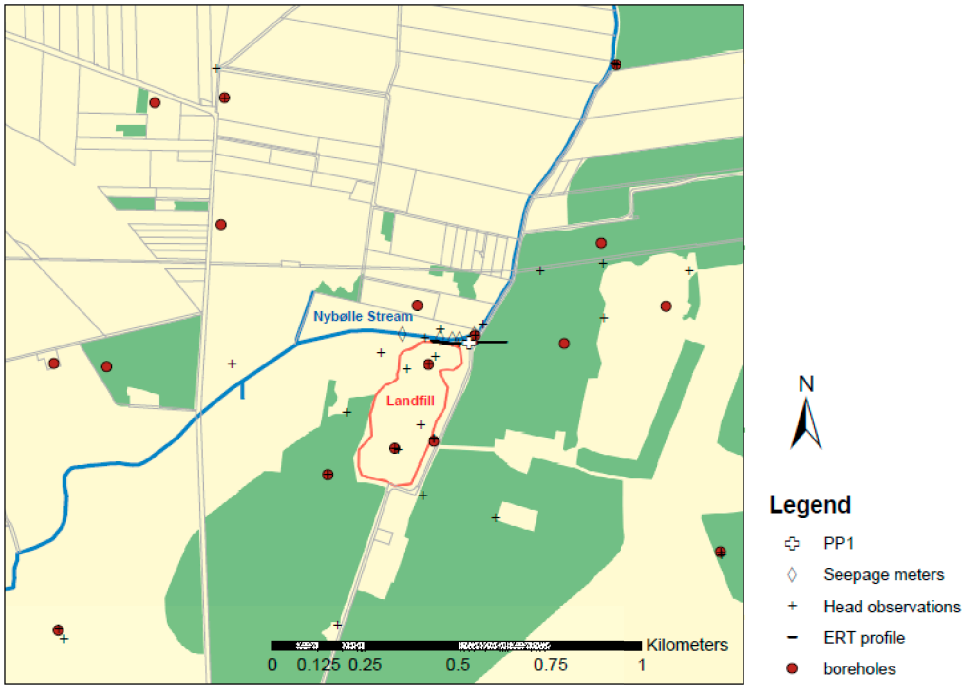

Figure 3.2 An overview of Risby Landfill and the collected measurement data that were used in paper **I**.

Risby landfill is located ca. 20 km west from Copenhagen, Denmark, and was chosen as a pilot-area in the RISKPOINT project to identify the dominant processes affecting the hydrogeological and geochemical interaction between the landfill, regional aquifer and the Nybølle stream. For this purpose boreholes have been drilled and leveled, together with the collection of indirect information using several geophysical methods. In Figure 3.2 a map is provided with the data that was used in paper **I**, comprising groundwater level measurements, seepage measurements in the Nybølle stream, borehole information and an ERT profile.

A detailed historical overview of Risby landfill was provided by [*Thomsen et al.*, 2011]. The geological setting of Risby landfill [*Gazoty et al.*, 2011, *Frederiksen et al.*, 2003; *Carl Bro A/S*, 1988] comprises pre-Quaternary limestone bedrock overlain by Quaternary glacial deposits. The pre-Quaternary limestone surface is located between -10 and +5 mamsl, corresponding to 20-30 m below the natural terrain surface. The Quaternary glacial deposits mainly consist of clay till, but intercalated sand lenses and sand layers are common. The sandy deposits range in thickness from a few centimeters to several meters.

In addition to the data that was used for paper **I**, water samples, ecological data and other geophysical data were collected in order to quantify contaminant fluxes from the landfill towards the stream and groundwater [*Milosevic et al.*, 2011, *Thomsen et al.,* 2011] and indentify which properties of a typical Danish landfill can be mapped using state-of-the-art geophysical techniques as magnetic methods, induced polarization and geo-electric methods [*Gazoty et al.*, 2011].

3.2 Monterey Bay, California

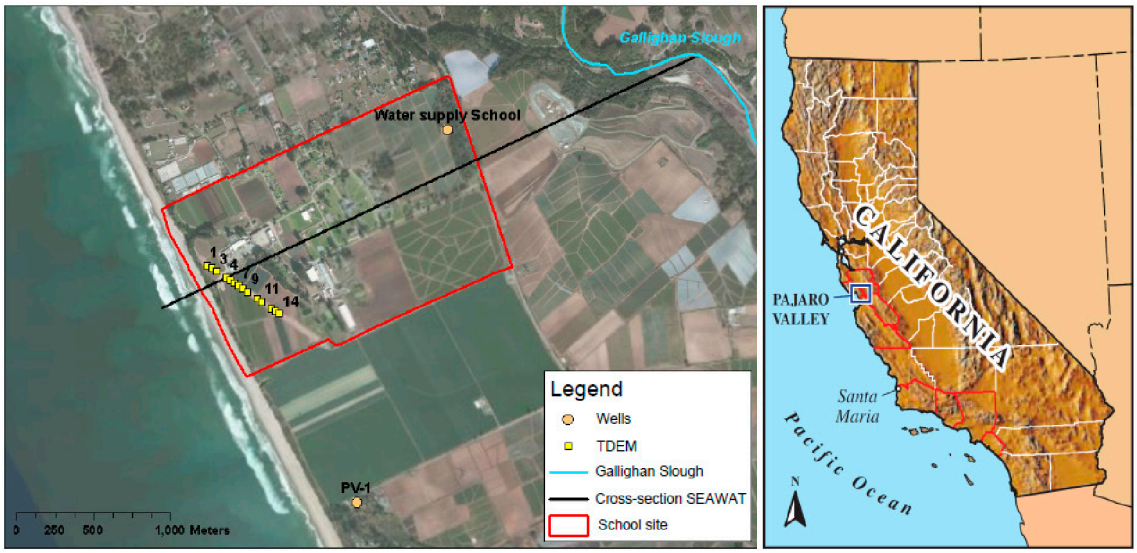

Figure 3.3 Right: Map of California, with a box highlighting Pajaro Valley, the water district where the School-site is located. Left: Overview of the School-site and the locations of the TDEM soundings.

At Monterey Bay, California, different electromagnetic (EM) methods were applied at two field sites, to evaluate the use of geophysical data for water managers in California. One of these field sites is called Monterey Bay Academy, to which we refer as the School-site. The other site is located 30 km south and is called Fort Ord. At Ford Ord there are plans to install a desalination plant that takes in salt water trough the upper aquifer system. [*Nenna et al.*, 2011] focus on the value of EM data at this site to inform local water managers about the current delineation of the salt water-fresh water interface and the presence of confining geological units that protect deep aquifers from induced salt water intrusion as a result of the placement of a desalination plant. Paper **II** is related to [*Nenna et al.*, 2011] and is focused on the TDEM data set collected at the School-site in relation to salt water intrusion at Monterey Bay. At the School-site 19 TDEM soundings were collected along an airstrip to obtain an electrical resistivity profile perpendicular to the coast that can be correlated to geological trends and changes in salt concentrations.

4 Inversion methodology

For the field sites in chapter 3, a hydrogeological model was employed to determine groundwater flow directions and quantify salt water intrusion, respectively. These hydrologic models require a significant amount of unknown input parameters, which have to be estimated based on prior knowledge or with an inversion approach using available measurement data. Measurement data include direct hydrologic observations but also indirect data such as geophysical measurements.

For both field sites in chapter 3 a CHI was applied, using a regional groundwater model in combination with TDEM or ERT data. When performing such a CHI a number of challenges were faced that are not taken in account in existing CHI-applications. The three most important challenges are:

- using the geophysical data to inform a hydrologic model about its input parameters
- allow for a separate estimation of essential geophysical parameters to achieve an acceptable geophysical data fit
- the large computational burden associated with the hydrologic model and the geophysical data sets

Ferré et al. [2009] provide a basic classification of hydrogeophysical inversion methods, which includes the division between CHI and SHI approaches. In addition to this classification, these CHI and SHI approaches can be divided into groups that couple geophysical models with a hydrologic model using the simulated hydrological state variables or the hydrologic input parameters. Paragraph 4.1 provides a short description of existing SHI and CHI approaches. Paragraph 4.2 describes the basics of performing a hydrogeophysical inversion using parameter and state coupling. In addition the differences are listed between existing CHI-applications and the CHI-frameworks that are developed in this thesis. Paragraph 4.3 concludes with a specification of the coupling constraints that can be used to inform hydrologic models with geophysical data, which we subdivide in geometric and petrophysical relationships.

4.1 Sequential and coupled hydrogeophysical inversion

Figure 4.1a and 4.1c show a Sequential Hydrogeophysical Inversion (SHI) approach. The first step in a SHI comprises a geophysical inversion in which a

geophysical parameter is estimated (e.g. electrical resistivity). Subsequently, the estimated geophysical parameter distribution is translated to a number of hydrologic observations or hydrologic input parameters. This can be done directly or with the use of a petrophysical relationship (e.g. Archie's law, Topp-equation). The way a hydrologic model is informed with the inverted geophysical model depends on the geophysical technique and the hydrologic interpretation of the estimated geophysical model. The final step in the SHI is to perform a hydrologic inversion, in which the hydrologic model parameters are estimated using the estimated geophysical parameters as observation data.

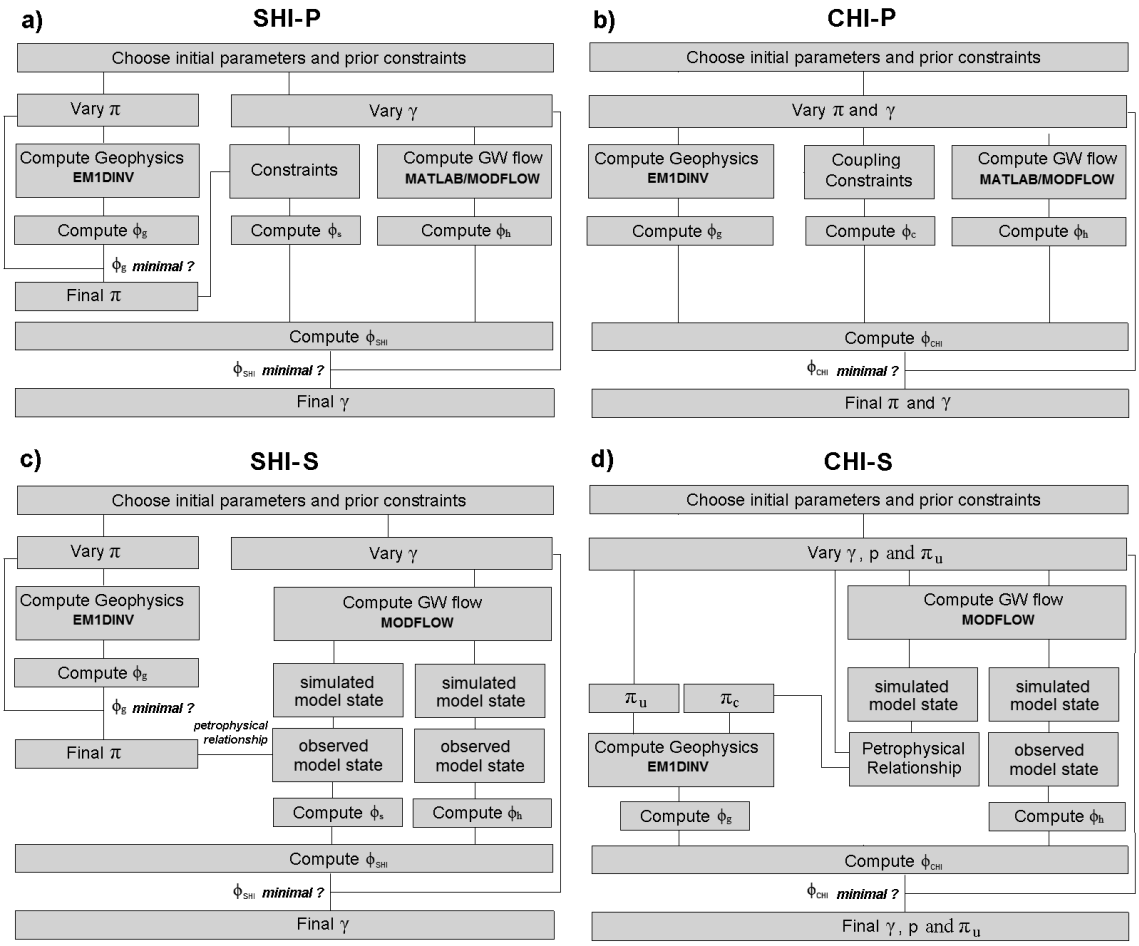

Figure 4.1 Inversion frameworks. Left: SHI, right: CHI. Up: Parameter coupling (P), down: State coupling (S). γ represents hydrologic parameters, π geophysical parameters and p petrophysical parameters. In Figure 4.1d π is divided into π_u and π_c, where π_u are uncoupled (u) geophysical parameters that are estimated independent from the hydrologic model.

In a SHI, the value of the geophysical data for informing the hydrologic models is not only influenced by the geophysical measurement errors, but also by the errors and assumptions associated with the geophysical forward model and the geophysical inversion. For example filter properties of a geophysical instrument

might not be modeled correctly [*Effersø et al.*, 1999] and regularization constraints used for the geophysical inversion might bias the hydrologic parameter estimates [*Day-Lewis et al.*, 2005]. Another important error component is the relationship with which geophysical parameters are correlated with hydrologic properties, which might neglect processes or properties that are important for fitting the geophysical measurement data, e.g. heterogeneity in petrophysical properties [*Hinnell et al.*, 2010].

Instead of performing a hydrologic and geophysical inversion separately, a Coupled Hydrogeophysical Inversion (CHI) can be employed, in which the hydrologic model is included in the geophysical inversion (Figure 4.1b and 4.1d).

This has a number of advantages compared to an SHI:

- A geophysical inversion can be undertaken, which is consistent according to an a priori hydrologic interpretation of the geophysical data [*Hinnell et al.*, 2010]
- The geophysical model can be updated according to the hydrologic observations
- Subjective geophysical parameter constraints (i.e. regularization) are partly substituted by a hydrologic model
- As the hydrologic model provides an advanced type of regularization framework for the geophysical inversion, the resolution of the geophysical model can be improved

Disadvantages of a CHI are:

- Larger computational burden
- Propagating errors associated with the hydrologic model into the geophysical model
- Not taking into account processes or properties of the subsurface that are essential for fitting the geophysical measurement data due to a poor coupling strategy between the geophysical and hydrologic model

4.2 State and parameter coupling

Instead of separating hydrogeophysical inversion methods into SHI and CHI approaches, these methods can be subdivided in another way. Many studies have used geo-electric methods to estimate moisture content based on electrical resistivity [*Robinson et al.*, 2008]. *Slater* [2007], *Purvance and Andricevic* [2000] and *Niwas and de Lima* [2003] discuss the estimation of hydraulic conductivity based on electrical resistivity. In contrast to moisture content, hydraulic conductivity is not a simulated state variable of a hydrologic model, but a static hydrologic input parameter. In addition, *Vanderborght et al.* [2005], *Hubbard et al.* [1999] and *Hyndman and Gorelick* [1996] provide examples were geostatistical properties of hydrologic input parameters are estimated using geophysical models. For this purpose this study divides hydrogeophysical inversion methods into a group that uses geophysical models to inform hydrologic models about its input parameters and a group of methods that is focused on simulated hydrologic state variables. We refer to these approaches as parameter (P) and state coupling approaches (S).

Figures 4.1a and 4.1b show the implementation framework for estimating hydrologic model parameters with geophysical data using a parameter coupling approach (SHI-P and CHI-P), where figures 4.1c and 4.1d show the use of a state coupling approach (SHI-S and CHI-S). Paper **I** provides a thorough theoretical description of using a parameter coupling approach. Paper **II** includes the theory for state coupling approaches. For SHI applications parameter and state coupling approaches are straightforward, as a geophysical inversion is undertaken after which the estimated geophysical parameters can be used as additional observations to constrain the hydrologic model. For CHI applications these coupling approaches are more difficult to implement due to the three challenges mentioned at the start of this chapter.

Existing CHI-applications by *Pollock and Cirpka* [2010] *Kowalsky et al.* [2005], *Hinnel et al.* [2010] and *Lambot et al.* [2009] only consider state coupling approaches (CHI-S). In these studies hydrologic and petrophysical parameters are estimated, after which the hydrologic simulations are translated to geophysical parameters to generate a geophysical forward response.

This thesis introduces a small modification with respect to the traditional CHI-S approach applied in *Pollock and Cirpka* [2010], *Kowalsky et al.* [2005], *Hinnel et al.* [2010] and *Lambot et al.* [2009]. This modification comprises the separate estimation of some geophysical parameters (in Figure 4.1d represented by π_u)

that are not coupled with the hydrologic model in order to fit the geophysical measurement data satisfactorily as some geophysical parameters cannot be calculated from the hydrologic simulations. For example in paper **II**, the electrical resistivity of the unsaturated zone needed to be estimated for the geophysical model. The hydrologic model, however, did not provide any information about this geophysical parameter.

The most important development in this thesis is the introduction of CHI-P, which is to our knowledge a new CHI-method. CHI-P employs a parameter coupling between the geophysical and hydrologic model. In the CHI-P both hydrologic and geophysical parameters are estimated. Within these two parameter groups, parameters are constrained using standard regularization constraints. Across the two parameter groups, parameters are coupled using coupling constraints.

The strength of both the CHI-S and CHI-P is their flexibility with which the hydrologic interpretation of the geophysical models can be coupled to the structure, parameters and simulations of a hydrologic model. In principle CHI-S and CH-P can be performed simultaneously, but for clarity reasons this topic will not be further discussed in both the thesis and in papers **I**, **II** and **III**.

4.3 Petrophysical and geometric coupling constraints

Relationships between geophysical parameters and hydrologic models can generally be divided in two groups, petrophysical and geometric relationships. Petrophysical relationships can be specified by empirical laws that describe the correlation between a geophysical parameter value and a hydrologic state variable or parameter. Geometric relationships are different as they apply to the spatial characteristics of the subsurface.

The most widely used examples of petrophysical relationships are given by *Archie* [1942] and *Topp et al.* [1980], which were discussed in paragraph 2.2.2. These laws describe the dependence of, respectively, electrical resistivity and permittivity on soil moisture content. These properties represent the natural characteristics (‘physics’) of the subsurface or rock (‘petro’ in Latin). Examples of studies where such petrophysical relationships are used can be found in [*Kemna et al.*, 2002; *Singha and Gorelick*, 2006].

Slater [2007], *Purvance and Andricevic* [2000] and *Niwas and de Lima* [2003] discuss another important petrophysical relationship, which includes the

estimation of hydraulic conductivity from geo-electric and IP-data. An important remark in these papers is the log-log relationship between electrical resistivity and hydraulic conductivity. In paper **I** we apply such a relationship in combination with a SHI-P and CHI-P using

$$\log 10(K) - \log 10(\rho_b) = P + e_s \tag{4.1}$$

In Equation 4.1, K represent the hydraulic conductivity [L/T] of a layer in the hydrologic model and ρ_b denotes the electrical resistivity in a TDEM or geo-electric model, where P is an expected value and e_s the assumed standard error associated with the petrophysical relationship. The assumption behind this relationship would be that the electrical resistivity is not influenced by another factor, e.g. the presence of a contaminant plume. The value for P and e_s depends on a priori knowledge and is site-specific.

In time-lapse applications of geophysical methods, petrophysical relationships can be employed differently. For example, ERT data can be used to monitor a salt tracer experiment. Salt tracer tests are commonly used to estimate the spatial distribution of hydraulic properties [e.g. *Kemna et al.*, 2002; *Vanderborght et al.*, 2005]. In such a setup concentration time series can be derived from the ERT data using a petrophysical relationship, which can be compared with simulated concentrations. Instead of comparing concentration time-series directly, temporal moments of the simulated and observed concentrations can be compared, which are a measure of the mean arrival time and the spread of a tracer [*Day-Lewis and Singha*, 2008]. For monitoring salt-tracer experiments with ERT data, *Singha and Gorelick* [2005] noted that only a fraction (25-50%) of the injected tracer was recovered from the inverted ERT model. To avoid such non-physical results, a CHI-S as in *Pollock and Cirpka* [2010] can be performed to consider the physics of the geophysical technique and the hydrologic process simultaneously.

The second type of coupling constraints between geophysical and hydrologic models comprises geometric constraints. Geometric constraints quantify spatial characteristics of hydrologic properties as the delineation of geological units and the spatial correlation structure of heterogeneous aquifer properties. Examples of studies which use such geometric constraints can be found in *Vanderborght et al.* [2005], *Hubbard et al.* [1999], *Hyndman and Gorelick* [1996] and many other papers. In paper **I** we use a geometric constraint to estimate the elevation of a geological layer in the groundwater model based on the thickness of a layer in the geophysical model.

5 Results

Each paragraph in this chapter successively addresses one of the three research objectives provided in paragraph 1.3 and the major findings in paper **I**, **II** and **III**.

5.1 Informing groundwater models with transient electromagnetic and geo-electric data

In paper **I** we present a CHI-P to inform a groundwater model with Time Domain Electromagnetic (TDEM) and Electrical Resistivity Tomography (ERT) data and compare the results with a SHI. The new aspect of the developed inversion strategy is the ability to constrain hydrologic model parameters with geophysical data. Previous studies about CHI have been applied using CHI-S only. As described in chapter 4 we developed a CHI-P approach. We tested our CHI-P approach for a synthetic groundwater model with TDEM measurements and a real-world groundwater model with ERT data.

For a synthetic study the CHI-P resulted in improved parameter estimates and a reduction in parameter uncertainty for both the groundwater model and the geophysical model compared with a SHI and a separate inversion. Figure 5.1 shows the estimates and confidence intervals for the synthetic groundwater and TDEM model parameters when performing a CHI-P. The x-axis of Figure 5.1 shows the strength of the coupling between the geophysical and groundwater model parameters, marked by e_c which denotes the standard deviation associated with the coupling constraint. When e_c is small, the coupling between the geophysical model and groundwater model is strong. In this analysis we generated 50 realizations of synthetic observation data which we used to estimate 3 groundwater model parameters and 3 geophysical model parameters. For smaller values for e_c, which again mark a stronger coupling between the geophysical and groundwater model, parameter estimates (dashed lines) approximate the truth (solid black line) more closely and parameter confidence intervals are reduced for all parameters. In Figure 5.1 the geophysical parameters are less impacted by the CHI-P.

For another study, considering a real-world groundwater model and an ERT section, a local sensitivity analysis for the groundwater model parameters showed that the use of petrophysical coupling constraints is likely to be of more importance compared to the use of geometric coupling constraints in order to improve groundwater model parameter estimates through a CHI-P. For this

second study, parameter uncertainty could not be reduced as well compared to a SHI and the computational burden associated with the CHI-P increased with a factor of ca. 2-3. However, the CHI-P clearly impacted the parameter estimates in both the groundwater model and geophysical model, resulting in consistent parameter estimates between the groundwater model and the geophysical model according to the hydrogeological interpretation of the geophysical model.

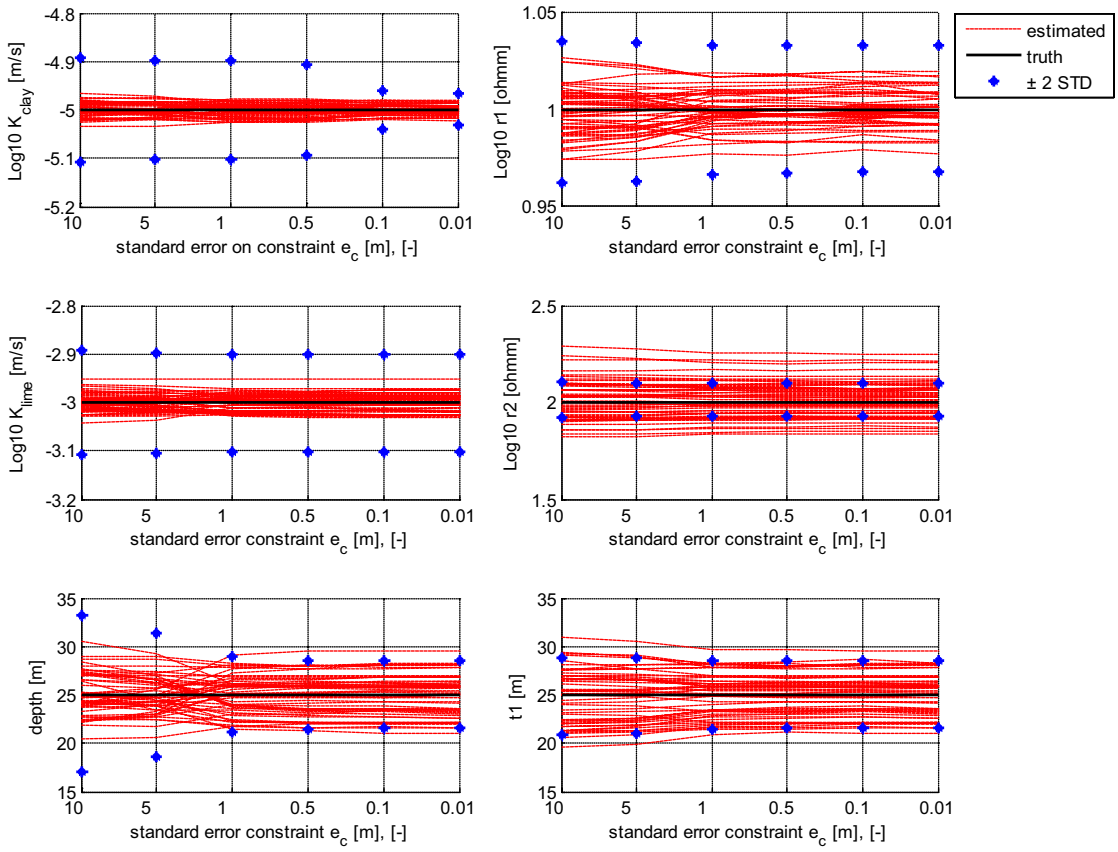

Figure 5.1 Parameter estimates (dashed red lines) for the synthetic example using a CHI with different e_c values for 50 realizations. Groundwater model parameters are shown in the left column of figures, geophysical parameters on the right. The straight black line marks the truth and the blued dots ± 2 standard deviations associated with the estimate. The x-axis shows the standard deviation of the two types of coupling constraints that were used, the geometrical constraint [m] between thickness clay and t1 and the petrophysical constraint between log10 K_{clay} and log10 r1 [-].

The impact by the CHI-P can be seen in Figure 5.2, which shows the inverted ERT model using a separate geophysical inversion and a CHI-P. Figure 5.2a shows a bottom layer of relatively resistive material of ca. 100 -150 Ωm, which dips down towards the east, which was interpreted as the regional limestone aquifer. The second layer at the right part of the profile with a resistivity of about

50 -80 Ωm was interpreted as a sandy deposit, while the first and second layer with a resistivity of ca. 10 Ωm in the left part of the profile were interpreted as clayey deposits. Figure 5.2c shows the uncertainty associated with the parameters that are estimated in the ERT model (layer resistivities: r1, r2, r3; layer thicknesses: t1, t2), expressed by their standard deviation as a percentage of the parameter estimate. This analysis included all the information provided by the data and parameter constraints. Note light colours in Figure 6c indicate relatively poorly resolved parameters, e.g. r1, r2 and t1 at the left part of the profile.

Figure 5.2b shows the inverted ERT model using a CHI-P with an e_c of 0.2. Compared with the result of a separate geophysical inversion in Figure 5.2a, the estimated resistivity of layer 2 decreased significantly from an average of 75 Ωm to ca. 30 Ωm for the first 10 resistivity models. Those were the models for which the electrical resistivity of layer 1 and 2 (r1 and r2) were coupled to the estimation of hydraulic conductivity of the clay in the groundwater model. In paper **I**, it can be seen in that the hydraulic conductivity of the clay was also impacted (Figure 8, paper **I**). Figure 5.2d shows the standard deviations associated with the estimated geophysical model obtained with the CHI-P. The parameter standard deviation of r2 indicates this parameter is not well-determined using the CHI-P as was the case in the separate geophysical inversion. r1 is determined with an approximate standard deviation of 10%. However, Figure 5.2d shows t1 is less well resolved for those model numbers where the petrophysical relationship was applied. The geometric coupling constraint does not show any effect on the estimated geophysical models in Figure 6.

With the results in paper **I** we show the main advantage of performing a CHI, a geophysical inversion that takes in account a hydrogeological interpretation of the geophysical data. *Hinnell et al.* [2010] point out that the formulation of a consistent framework for inference and solution between the geophysical model and hydrologic model is essential when performing a CHI. Our method would provide a very flexible framework to apply a CHI for hydrologic model parameters, which takes in account that 1) only part of a geophysical model can be coupled with a hydrologic model, 2) confidence associated with the hydrologic interpretation of a geophysical model can be altered using different weights for the employed coupling constraints and 3) scale issues can be overcome by coupling several geophysical parameters to hydrologic parameters and vice versa.

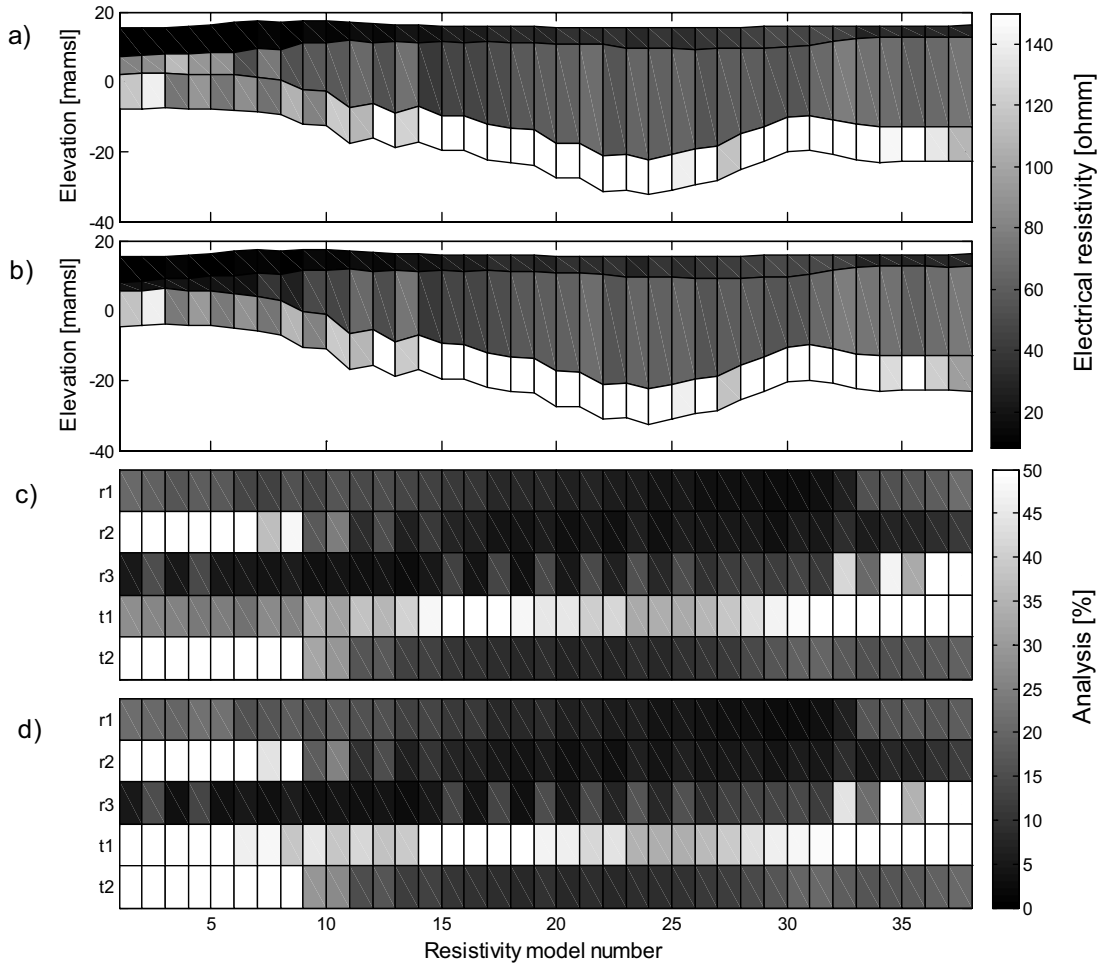

Figure 5.2 Inverted ERT model obtained after a separate geophysical inversion (a) and using the CHI with e_c=0.2 (b) together with a parameter uncertainty analysis expressed by their standard deviation relative to the parameter estimate. A gray scale marks well (dark coloured) and undetermined parameters (light coloured) for the separate geophysical inversion (c) and a CHI-P with e_c=0.2 (d).

5.2 Calibrating a saltwater intrusion model with time domain electromagnetic data

Attempts have been made to calibrate salt water intrusion models with different geophysical data [*Duque et al.*, 2008, *Langevin et al.*, 2003b, *Guérin et al.*, 2001], but all these approaches have been using a SHI (with the exception of *Bauer-Gottwein et al.*, 2010]. A SHI can induce a number of errors related to inconsistent scales between the geophysical and hydrologic models and the assumption behind the petrophysical relationship that converts the simulations of the hydrologic model to a geophysical parameter distribution. For this purpose we apply a CHI-S approach for a small pilot area in California in which we calibrate a salt water intrusion model with TDEM measurement data.

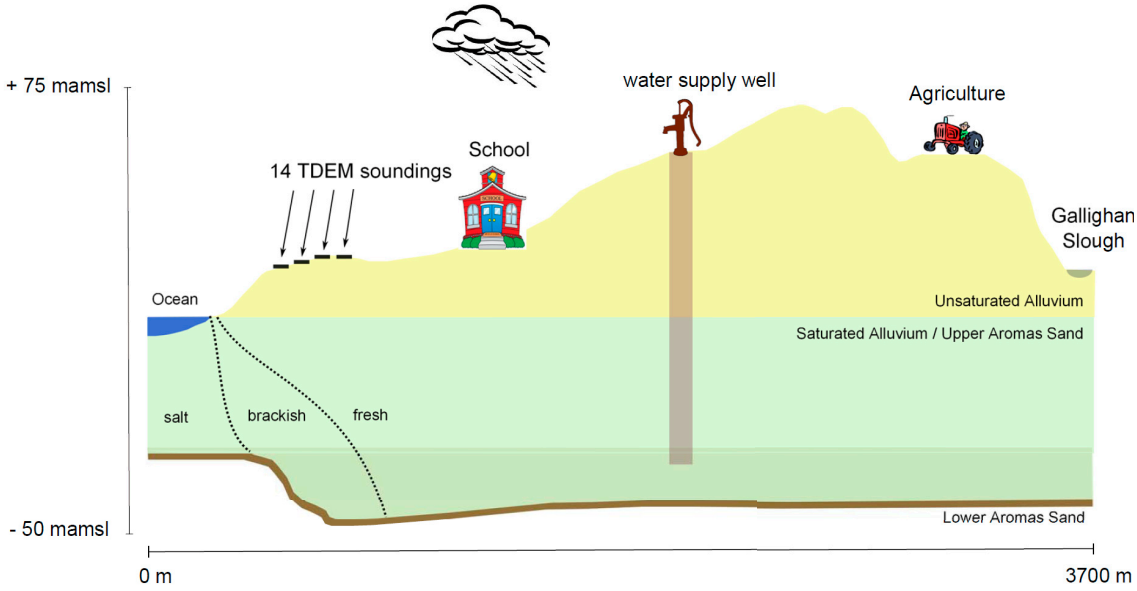

Figure 5.3 Hydrogeological schematization of the School site.

The CHI-P was applied for a semi-synthetic example, based on a real TDEM data set at a site in Monterey, California. For this site 14 TDEM soundings were available and we assumed a cross-sectional model with uniform aquifer properties. The geology and hydrologic processes that are represented by the salt water intrusion model are given by a conceptual hydrogeological cross-section in Figure 5.3, which only represents the water table aquifer that is found in this area, which is separated from the deep aquifer system by a clay unit marked by the Lower Aromas Sand formation. The current extent of the freshwater/salt water interface is the result of pumping activities at this site over a time period of 67 years. For the site no water level or salt concentration data were available and exact properties of the present and past water supply wells are unknown. For this aquifer we want to estimate five uniform aquifer properties (diffusion, dispersion, hydraulic conductivity, anisotropy and porosity) and one petrophysical shape parameter (m in Archie's law) by fitting the collected TDEM data (more than 300 apparent resistivities).

Except for the data at early time gates pertaining to three soundings all the TDEM data could be fitted with a RMSE close to 1 (Figure 6, paper **II**). Possible explanations for the poor data fit for these three soundings are the neglecting of spatial heterogeneity in the salt water intrusion model and not taking in account 3D effects for generating the TDEM forward responses.

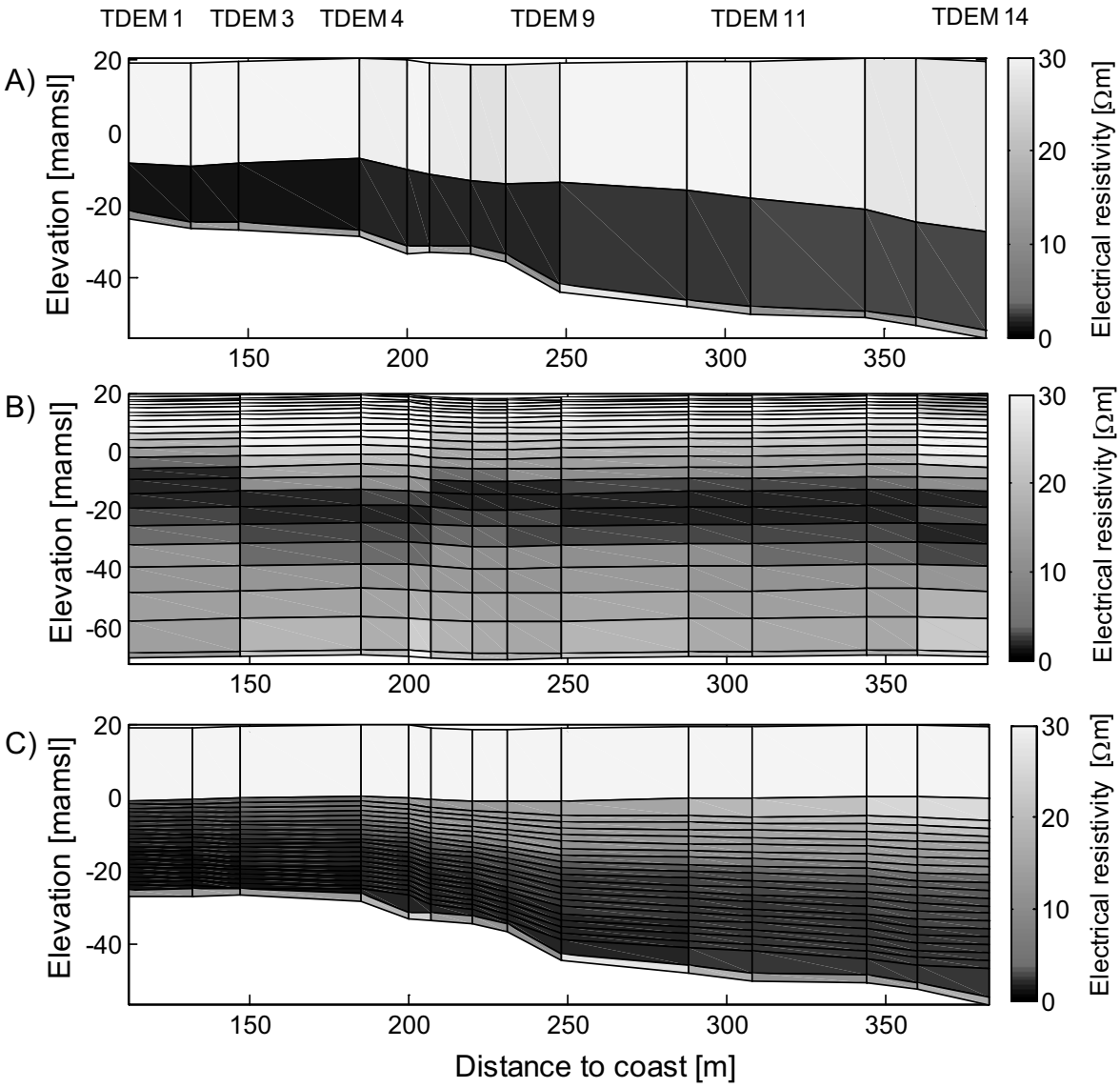

Figure 5.4 Inversion results of the 14 TDEM soundings using A) a 3-layer electrical resistivity model, B) 25-layer smooth inversion and C) CHI-S inversion.

Figure 5.4a presents the inverted 3-layer resistivity models for TDEM sounding 1-14 as a function of the distance with respect to the coast. All electrical resistivity models show a first layer with a high resistivity, a second layer with a very low electrical resistivity and a third layer with a higher resistivity compared to the second layer. The first TDEM-layer can be interpreted as a layer comprising both the dry deposits and the freshwater saturated aquifer, where the second layer with a very low electrical resistivity of less than 1 Ωm represents the salt water saturated sediments. The final third layer in Figure 5.4a is remarkable as it shows an increased electrical resistivity compared with the layer above. This layer has been interpreted as a freshwater saturated clay deposit. In

Figure 4a a dip can be seen associated with the clay layer. Figure 5.4b shows the inversion result for the 25-layer smooth model. The pattern is consistent with 5.4a, showing both the clay layer and the salt water saturated layer. The dip of the clay layer is not very obvious in Figure 5.4b, but provides more information about the distribution of fresh and salt water in the aquifer.

Figure 5.4c shows the resulting TDEM model using a CHI-S. The bottom layer is the same in both Figures 5.4a and 5.4c, representing the clay layer that is present at the site. We fixed the particular geophysical parameters for this clay layer when performing the CHI-S as the salt water intrusion model does not provide any information about this layer. The second commonality between 5.4c and the geophysical inversion results is the high electrical resistivity of the top layer. The difference, however, is the much higher amount of detail for the electrical resistivity in the aquifer. The electrical resistivity model resulting from the 25-layer smooth inversion has a similar resolution, but shows a much less consistent pattern about the distribution of salt and fresh water in the aquifer. Given the simple SEAWAT model, the data fit and the small amount of parameters which could be resolved well (Table 3, paper **II**), obviously the hydrologic model provided a well defined regularization or interpretation framework for inverting the TDEM data.

We think our CHI-S approach provides a great method to extract the huge amount of hydrogeological information that might be available within existing and future TDEM datasets with which salt water intrusion models can be constrained. This could improve the simulation of the past system state of a coastal aquifer, but also provides an opportunity to use TDEM data and salt water intrusion models together as a consistent real-time monitoring and simulation tool to support current coastal water management.

5.3 Monitoring aquifer pumping tests with time-lapse gravity and magnetic resonance sounding data

The previous two applications of applying a CHI were related to relative large scale hydrologic problems. To inform large scale simulation models aquifer pumping tests are conducted, to provide an indication of local aquifer properties as hydraulic conductivity and aquifer storage characteristics. *Blainey et al.* [2007] and *Damiata and Lee* [2004] provided a specific application of time-lapse signals retrieved with relative gravimetry (TL-RG) to estimate aquifer properties for aquifer pumping tests using a CHI-S.

Table 5.1 Properties of the different pumping test scenarios investigated in paper **III**.

Property	Scenario					
	Fully Penetrating	*High Noise*	*Partially Penetrating*	*Delayed Yield*	*Partially Penetrating & Delayed Yield & High Noise*	*Correlated Noise Gravity*
Thickness of aquifer (D), m	50					
Depth to initial water level (hi), m	25					
Hydraulic conductivity (Kh), m/s	10^{-4}					
Anisotropy Kh/Kz	1	1	10	1	10	1
Specific yield (Sy)	0.25					
Radius of borehole, m	0.1					
Well type	Fully Penetrating	Fully Penetrating	Partially Penetrating	Fully Penetrating	Partially Penetrating	Fully Penetrating
Screen interval, m below initial water level	0-50	0-50	40-50	0-50	40-50	0-50
Density of groundwater, kg/m3	1000					
Flow rate (Q), m3/s	0.06309					
Duration of pumping, d	7					
Locations observation wells, m from pumping well	5, 8.3, 13.9, 23.2, 38.7, 64.6, 107.8, 179.8, 300					
Locations RG observations, m from pumping well	5, 8.3, 13.9, 23.2, 38.7, 64.6, 107.8, 179.8, 300					
Locations MRS observations, m from pumping well	5, 179.8					
Measurement error drawdown, cm	5					
Measurement error TL-RG, µGal	2	4	2	2	4	4
Measurement error TL-MRS, nV	10	20	10	10	20	-
Delay index $1/\alpha_d$ [Boulton, 1970], d	0	0	0	2	2	0

In paper **III** we investigate this particular application of CHI-S, as these studies considered highly idealized conditions considering the configuration of the pumping test and accuracy of the geophysical methods. The aim of paper **III** is twofold: 1) major issues are investigated which likely limit the practical utility of TL-RG for pumping test monitoring and 2) we introduce TL-MRS data using a similar CHI-S framework and compare the performance of TL-MRS and TL-RG for pumping test monitoring.

The investigations were performed for a virtual aquifer pumping test, for which synthetic drawdown data was generated together with synthetic TL-MRS and TL-RG measurement data. Subsequently aquifer parameters were estimated using a CHI-S for 6 different scenarios listed in Table 5.1, which comprise respectively (1) a fully penetrating well with low-noise geophysical data, (2) a fully penetrating well with high-noise geophysical data, (3) a partially penetrating well in an anisotropic aquifer, (4) a fully penetrating well in an aquifer showing delayed drainage effects, (5) a real-world scenario of a partially penetrating well in an anisotropic aquifer showing delayed yield in combination with high-noise geophysical data and (6) TL-RG data with correlated measurement errors. Table 5.1 summarizes the assumed properties for the six pumping tests scenarios that were investigated, including the observation locations, the aquifer properties, the pumping test design variables and the standard deviation of the measurement errors that were assumed to generate synthetic observation data.

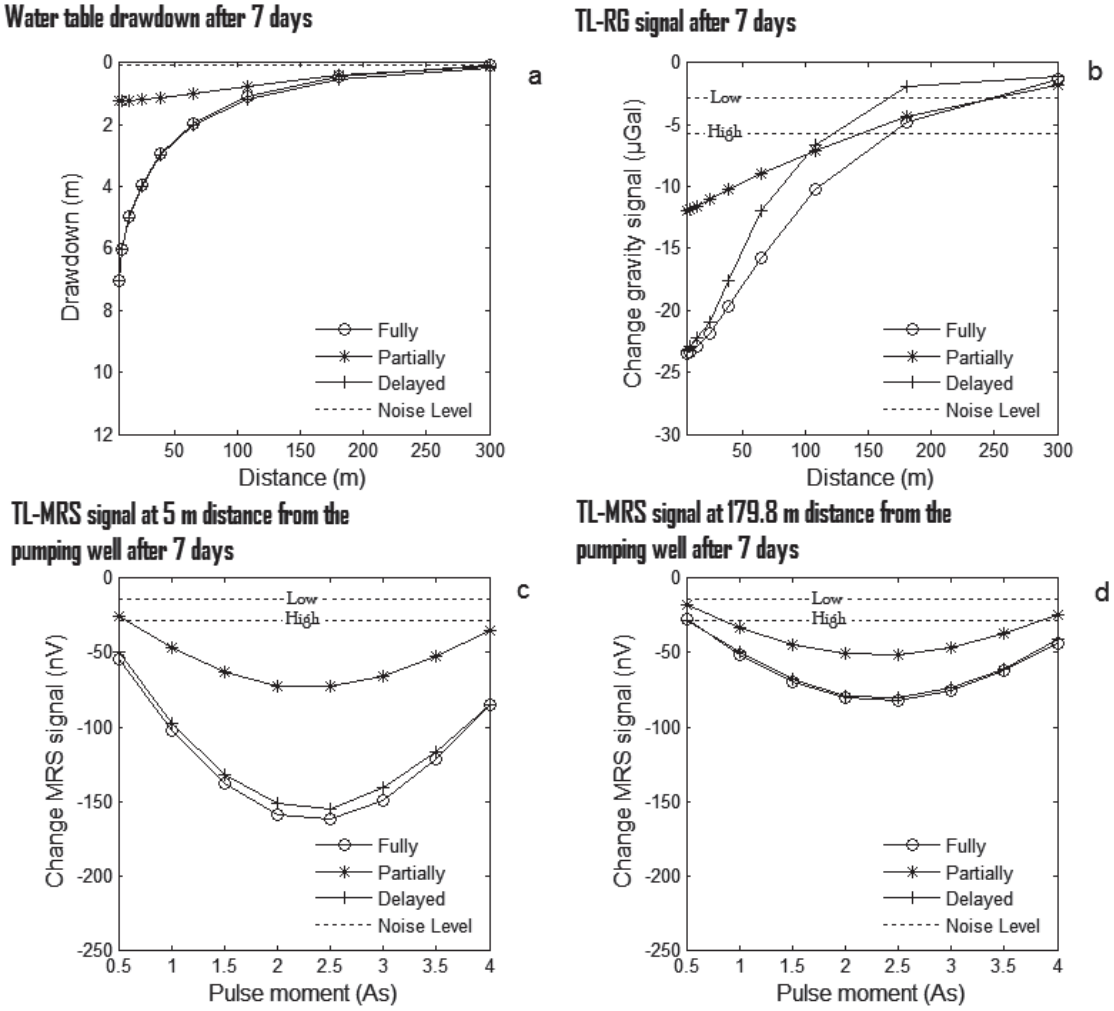

Figure 5.5 Water table drawdown (a) and simulated TL-RG data (b) after seven days of pumping for a fully and partially penetrating well and the inclusion of delayed yield. (c) and (d) show the TL-MRS signal at respectively 5.0 and 179.8 m from the extraction well. Note this figure shows the synthetic data without the added measurement errors. Indicated by the dashed lines are the standard deviations of the measurement errors ("Noise level") that were used to generate the synthetic TL-RG and TL-MRS observations.

In Figure 5.5 the synthetic drawdown, TL-RG and TL-MRS data are plotted without the added measurement errors, for scenrario "Fully Penetrating", "Partially Penetrating" and "Delayed Yield". Figure 5.5a shows the drawdown data of 9 different monitoring wells after 7 days of pumping, which marks an exponential decreasing water table drawdown when moving further away from the extraction well for scenario "Fully Penetrating" and "Delayed Yield". For scenario "Partially Penetrating" water table drawdown is much smaller closer to the pumping well compared with the other scenarios. Figure 5.5b shows the corresponding change in gravity signal together with the measurement errors we investigated for this data type. Figure 5.5c and d show the change in MRS signal

(initial amplitude data only) for 8 pulse lengths at two locations with respect to the pumping well (5m and 179.8 m). Remarkable is the large size of the measurement error for the geophysical data compared to the actual signal (signal-to-noise ratio). This signal-to-noise ratio is one of the factors that might limit the sensitivity of TL-RG and TL-MRS to estimate aquifer parameters for a pumping test.

In Table 5.2 we listed the CHI-S results for the 6 different scenarios. Based on this table, we can conclude that more conservative TL-RG and TL-MRS data error estimates (according our own field experience) strongly limits the informative value of the TL-RG data; TL-MRS data was less affected by this. For a partially penetrating well under anisotropic conditions parameter uncertainty could be reduced more effectively compared to a fully penetrating well. Delayed drainage effects did not limit the ability of the TL-MRS and TL-RG data to reduce parameter uncertainty significantly. The incorporation of representative correlated measurement error in the TL-RG data neither affected its informative value.

A local sensitivity analysis showed that TL-RG and TL-MRS observations were most sensitive to the pumping rate and the thickness, specific yield and hydraulic conductivity of the aquifer. The inclusion of TL-MRS data proved to be more effective to constrain the aquifer parameters compared with TL-RG. The inclusion of both TL-RG and TL-MRS had a limited added value compared to TL-MRS only. We conclude that this particular application of CHI-S has a limited potential for TL-RG, while TL-MRS appears to be a more promising method.

Table 5.2 Inversion results showing data misfit, parameter cross-correlation, estimated values, uncertainty ranges and uncertainty reduction percentages for the hydraulic conductivity and specific yield for different observation data sets and each scenario described in Table 5.1.

Calibration dataset	RMSE[a]	Cr-Corr[b] Sy-Kh	Kh[c] (m/s)	Parameter uncertainty (%)[d]	Uncertainty reduction [%][e]	Sy[c] (-)	Parameter uncertainty (%)[d]	Uncertainty reduction [%][e]	Scenario
Truth	-	-	$1 \cdot 10^{-4}$	-	-	0.25	-	-	Truth
Heads	0.82	-0.86	$9.99 \cdot 10^{-5} \pm 2.35 \cdot 10^{-6}$	2%	-	0.251 ± 0.022	9%	-	Fully Penetrating
Gravity	0.77	1.00	$1.07 \cdot 10^{-4} \pm 2.60 \cdot 10^{2}$	>> 100 %	-	0.259 ± 2.248	>> 100 %	-	
MRS	0.86	0.99	$1.07 \cdot 10^{-4} \pm 1.96 \cdot 10^{-4}$	>> 100 %	-	0.278 ± 0.339	>> 100 %	-	
Heads & Gravity	0.86	-0.80	$1.00 \cdot 10^{-4} \pm 1.79 \cdot 10^{-6}$	2%	24%	0.250 ± 0.016	6%	27%	
Heads & MRS	0.92	-0.82	$9.98 \cdot 10^{-5} \pm 1.58 \cdot 10^{-6}$	2%	33%	0.252 ± 0.014	6%	34%	
Heads & Gravity & MRS	0.92	-0.77	$1.00 \cdot 10^{-4} \pm 1.45 \cdot 10^{-6}$	1%	38%	0.251 ± 0.013	5%	42%	
Heads	0.82	-0.86	$9.99 \cdot 10^{-5} \pm 2.35 \cdot 10^{-6}$	2%	-	0.251 ± 0.022	9%	-	High Noise
Heads & Gravity	0.93	-0.84	$9.99 \cdot 10^{-5} \pm 2.08 \cdot 10^{-6}$	2%	11%	0.252 ± 0.019	8%	12%	
Heads & MRS	0.95	-0.85	$1.00 \cdot 10^{-4} \pm 1.73 \cdot 10^{-6}$	2%	26%	0.250 ± 0.016	6%	28%	
Heads & Gravity & MRS	0.92	-0.84	$1.00 \cdot 10^{-4} \pm 1.74 \cdot 10^{-6}$	2%	26%	0.251 ± 0.016	6%	27%	
Heads	0.83	-0.87	$9.99 \cdot 10^{-5} \pm 2.43 \cdot 10^{-6}$	2%	-	0.251 ± 0.023	9%	-	Delayed yield
Heads & Gravity	0.86	-0.83	$1.00 \cdot 10^{-4} \pm 1.89 \cdot 10^{-6}$	2%	22%	0.250 ± 0.018	7%	24%	
Heads & MRS	0.93	-0.83	$9.98 \cdot 10^{-5} \pm 1.60 \cdot 10^{-6}$	2%	34%	0.252 ± 0.015	6%	35%	
Heads & Gravity & MRS	0.92	-0.79	$1.00 \cdot 10^{-4} \pm 1.49 \cdot 10^{-6}$	1%	39%	0.251 ± 0.014	5%	41%	
Heads	0.76	-0.97	$1.01 \cdot 10^{-4} \pm 5.91 \cdot 10^{-5}$	58%	-	0.250 ± 0.057	23%	-	Partially Penetrating
Heads & Gravity	0.83	-0.96	$1.04 \cdot 10^{-4} \pm 4.97 \cdot 10^{-5}$	33%	42%	0.247 ± 0.036	14%	38%	
Heads & MRS	0.90	-0.93	$9.74 \cdot 10^{-5} \pm 3.02 \cdot 10^{-5}$	31%	49%	0.254 ± 0.033	13%	43%	
Heads & Gravity & MRS	0.83	-0.92	$9.94 \cdot 10^{-5} \pm 2.91 \cdot 10^{-5}$	29%	51%	0.251 ± 0.032	13%	44%	
Heads	0.77	-0.98	$1.02 \cdot 10^{-4} \pm 4.46 \cdot 10^{-5}$	44%	-	0.250 ± 0.061	25%	-	Partially Penetrating & High Noise & Delayed yield
Heads & Gravity	0.92	-0.97	$1.00 \cdot 10^{-4} \pm 3.61 \cdot 10^{-5}$	36%	19%	0.250 ± 0.052	21%	15%	
Heads & MRS	0.92	-0.97	$1.00 \cdot 10^{-4} \pm 2.81 \cdot 10^{-5}$	27%	37%	0.249 ± 0.041	16%	34%	
Heads & Gravity & MRS	0.96	-0.97	$1.00 \cdot 10^{-4} \pm 2.76 \cdot 10^{-5}$	27%	38%	0.251 ± 0.040	16%	34%	
Heads & Gravity	0.84	-0.84	$1.00 \cdot 10^{-4} \pm 1.97 \cdot 10^{-6}$	2%	16%	0.250 ± 0.018	7%	17%	Correlated Noise Gravity

[a] Root Mean Square Error, [b] Cross-correlation, [c] Mean ± 2 standard deviations, [d] relative to the estimated parameter value, [e] percentual decrease of parameter ucertainty

6 Conclusions

The combination of hydrologic models and geophysical datasets is powerful as a united characterization tool. Where geophysical techniques are able to provide high resolution datasets that can be correlated with hydrogeological properties, hydrologic models can provide a method to understand and identify the relevant physical processes underlying the geophysical parameter distributions.

This study focused on development of new and the application of existing methods to inform groundwater models with near-surface geophysical data in a consistent way. In paper **I**, **II** and **III** the following key-findings and developments have been made:

- A new Coupled Hydrogeophysical Inversion (CHI) approach has been developed, which is called CHI-P. CHI-P uses a parameter coupling approach, which can be used to estimate hydrologic input parameters with geophysical data by coupling the estimation process of geophysical and hydrologic parameters directly. To our knowledge, existing CHI methods are only focused on CHI-S, in which hydrologic model simulations are transformed to a geophysical model, not on parameter coupling. We believe our CHI-P method increases the flexibility of performing a CHI greatly, especially for the estimation of hydraulic conductivity in groundwater models.

- A minor change was made with respect to the existing CHI-S approaches [*Pollock and Cirpka*, 2010; *Kowalsky et al.*, 2005; *Hinnel et al.*, 2010; *Lambot et al.*, 2009], in order to allow for the separate estimation of geophysical parameters that cannot be computed from simulated hydrological state variables.

- Compared with a Sequential Hydrogeophysical Inversion (SHI), the CHI-P resulted in improved parameter estimates and a reduction in parameter uncertainty for a synthetic groundwater and a Time Domain Electromagnetic (TDEM) model. For a real-world groundwater model and a geo-electric profile, the CHI-P resulted in significant parameter changes in both the geophysical as the groundwater model, which were consistent with the coupling constraints that represented the hydrogeological interpretation of the geophysical model. Parameter uncertainty was not

reduced significantly. The computational burden associated with the CHI-P increased with a factor of ca. 2-3 compared with a SHI.

- We successfully applied a CHI-S to estimate an acceptable range of parameter values for the main hydraulic properties of an aquifer, using the data of 14 TDEM soundings in combination with a salt water intrusion model. Given the simple parameterization of the saltwater intrusion model, the data fit and narrow parameter confidence intervals, we think the saltwater intrusion model provided an excellent spatial correlation structure for the geophysical model, yielding a superior resolution which could never be obtained with a separate geophysical inversion and standard regularization constraints.

- We successfully applied a CHI-S to evaluate the potential for time-lapse relative gravimetry (TL-RG) and magnetic resonance sounding (TL-MRS) to estimate aquifer properties during a pumping test. We investigated four practical issues that might limit the sensitivity of these techniques which are (1) a partially penetrating well in an anisotropic aquifer, (2) typical environmental noise properties for TL-RG, (3) delayed yield and (4) correlated measurement error. The findings of this thesis suggest a limited applicability of a CHI-S with TL-RG data for practical pumping tests, but inversion results proved to be more optimistic than we expected beforehand, especially for the partially penetrating well. The inclusion of TL-MRS data appeared more promising compared to the TL-RG data, as parameter uncertainty could be reduced with ca. 30 % for most of the investigated scenarios in this paper.

7 Perspectives

A CHI offers a great opportunity to integrate geophysical information into groundwater models, but like all methods it should fit a clear purpose. Factors determining the suitability of a CHI will depend on whether the targeted prediction is sensitive with respect to the geophysical data, whether the geophysical model will be significantly impacted by the CHI and whether there is enough data to support the assumption behind the coupling relationships between the geophysical and hydrologic model.

Based on this research, we like to address some future challenges and opportunities:

- In Denmark, Australia and the United States large airborne electromagnetic data sets have been collected to map salt water intrusion and delineate groundwater protection zones. At the same time, large regional models are available to simulate salt water intrusion and groundwater flow. According to the results in this thesis, the computational time and the CHI-approach are no practical limitations to perform a CHI on this scale. However, the main question is whether the improvement in groundwater and geophysical models will outweigh the additional effort of performing a CHI.

- In general, large-scale hydrologic models are supported by less data compared to geophysical models. This means the hydrologic model can incorporate large conceptual errors which should not be propagated to the geophysical model by using a CHI. Additional research could focus on the transfer of such conceptual errors and a set of general guidelines about when to use a SHI instead.

- A real aquifer pumping test should be performed in combination with time-lapse magnetic resonance sounding (TL-MRS) and relative gravimetry. For selecting a potential site, aquifer properties and environmental noise properties should be assessed. At three sites in Denmark the environmental noise properties for MRS seem acceptable, which are Skive [paper **I**], Dalby and Bredal [*Chalikakis et al.*, 2008]. To assess the suitability of these field sites, synthetic simulations as in paper **I** need to be performed, in which a rough estimate of the local aquifer characteristics and the intended pumping test design are taken in account.

8 References

Archie, G. E., The electrical resistivity log as an aid in determining some reservoir characteristics, Transactions of the American Institute of Mining and Metallurgical Engineers, 146, 54-61, 1942.

Auken, E. and A. V. Christiansen, Layered and laterally constrained 2D inversion of resistivity data, Geophysics, 69(3), 752-761, 2004.

Auken, E., A. V. Christiansen, L. H. Jacobsen and K. I. Sorensen, A resolution study of buried valleys using laterally constrained inversion of TEM data, Journal of Applied Geophysics, 65(1), 10-20, 2008.

Baxter, G. P. and C. C. Wallace, Changes in volume upon solution in water of the halogen salts of the alkali metals II, Journal of the American Chemical Society, 38, 70-105, 1916.

Bauer-Gottwein, P., B. N. Gondwe, L. Christiansen, D. Herckenrath, L. Kgotlhang and S. Zimmermann, Hydrogeophysical exploration of three-dimensional salinity anomalies with the the time-domain electromagnetic method (TDEM), Journal of Hydrology, 2009.

Binley, A., P. Winship, R. Middleton, M. Pokar and J. West, High-resolution characterization of vadose zone dynamics using cross-borehole radar, Water Resources Research, 37(11), 2639-2652, 2001.

Bjerg, P.L., Tuxen, N., Reitzel, L.A., Albrechtsen, H.-J., Kjeldsen, P., Natural attenuation processes in landfill leachate plumes at three Danish sites. Ground Water, 2011.

Blainey, J. B., T. P. A. Ferré and J. T. Cordova, Assessing the likely value of gravity and drawdown measurements to constrain estimates of hydraulic conductivity and specific yield during unconfined aquifer testing, Water Resour. Res., 43(12), 2007.

Carmichael, R.S., Henry Jr., G., Gravity exploration for groundwater and bedrock topography, Geophysics, 42, 850–859, 1977.

Cassiani, G., G. Bohm, A. Vesnaver and R. Nicolich, A geostatistical framework for incorporating seismic tomography auxiliary data into hydraulic conductivity, Journal of Hydrology, 206(1-2), 58-74, 1998.

Chalikakis, K., M. R. Nielsen and A. Legchenko, MRS applicability for a study of glacial sedimentary aquifers in Central Jutland, Denmark, Journal of Applied Geophysics, 66(3-4), 176-187, 2008.

Cassiani, G., V. Bruno, A. Villa, N. Fusi and A. M. Binley, A saline trace test monitored via time-lapse surface electrical resistivity tomography, Journal of Applied Geophysics, 59(3), 244-259, 2006.

Chambers, J. E., M. H. Loke, R. D. Ogilvy and P. I. Meldrum, Noninvasive monitoring of DNAPL migration through a saturated porous medium using electrical impedance tomography, Journal of Contaminant Hydrology, 68(1-2), 1-22, 2004.

Chambers, J. E., O. Kuras, P. I. Meldrum, R. D. Ogilvy and J. Hollands, Electrical resistivity tomography applied to geologic, hydrogeologic, and engineering investigations at a former waste-disposal site, Geophysics, 71(6), B231-B239, 2006.

Chen, J., S. Hubbard, J. Peterson, K. Williams, M. Fienen, P. Jardine and D. Watson, Development of a joint hydrogeophysical inversion approach and application to a contaminated fractured aquifer, Water Resources Research, 42(6), 2006.

Chen, J. S., S. Hubbard, Y. Rubin, C. Murray, E. Roden and E. Majer, Geochemical characterization using geophysical data and Markov Chain Monte Carlo methods: A case study at the South Oyster bacterial transport site in Virginia, Water Resources Research, 40(12), 2004.

Christiansen, L., P. Binning, D. Rosbjerg, O. Andersen and P. Bauer-Gottwein, Using time-lapse gravity for groundwater model calibration: An application to alluvial aquifer storage, Water Resources Research, 47, 2011.

Dahlin, T., Leroux, V. and J. Nissen, Measuring techniques in induced polarisation imaging, Journal of Applied Geophysics, 50, 279– 298, 2002

Damiata, B. N. and T. C. Lee, Simulated gravitational response to hydraulic testing of unconfined aquifers, Journal of Hydrology, 318(1-4), 348-359, 2006.

Day-Lewis, F. D., J. W. Lane, J. M. Harris and S. M. Gorelick, Time-lapse imaging of saline-tracer transport in fractured rock using difference-attenuation radar tomography, Water Resources Research, 39(10), 2003.

Day-Lewis, F. D., K. Singha and A. M. Binley, Applying petrophysical models to radar travel time and electrical resistivity tomograms: Resolution-dependent limitations, Journal of Geophysical Research-Solid Earth, 110(B8), 2005.

Day-Lewis, F. D., K. Singha, Geoelectrical inference of mass transfer parameters using temporal moments, Water Resources Research, 44, 2008.

Duffield, G. M. AQTESOLV for Windows Version 4.0 Professional. 2011. HydroSOLVE, Inc.

Duque, C., M. L. Calvache, A. Pedrera, W. Martin-Rosales and M. Lopez-Chicano, Combined time domain electromagnetic soundings and gravimetry to determine marine intrusion in a detrital coastal aquifer (Southern Spain), Journal of Hydrology, 349(3-4), 536-547, 2008.

Efferso, F., Auken, E., and Sorensen, K.I., Inversion of band-limited TEM responses. Geophysical Prospecting, 47 (4): 551-564, 1999.

Fetter, C. W., Applied Hydrogeology. Prentice-Hall, New Jersey, USA, 3rd edition, ISBN: 0-02-336490-4, 1994.

French, H. and A. Binley, Snowmelt infiltration: monitoring temporal and spatial variability using time-lapse electrical resistivity, Journal of Hydrology, 297(1-4), 174-186, 2004.

Gazoty, A., Behroozmand, A., Fiandaca, G. and E. Auken, Landfill characterization with geophysical methods: the Risby case study, Applied Geophysics, submitted, 2011.

Giambastiani, B. M., M. Antonellini, G. H. Essink and R. J. Stuurman, Saltwater intrusion in the unconfined coastal aquifer of Ravenna (Italy): A numerical model, Journal of Hydrology, 340(1-2), 91-104, 2007.

Guérin, R., Descloitres, M., Talbi, A., Coudrain, A., Gallaire, R., Geophysical surveys for identifying saline groundwater in the semi-arid region of the central Altiplano, Bolivia. Hydrologic Processes 15, 3287–3301, 2001.

Harbaugh, A. W., E. R. Banta, M. C. Hill and M. G. McDonald, MODFLOW-2000: The U.S. Geological Survey modular ground-water model: User guide to modularization concepts and the groundwater flow process, 00-92, 2000.

Henriksen, H. J., L. Troldborg, P. Nyegaard, T. O. Sonnenborg, J. C. Refsgaard and B. Madsen, Methodology for construction, calibration and validation of a national hydrological model for Denmark, Journal of Hydrology, 280(1-4), 52-71, 2003.

Hinnell, A., T. Ferre, J. Vrugt, J. Huisman, S. Moysey, J. Rings and M. Kowalsky, Improved extraction of hydrologic information from geophysical data through coupled hydrogeophysical inversion, Water Resources Research, 46, 2010.

Hubbard, S. S., Y. Rubin and E. Majer, Spatial correlation structure estimation using geophysical and hydrogeological data, Water Resources Research, 35(6), 1809-1825, 1999.

Huisman, J., S. Hubbard, J. Redman and A. Annan, Measuring Soil Water Content with Ground Penetrating Radar: A Review, Vadose Zone Journal, 2(4), 476-491, 2003.

Hyndman, D. W. and S. M. Gorelick, Estimating lithologic and transport properties in three dimensions using seismic and tracer data: The Kesterson aquifer, Water Resources Research, 32(9), 2659-2670, 1996.

Kearey, P., M. Brooks and I. Hill, An introduction to geophysical exploration, Blackwell Publishing, 2002.

Kemna, A., J. Vanderborght, B. Kulessa and H. Vereecken, Imaging and characterisation of subsurface solute transport using electrical resistivity tomography (ERT) and equivalent transport models, Journal of Hydrology, 267(3-4), 125-146, 2002.

Kirsch, R., Petrophysical properties of permeable and low-permeable rocks, Groundwater Geophysics, Springer Berlin Heidelberg, ISBN: 978-3-540-29387-3, 2006.

Kjeldsen, P., M. A. Barlaz, A. P. Rooker, A. Baun, A. Ledin and T. H. Christensen, Present and long-term composition of MSW landfill leachate: A review, Critical Reviews in Environmental Science and Technology, 32(4), 297-336, 2002.

Knight, R., Ground penetrating radar for environmental applications, Annual Review of Earth and Planetary Sciences, 29, 229-255, 2001.

Kowalsky, M. B., S. Finsterle, J. Peterson, S. Hubbard, Y. Rubin, E. Majer, A. Ward and G. Gee, Estimation of field-scale soil hydraulic and dielectric parameters through joint inversion of GPR and hydrological data, Water Resources Research, 41(11), 2005.

Lambot, S., E. Slob, M. Vanclooster and H. Vereecken, Closed loop GPR data inversion for soil hydraulic and electric property determination, Geophysical Research Letters, 33(21), 2006.

Lambot, S., E. Slob, J. Rhebergen, O. Lopera, K. Z. Jadoon and H. Vereecken, Remote Estimation of the Hydraulic Properties of a Sand Using Full-Waveform Integrated Hydrogeophysical Inversion of Time-Lapse, Off-Ground GPR Data, Vadose Zone Journal, 8(3), 743-754, 2009.

Langevin, C. D., Simulation of submarine ground water discharge to a marine estuary: Biscayne Bay, Florida, Ground Water, 41(6), 758-771, 2003a.

Langevin, C. D., D. Fitterman and M. Deszcz-Pan, Calibration of a Variable-Density Groundwater Flow Model Using Detailed Airborne Geophysical Data, Second International Conference on Saltwater Intrusion and Coastal Aquifers— Monitoring, Modeling and Management, Merida, Mexico, 2003b.

Langevin, C. D. and W. X. Guo, MODFLOW/MT3DMS-based simulation of variable-density ground water flow and transport, Ground Water, 44(3), 339-351, 2006.

Legchenko, A., J. M. Baltassat, A. Beauce and J. Bernard, Nuclear magnetic resonance as a geophysical tool for hydrogeologists, Journal of Applied Geophysics, 50(1-2), 21-46, 2002.

Legchenko, A. and P. Valla, A review of the basic principles for proton magnetic resonance sounding measurements, Journal of Applied Geophysics, 50(1-2), 3-19, 2002.

Leroy, P. and A. Revil, A mechanistic model for the spectral induced polarization of clay materials, Journal of Geophysical Research-Solid Earth, 114, 2009.

Lesmes, D. P. and S. P. Friedman, Relationships between the Electrical and Hydrogeological Properties of Rocks and Soils, Water Science and Technology Library, Volume 50, Part 2, 87-128, 2005.

Linde, N., S. Finsterle and S. Hubbard, Inversion of tracer test data using tomographic constraints, Water Resources Research, 42(4), 2006.

Looms, M. C., K. H. Jensen, A. Binley and L. Nielsen, Monitoring unsaturated flow and transport using cross-borehole geophysical methods, Vadose Zone Journal, 7(1), 227-237, 2008.

Lorah, M. M., I. M. Cozzarelli and J. Boehlke, Biogeochemistry at a wetland sediment-alluvial aquifer interface in a landfill leachate plume, Journal of Contaminant Hydrology, 105(3-4), 99-117, 2009.

Macaulay, S. and I. Mullen, Predicting salinity impacts of land-use change: Groundwater modelling with airborne electromagnetics and field data, SE Queensland, Australia, International Journal of Applied Earth Observation and Geoinformation, 9(2), 124-129, 2007.

Meju, M. A., Geoelectrical investigation of old/abandoned, covered landfill sites in urban areas: model development with a genetic diagnosis approach, Journal of Applied Geophysics, 44(2-3), 115-150, 2000.

Michot, D., A. Dorigny and Y. Benderitter, Determination of water flow direction and corn roots-induced drying in an irrigated Beauce CALCISOL, using electrical resistivity measurements, Comptes Rendus de l Academie des Sciences Serie Ii Fascicule A-Sciences de la Terre et des Planetes, 332(1), 29-36, 2001.

Miljøstyrelsen. Redegørelse om jordforurening 2009. 2011.

Milošević, N., Thomsen, N.I., Juhler, R. K., Albrechtsen, H. J. and P.L. Bjerg, Identification of discharge zones and quantification of contaminant mass discharges into a local stream from a landfill in a heterogeneous geologic setting, Journal of Hydrology, 2011.

Miller, R. D., D. W. Steeples and M. Brannan, Mapping A Bedrock Surface Under Dry Alluvium with Shallow Seismic Reflections, Geophysics, 54(12), 1528-1534, 1989.

Mohnke, O. and U. Yaramanci, Pore size distributions and hydraulic conductivities of rocks derived from Magnetic Resonance Sounding relaxation data using multi-exponential decay time inversion, Journal of Applied Geophysics, 66(3-4), 73-81, 2008.

Montgomery, E. L., Determination of Specific Yield Using Gravity Measurements, Transactions-American Geophysical Union, 52(4), 205-&, 1971.

Naudet, V., A. Revil, E. Rizzo, J. Y. Bottero and P. Begassat, Groundwater redox conditions and conductivity in a contaminant plume from geoelectrical investigations, Hydrology and Earth System Sciences, 8(1), 8-22, 2004.

Nenna, V., D. Herckenrath, N. Odlum and R. Knight, Sentinel geophysics for coastal aquifers in northern California: Application and evaluation of electromagnetic methods, Journal of Applied Geophysics, Submitted, 2011.

Niwas, S. and O. A. L. de Lima, Aquifer parameter estimation from surface resistivity data, Ground Water, 41(1), 94-99, 2003.

Paine, J. G., Determining salinization extent, identifying salinity sources, and estimating chloride mass using surface, borehole, and airborne electromagnetic induction methods, Water Resources Research, 39(3), 2003.

Pelton, W. H., Ward, S. H., Hallof, P. G., Sill, W. R. and P. H. Nelson, Mineral discrimination and removal of inductive coupling with multifrequency IP, Geophysics, 43, 588–609, 1978.

Pollock, D. and O. A. Cirpka, Fully coupled hydrogeophysical inversion of synthetic salt tracer experiments, Water Resources Research, 46, 2010.

Purvance, D. T. and R. Andricevic, On the electrical-hydraulic conductivity correlation in aquifers, Water Resources Research, 36(10), 2905-2913, 2000.

Radulescu, M., C. Valerian and J. Yang, Time-lapse electrical resistivity anomalies due to contaminant transport around landfills, Annals of Geophysics, 50(3), 453-468, 2007.

Revil, A. and N. Florsch, Determination of permeability from spectral induced polarization in granular media, Geophysical Journal International, 181(3), 1480-1498, 2010.

Rubin, Y. and S. S. Hubbard, Water Science and Technology Library - Hydrogeophysics, Springer, Netherlands, 2011.

Singha, K. and S. M. Gorelick, Saline tracer visualized with three-dimensional electrical resistivity tomography: Field-scale spatial moment analysis, Water Resources Research, 41(5), 2005.

Singha, K. and S. M. Gorelick, Effects of spatially variable resolution on field-scale estimates of tracer concentration from electrical inversions using Archie's law, Geophysics, 71 (3), G83-G91, 2006.

Slater, L., Near surface electrical characterization of hydraulic conductivity: From petrophysical properties to aquifer geometries - A review, Surveys in Geophysics, 28(2-3), 169-197, 2007.

Sogade, J. A., F. Scira-Scappuzzo, Y. Vichabian, W. Shi, W. Rodi, D. P. Lesmes and F. D. Morgan, Induced-polarization detection and mapping of contaminant plumes, Geophysics, 71(3), B75-B84, 2006.

Supper, R., K. Motschka, A. Ahl, P. Bauer-Gottwein, B. Gondwe, G. M. Alonso, A. Roemer, D. Ottowitz and W. Kinzelbach, Spatial mapping of submerged cave systems by means of airborne electromagnetics: an emerging technology to support protection of endangered karst aquifers, Near Surface Geophysics, 7(5-6), 613-627, 2009.

Tan, K., H. Apps, L. Halas, D. Gibson and K. Lawrie, Utilizing Airborne Electromagnetic Data To Model The Subsurface Salt Load In A Catchment, Bland Basin, NSW, Modsim 2005: International Congress on Modelling and Simulation: Advances and Applications for Management and Decision Making: Advances and Applications for Management and Decision Making, 1478-1484, 2005.

Telford, W. M., L. P. Geldart, and R. E. Sheriff, Applied Geophysics, 770 pp., Cambridge Univ. Press, New York, 1990.

Thomsen, R., V. H. Sondergaard and K. I. Sorensen, Hydrogeological mapping as a basis for establishing site-specific groundwater protection zones in Denmark, Hydrogeology Journal, 12 (5), 550-562, 2004.

Topp, G. C., J. L. Davis and A. P. Annan, Electromagnetic Determination of Soil-Water Content - Measurements in Coaxial Transmission-Lines, Water Resources Research, 16(3), 574-582, 1980.

Vanderborght, J., A. Kemna, H. Hardelauf and H. Vereecken, Potential of electrical resistivity tomography to infer aquifer transport characteristics from tracer studies: A synthetic case study, Water Resources Research, 41(6), 2005.

van Gelderen, M., Haagmans, R., Bilker, M., Gravity changes and natural gas extraction in Groningen, Geophysical Prospecting, 47, 979–993, 1999.

Vereecken, H., A. Binley, G. Cassiani, A. Revil and K. Titov, Applied hydrogeophysics, Applied Hydrogeophysics, 71, 1-8, 2006.

Vouillamoz, J., G. Favreau, S. Massuel, M. Boucher, Y. Nazoumou and A. Legchenko, Contribution of magnetic resonance sounding to aquifer characterization and recharge estimate in semiarid Niger, Journal of Applied Geophysics, 64(3-4), 99-108, 2008.

Vozoff, K. and D. L. B. Jupp, Joint Inversion of Geophysical Data, Geophysical Journal of the Royal Astronomical Society, 42(3), 977-991, 1975.

Vaudelet, P., A. Revil, M. Schmutz, M. Franceschi and P. Begassat, Induced polarization signatures of cations exhibiting differential sorption behaviors in saturated sands, Water Resources Research, 47, 2011.

Yeh, T. C. J., S. Liu, R. J. Glass, K. Baker, J. R. Brainard, D. Alumbaugh and D. LaBrecque, A geostatistically based inverse model for electrical resistivity surveys and its applications to vadose zone hydrology, Water Resources Research, 38(12), 2002.

Zawila, J.S., B.N. Damiata, S.C. Biehler, T.C. Lee, Gravity mapping of subsurface structures in batholithic terrain, Symposium on the Application of Geophysics to Engineering and Environmental Problems, 801–810, Reno, 1997

Zhang, Q., R. E. Volker and D. A. Lockington, Numerical investigation of seawater intrusion at Gooburrum, Bundaberg, Queensland, Australia, Hydrogeology Journal, 12(6), 674-687, 2004.

9 Papers

I. Herckenrath, D., Legaz-Gazoty, A., Fiandaca, G., Auken, E., Christensen, M., Balicki, M. and P. Bauer-Gottwein, Sequential and Coupled Hydrogeophysical Inversion of a Groundwater Model using Geoelectric and Transient Electromagnetic Data, *Journal of Hydrology*, submitted.

II. Herckenrath, D., Odlum, N., Nenna, V., Auken, E., and P. Bauer-Gottwein, Calibrating salt water intrusion models with Time-Domain Electromagnetic Data, *Groundwater*, submitted. Herckenrath, D., Behroozmand, A., Christiansen, L., Auken, E., and P. Bauer-Gottwein, *Groundwater*, submitted.

III. Coupled hydrogeophysical inversion using time-lapse magnetic resonance sounding and time-lapse gravity data for hydraulic aquifer testing: potential and limitations, *Water Resources Research*, in review.

I

Sequential and Coupled Hydrogeophysical Inversion of a Groundwater Model using Geoelectric and Transient Electromagnetic Data

Herckenrath, D., Legaz-Gazoty, A., Fiandaca, G., Auken, E., Christensen, M., Balicki, M. and P. Bauer-Gottwein

Journal of Hydrology, submitted

Sequential and Coupled Hydrogeophysical Inversion of a Groundwater Model using Geoelectric and Transient Electromagnetic Data

Daan Herckenrath[1,*], Aurelie Gazoty[2], Gianluca Fiandaca[2,3], Esben Auken[2], Mette Christensen[1], Monika Balicki[1] and Peter Bauer-Gottwein[1]

1 Department of Environmental Engineering, Technical University of Denmark, Miljøvej, Building 113,DK-2800, Kgs. Lyngby, Denmark

2 Department of Earth Sciences, Aarhus University, Høegh-Guldbergs Gade 2, 8000 Aarhus C, Denmark

3 Department of Mathematics and Informatics, University of Palermo, Italy

** Corresponding author: daah@env.dtu.dk*

Abstract

This paper presents a new coupled hydrogeophysical inversion approach (CHI) to inform a groundwater model with Time Domain Electromagnetic (TDEM) and Electrical Resistivity Tomography (ERT) data and compares the results with a sequential inversion approach (SHI). The SHI uses an inverted geophysical image to constrain the calibration process of the groundwater model using geometric and petrophysical relationships. In the CHI we consider two groups of parameters to be estimated: parameters determining the groundwater flow only and parameters determining the geophysical response only. Within the parameter groups, parameters are coupled using standard regularization constraints. Across the parameter groups, parameters are coupled using coupling constraints. The strength of this approach is the flexibility of the coupling constraints with which the hydrogeological interpretation of the geophysical models can be coupled to the structure and parameters of the groundwater model. Coupling constraints can be based on petrophysical relationships (e.g. between electrical resistivity and hydraulic conductivity) or geometric relationships (e.g. correspondence of layer interfaces). The weight of individual constraints can be adjusted depending on the quality of the petrophysical or geometric relationships. The utility of the developed coupled hydrogeophysical inversion approach is tested for a synthetic groundwater model with TDEM measurements and a real-world groundwater model with ERT data. When applying the CHI for both the synthetic and real-world example, parameter estimates in the geophysical and groundwater models were more consistent and the parameter uncertainty was reduced, particularly for those parameters that were subjected to the coupling constraints. Compared with the SHI, the computational burden increased with a factor 2-3.

1. Introduction

Over the last decade, interest in geophysical methods for hydrogeological site characterization has been increasing (e.g. *Hubbard and Rubin*, 2000; *Vereecken et al.*, 2004). This growing interest is due to the ability of many geophysical methods to provide spatially distributed models of subsurface properties, which are difficult to obtain from sparse borehole information. Geophysical imaging of the subsurface is increasingly being used to conceptualize and develop geophysical and hydrologic models.

Hinnell et al. [2010] provide an extended list of references to case study applications using different types of approaches in which geophysical models and hydrologic models are integrated. A number of joint inversion methods have been developed to use multiple geophysical methods to improve their structural models [e.g., *Vozoff and Jupp*, 1975; *Gallardo and Meju*, 2003, 2004; *Linde et al.*, 2006a]. For example, geostatistical methods have been employed to estimate hydrologic properties based on statistical correlations in geophysical images [*Cassiani et al.*, 1998; *Hubbard et al.*, 1999; *Yeh et al.*, 2002; *Chen et al.*, 2004] and hydrologic structures and parameter distributions have been estimated simultaneously using geophysical and hydrologic data [*Hyndman and Gorelick*, 1996; *Dam and Christensen*, 2003; *Chen et al.*, 2006, *Linde et al.*, 2006]. In other studies geo-electrical [*Kemna et al.*, 2002; *Vanderborght et al.*, 2005; *Cassiani et al.*, 2006], electromagnetic [*Binley et al.*, 2001; *Day-Lewis et al.*, 2003; *Lambot et al.*, 2004; *Looms et al.*, 2008b] and ground penetrating radar (GPR) [*Knight*, 2001; *Huisman et al.*, 2003] are used to monitor changes in water content or solute concentrations with time.

Many previous applications in which hydrologic models are informed with geophysical data use a sequential inversion approach (SHI), where geophysical data is inverted to estimate the distribution of a geophysical property (e.g. electrical resistivity, chargeability), after which a petrophysical relation [e.g., *Archie*, 1942; *Topp et al.*, 1980] is used to convert the geophysical property to hydrologic state distributions (e.g. solute concentrations, water content), which are then used to calibrate a hydrologic model. In a SHI measurement errors and parameter uncertainties associated with the independent inversion of the geophysical data are propagated to the hydrologic analysis through a petrophysical relation. Not only geophysical parameter uncertainty is propagated with these petrophysical relationships, but also the uncertainty pertaining to parameters of the petrophysical relationship (e.g. shape factors in Archie's law).

Another issue is the large number of parameters that is estimated in geophysical models, which commonly requires the use of extensive regularization (e.g. smoothness constraints) to stabilize the geophysical inversion [e.g., *Menke*, 1984]. These regularization constraints do not necessarily reflect the hydrologic conditions and can limit the value of hydrologic state estimates derived from geophysical observations [*Day-Lewis et al.*, 2005; *Chen et al.*, 2006; *Slater*, 2007].

Hinnell et al. [2010], *Ferré et al.* [2009], *Kowalsky et al.* [2005], *Lambot et al.* [2006, 2009], *Christiansen et al.* [2011] and *Herckenrath et al.* [2011] describe a coupled hydrogeophysical inversion approach (CHI), in which a hydrologic model is part of the geophysical inversion process and a single objective function is minimized which comprises both a geophysical and hydrologic component. In these studies the coupling of both models is predominantly done by translating simulated hydrological state variables (e.g. soil moisture content) to a geophysical parameter distribution (e.g. electrical conductivity). We refer to this methodology as "state coupling". However, not only hydrologic states can be correlated with geophysical parameter distributions, but also hydrologic parameters (e.g. electrical resistivity and hydraulic conductivity [*Purvance and Andricevic*, 2000; *Niwas and de Lima*, 2003]). For this purpose, we investigate another way to conduct a CHI to which we refer as "parameter coupling" in which parameters of hydrologic and geophysical models are coupled. To our knowledge this concept is fairly new as no appropriate references were found to clearly illustrate this type of CHI.

The main purpose for doing a CHI is to provide a context of interpretation for the geophysical measurements through the hydrologic model and use this interpretation in the geophysical inversion [*Hinnell et al.,* 2010]. One severe drawback of a CHI is the fact that all conceptual errors pertaining to the hydrologic model, as well as errors associated with the hydrologic measurements, are transferred to the geophysical model. The influence of these conceptual model errors is application dependent, and their contribution is ultimately unknown. *Linde et al.* [2006b] discuss the factors that influence a successful integration of hydrogeological and geophysical data and identify the critical choices and considerations. For example the applicability of a certain geophysical technique in combination with a hydrologic model heavily depends on the site, the research objective and the available a priori knowledge.

In this research we consider a groundwater model together with Time Domain Electromagnetic (TDEM) and Electrical Resistivity Tomography (ERT) data. Our objective is to constrain the hydrogeological parameters of the groundwater model with these geophysical datasets using a CHI. For this purpose we will use a parameter coupling approach. Several complications arise when performing a SHI and CHI for a groundwater model together with ERT and TDEM data. The first complication arises due to the fact that the conceptual framework of many groundwater models is prone to large uncertainties [*Refsgaard et al.*, 2006]. These differences are the result of limited data availability to characterize the hydrogeological properties of an area and the use of many simplifying assumptions associated with the geological setup and the boundary conditions used in the groundwater model. The second complication pertains to the difference in scales between the groundwater and geophysical models, while the third problem is the accuracy and error associated with the assumed petrophysical relationship between geophysical and groundwater model parameters. Error and accuracy in the petrophysical relationship should be clearly distinguished, as its accuracy pertains to processes that are not taken in account in the petrophysical relationship (e.g. surface conductivity in Archie's law [*Winsauer and McCardell*, 1953]) and its error is associated with defining the parameters of the petrophysical relationship (e.g. pore space tortuosity factor in Archie's law). The fourth issue involves processes that significantly affect the geophysical model which are not included in the hydrogeological model. An example would be a geological layer that was not defined in the groundwater model which is of significant importance for the geophysical model. Based on these four problems, we cannot expect to generate a decent geophysical signal based on the parameters and states of a groundwater model only in order to fit the geophysical data satisfactorily. These four issues suggest a modification of the coupled inversion framework described in *Hinnel et al*. [2010] by not letting the entire interpretation of the geophysical model be done by the hydrologic model, but only couple those parts of the geophysical models that are relevant to the groundwater model. Another difficulty is the large computational burden associated with a groundwater model and the huge amount of parameters in the geophysical models, limiting parameter estimation to gradient-search algorithms [e.g. *Doherty*, 2010] instead of Markov-Chain Monte Carlo based methods [e.g. *Vrugt et al.*, 2008]. To realize an approach that meets the above constraints we developed a new flexible CHI approach in which only parts of a geophysical model are coupled to a groundwater model by introduction of additional coupling constraints depending on the hydrogeological interpretation of the geophysical models.

In the next section concepts of the applied sequential hydrogeophysical inversion (SHI) and the coupled hydrogeophysical inversion (CHI) approach are explained. Section 3 shows the application of both the SHI and CHI for a synthetic groundwater model with Time-Domain Electromagnetic (TDEM) data. The implementation of CHI for a real-world groundwater model and geo-electric data (ERT) is described in section 4. Results for both methods are given in terms of parameter estimates, parameter uncertainty, model misfit and computational effort. The paper concludes with a summary of the benefits and disadvantages of the presented coupling procedures.

2. Methodology

2.1 Geophysical Inversion

Consider a dataset of geophysical observations assembled in vector d_g

$$d_g = \left(\rho_1, \rho_2, ..., \rho_{N_g}\right)^T \tag{2}$$

The symbol ρ denote the geophysical observations, e.g. apparent resistivities. Subscript N_g is the number of available geophysical observations. The geophysical model parameters to be estimated are assembled in vector π

$$\pi = (r_1, ..., r_{M_r}, t_1 ..., t_{M_t})^T \tag{3}$$

In this paper π contains a number of layer thicknesses and layer resistivities to be estimated for a 1D electrical resistivity model. M_r and M_t represent the number of parameters for each parameter type and their sum (M_r+M_t) is represented by M_g.

The SHI starts with a geophysical inversion in which geophysical parameters in π are estimated by fitting the geophysical observations in d_g. For this purpose we follow a well established iterative least-squares inversion approach [*Tarantola and Valette*, 1982; *Menke*, 1984), using linearized approximation with the first term of the Taylor expansion, we obtain

$$d_g + e_{obs} \cong g_g(\pi_{prior}) + G_g(\pi_{true} - \pi_{prior}) \tag{4}$$

for an initial combination of geophysical parameters π_{prior} that is sufficiently close to the true model π_{true} for the linear approximation to be good. In short we write,

$$\partial d_g = G_g \delta\pi + e_g \tag{5}$$

where ∂d_g represents the difference between the simulated geophysical forward response and the observed data, $\delta\pi$ symbolizes the parameter update and where Jacobian G_g contains all partial derivatives of the geophysical mapping

$$G_{ij} = \frac{\partial d_i}{\partial \pi_j} \tag{6}$$

for every j^{th} model parameter and every i^{th} observation. The estimate of π_{true} also needs to honor a number of parameter constraints. Four types of parameter constraints are used in this research: prior parameter constraints, prior depth constraints, vertical constraints and lateral constraints. These result in four additional operators I, P_h, R_p and R_h and contribute to the total geophysical observation error e_g'. The implementation and derivation of these constraints is explained in more detail in *Auken and Christiansen* [2004]. When joining equation 4 and equations 9, 11, 15 and 19 in *Auken and Christiansen* [2004], the inversion problem can be written as

$$\begin{bmatrix} G_g \\ I \\ P_h \\ R_p \\ R_h \end{bmatrix} \cdot \delta\pi = \begin{bmatrix} \delta d_g \\ \delta\pi_{prior} \\ \delta\pi_{h-prior} \\ \delta r_p \\ \delta r_h \end{bmatrix} + \begin{bmatrix} e_g \\ e_{prior} \\ e_{h-prior} \\ e_p \\ e_h \end{bmatrix} \tag{7}$$

where $\delta\pi_{prior}$, $\delta\pi_{h\text{-}prior}$, δr_p and δr_h express the deviation with respect to the expected value for the prior parameter constraints, prior depth constraints, vertical constraints and lateral constraints, where e_{prior}, $e_{h\text{-}prior}$, e_p and e_h are the errors associated with these constraints. More compact equation 7 is

$$G_g' \cdot \delta\pi = \delta d_g' + e_g' \tag{8}$$

The covariance matrix C_g' of the joint geophysical observation error e_g' is expressed as

$$C_g' = \begin{bmatrix} C_g & 0 & \cdots & \cdots & 0 \\ 0 & C_{prior} & \ddots & & \vdots \\ \vdots & \ddots & C_{h-prior} & \ddots & \vdots \\ \vdots & & \ddots & C_{Rp} & 0 \\ 0 & \cdots & \cdots & 0 & C_{Rh} \end{bmatrix} \tag{9}$$

The geophysical model estimate π_{est} is updated as given in equation 10

$$\delta\pi_{est} = \left[G_g'^T \, C_g'^{-1} \, G_g' \right]^{-1} G_g'^T \, C_g'^{-1} \, \delta d_g' \tag{10}$$

by minimizing the objective function

$$\phi_g = \left(\sum_{i=1}^{N_g} \delta d_g{}^T \cdot C_g{}^{-1} \cdot \delta d_g{}^T \right)^{\frac{1}{2}} + \phi_{prior} + \phi_{h-prior} + \phi_{Rp} + \phi_{Rh} \qquad (11)$$

where ϕ_{prior}, $\phi_{h\text{-}prior}$, ϕ_{Rp}, and ϕ_{Rh} represent the objective function component for the prior parameter constraints, depth constraints, vertical constraints and lateral parameter constraints, respectively.

The posterior standard deviation of the estimated geophysical parameters is calculated based on a post-calibrated parameter covariance matrix, defined as

$$C_{gest} = \left[G_g{}'^T \, C_g{}'^{-1} \, G_g{}' \right]^{-1} \qquad (12)$$

As all model parameters are estimated in logarithmic space, confidence intervals are subsequently calculated as the square root of the diagonal elements of C_{gest} using

$$STD(\pi_s) = \exp(\sqrt{C_{gest}(s,s)}) \qquad (13)$$

2.2 Sequential Hydrogeophysical Inversion

The traditional hydrogeological observations are listed in vector d_h,

$$d_h = \left(h_1, h_2, ..., h_{N_{h1}} \right)^T \qquad (14)$$

subscript N_h indicates the number of hydrogeological observations represented by h, which can include for instance head data and observed water fluxes. The hydrogeological parameters are listed by vector

$$\gamma = (\gamma_1, \gamma_2, ..., \gamma_{M_h})^T \qquad (15)$$

where M_h represents the number of hydrogeological parameters; in this paper the parameters representing hydraulic conductivities and thicknesses of geological layers. As for the geophysical model, an iterative least squares approach is used to estimate the parameters listed in γ. For the hydrogological data we write

$$\partial d_h = G_h \delta\gamma + e_h \qquad (16)$$

where G_h is the Jacobian containing all partial derivatives associated with the hydrogeological forward mapping and where e_h represents the observation errors of the hydrogeological data.

The second step of the SHI is to calibrate the hydrogeological model using the traditional hydrologic data in vector d_h and a number of estimated geophysical model parameters π_{est} together with their posterior standard deviations. When a

petrophysical relationship is used, π_{est} is first transformed to another property (e.g. hydraulic conductivity). This yields an additional set of hydrogeological observations comprised by vector $s_{h,}$

$$s_h = \left(\pi_{est1}, \pi_{est2}, ..., \pi_{estN_s}\right)^T \tag{17}$$

where N_s is the number of geophysical parameters that are used as observation to constrain the hydrogeological model parameters (e.g. thickness of a geological layer). These observations are connected to the hydrogeological parameters as given in equation 18

$$\partial s_h = R_s \delta\gamma + e_s \tag{18}$$

where R_s is a matrix with the dimensions of vectors γ and $N_{s,}$ containing ones for the hydrogeological parameters that are constrained by the estimated geophysical parameters in s_h and zeros for the hydrogeological parameters that are not constrained. e_s represents the posterior standard deviations associated with the geophysical parameters. This approach is analogous to the use of the prior parameter constraints in the geophysical inversion. The hydrogeological inverse problem can therefore be described as

$$\begin{bmatrix} G_h \\ R_s \end{bmatrix} \cdot \delta\gamma = \begin{bmatrix} \delta d_h \\ \delta s_h \end{bmatrix} + \begin{bmatrix} e_h \\ e_s \end{bmatrix} \tag{19}$$

or more compact as

$$G_h' \cdot \delta\gamma = \delta d_h' + e_h' \tag{20}$$

with parameter update

$$\delta\gamma_{est} = \left[G_h'^T \, C_h'^{-1} \, G_h'\right]^{-1} G_h'^T \, C_h'^{-1} \, \delta d_h' \tag{21}$$

where C_h' is the joint observation error comprising the error covariance matrix C_h for the hydrogeological observations and C_s for the geophysical observations. Equation 21 minimizes the objective function ϕ_{SHI} in the SHI approach

$$\phi_{SHI} = \phi_h + \phi_s = \left(\sum_{i=1}^{N_h} \delta d_h^{\,T} \cdot C_h^{\,-1} \cdot \delta d_h'^T \right)^{\frac{1}{2}} + \left(\sum_{i=1}^{N_s} \delta s_h^{\,T} \cdot C_s^{\,-1} \cdot \delta s_h^{\,T} \right)^{\frac{1}{2}} \tag{22}$$

Parameter uncertainty is calculated using a posterior parameter covariance matrix in the same way as for the geophysical inversion, described in the previous paragraph.

2.3 Coupled Hydrogeophysical Inversion (CHI)

In contrast to the SHI, we perform one single inversion for both the geophysical and the hydrogeological model. For this we assemble the parameters of both model types in vector m,

$$m = (\gamma_1, \gamma_2, ..., \gamma_{M_h}, \pi_1, \pi_2, ..., \pi_{M_g})^T \tag{23}$$

We introduce a number of so-called coupling constraints between the geophysical and hydrogeological parameters that are connected to the true model as

$$P_c \delta m = \delta r_c + e_c \tag{24}$$

where e_c denotes the error associated with the coupling constraint. As δr_c is only related to estimable parameters, e_c is unknown and has to be defined by the user. Its definition depends upon the confidence in the coupling constraint. In this CHI framework, e_c plays a key role. Operator P_c can have many forms. For example, when we introduce two coupling constraints which implies that the hydrogeological parameters γ_1 and γ_2 (thicknesses of geological layers) have to be equal to respectively π_1 and π_2 (e.g. layer thicknesses), equation 24 takes the following form

$$\begin{bmatrix} 1 & 0 & \cdots & 0 & -1 & 0 & \cdots & \cdots & 0 \\ 0 & 1 & 0 & \cdots & 0 & -1 & 0 & \cdots & 0 \end{bmatrix} \begin{bmatrix} \gamma_1 \\ \gamma_2 \\ \vdots \\ \gamma_{M_h} \\ \pi_1 \\ \pi_2 \\ \vdots \\ \pi_{M_g} \end{bmatrix} = 0 + e_c \tag{25}$$

When relationships between parameter groups γ and π are defined a coupled inversion can be undertaken. Equation 26 is the result of combining equations 11 and 16 with the coupling constraints in equation 24

$$\begin{bmatrix} G_g' \\ G_h \\ P_c \end{bmatrix} \cdot \delta m = \begin{bmatrix} \delta d_g \\ \delta d_h \\ \delta r_c \end{bmatrix} \begin{bmatrix} e_g \\ e_h \\ e_c \end{bmatrix} \tag{26}$$

which can be written more compactly as

$$G' \cdot \delta m = \delta d + e' \tag{27}$$

Many of the entries in Jacobian G' are equal to 0 as some of the hydrogeological parameter estimates are not affected by the geophysical observation and constraints and vice versa. The joint observation error e' is denoted by covariance matrix C'

$$C' = \begin{bmatrix} C_g' & 0 & 0 \\ 0 & C_h & 0 \\ 0 & 0 & C_c \end{bmatrix} \tag{28}$$

The model estimate becomes

$$\delta m_{est} = \left[G'^T \, C'^{-1} \, G' \right]^{-1} G'^T \, C'^{-1} \, \delta d' \tag{29}$$

which minimizes the objective function

$$\phi_{total} = \phi_g + \phi_h + \phi_c \tag{30}$$

where ϕ_h is the hydrogeological data misfit and ϕ_c the objective function term associated with the coupling constraints.

2.4 Implementation

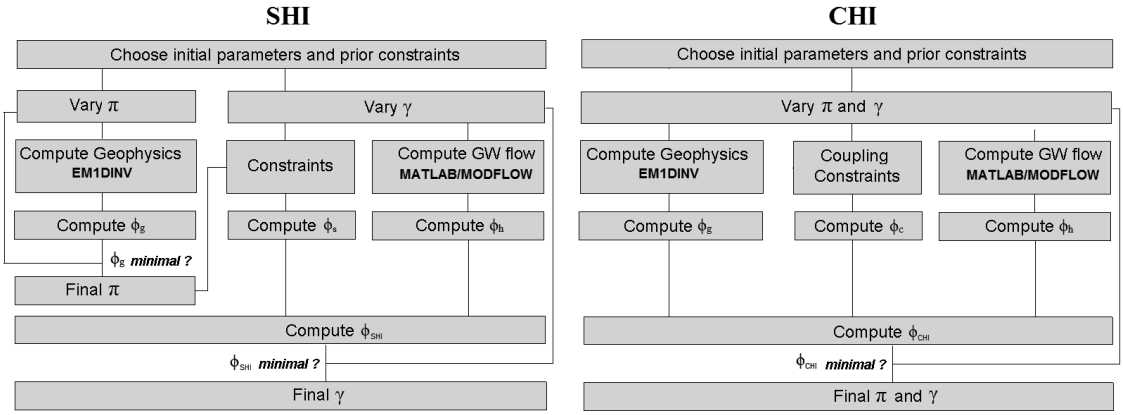

Figure 1 Implementation of the SHI (left) and CHI approach (right). π and γ respectively indicate the geophysical and groundwater model parameters, where the bold formatted text mentions the specific software used in this paper.

Figure 1 shows a visual summary and practical implementation of the SHI and the new CHI approach. Initial parameter values for the geophysical and groundwater models are given by a prior separate inversion for both models. The TDEM forward algorithm EM1DINV [HGG, 2008] is based on *Ward and Hohmann* [1988] and includes the modeling of low-pass filters [*Effersø et al.*, 1999] and the turn-on and turn-off ramps described in [*Fitterman and Anderson*,

1986]. EM1DINV is also used to generate a forward response for the ERT data [*Auken et al.*, 2002]. The geophysical model that is estimated for the TDEM is a 1D resistivity model (Figure 2b), in which typically a number of layer thicknesses and layer resitivities are estimated. For the ERT data, this would be a number of 1D resistivity models (Figure 6a) tied by lateral constraints [*Auken et al.*, 2002]. The ERT forward model is described in [*Auken et al*., 2002]. The groundwater model in the synthetic example was implemented in Matlab (PDE-tool) and in MODFLOW [*Harbaugh et al.*, 2000] for the real-world example. More details about the groundwater models are given in the next section.

3. Example 1: Synthetic study TDEM

3.1 Setup

Our first application of the CHI approach considers a synthetic cross-sectional groundwater model and a TDEM sounding. The groundwater model consists of two layers, similar to the geological setup of the field study we discuss in the second example. The upper layer, with a thickness of 25 m, is considered to be clayey sand with a hydraulic conductivity of 10^{-5} m/s and the bottom layer represents limestone with a hydraulic conductivity of 10^{-2} m/s. Constant heads are applied as boundary conditions (right: 1 m; left: 0 m) and in the middle of the model domain a river is assumed to be located with a fixed head of 0. This results in flow from left to right and flow towards the river. Figure 2a marks 6 observations, 4 head and 2 flux measurements.

TDEM measures apparent resistivities by applying electrical pulses through a transmitter loop that produces a primary magnetic field. After the turnoff of each electrical pulse, a secondary magnetic field is generated that decays over time. The rate of change of the secondary field is recorded for a number of time gates and is converted into a series of apparent resistivities ρ, which represent the geophysical observations in this example. This procedure is repeated a number of times to obtain a data stack, based on which the measurement errors can be calculated. The geophysical model used in the synthetic example consists of 1 layer thickness and 2 layer resistivities to be estimated using 30 “observed” apparent resistivities. The simplified 1D description of the geophysical model is used because of the negligible effect of the water table variation and unsaturated zone thickness in the model, compared to the geometry of the model and the TDEM resolution.

For the synthetic example we want to estimate 6 parameters, 3 for both the geophysical model and the groundwater model. To test the SHI and CHI, we generated 50 observation realizations of hydrologic data (heads and fluxes) and geophysical data (apparent resistivities) by adding uncorrelated noise to a model generated truth. The true parameter values are shown as black lines in Figure 3. The 50 sets of added noise had a standard deviation of 2 cm for the head observations and 10% of the measurement value for the fluxes. The measurement error added to the apparent resistivities had a standard deviation of ca. 3% of the measurement value and was based on a real-world TDEM sounding. This measurement error does not only reflect the standard deviation of the data stack, which typically shows much smaller standard deviations, especially for apparent resistivities measured at early time gates (less than 1 ms after pulse turn-off). However, this value of ca. 3% includes an additional error component to take in account the assumption of neglecting 3D effects and imperfect instrument specifications (e.g. filters, wave form of the applied pulses). This additional error component would typically yield correlated measurement errors. For example [*Effersø et al.*, 1999] provide the effect of different low pass filters on the TDEM forward response. When these filters are not accurately included in the TDEM forward model the result would be a structural over- or underestimation of the apparent resistivities at early time gates. In this research, however, we do not investigate correlated errors and thus add uncorrelated measurement error to the TDEM data to be consistent with the Gaussian assumptions of least-squares inversion theory [*Tarantola*, 2005]. Different starting parameters were used for the calibration of the geophysical and groundwater model with each observation realization.

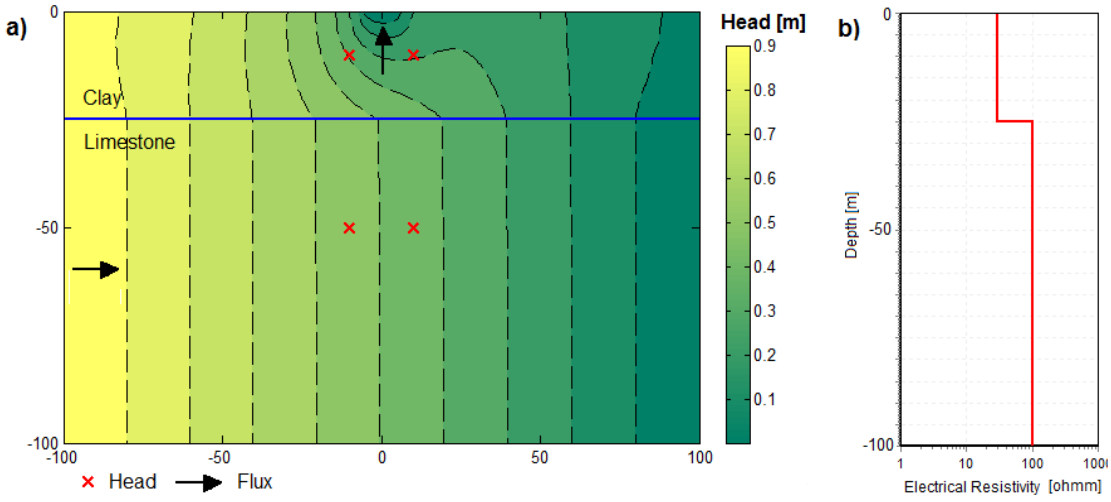

Figure 2 Groundwater model (a) and TDEM model (b) setups. Crosses mark head observations, arrows represent the flux observations used for the CHI exercise.

Table 1 Model properties used in the synthetic example.

Model Property	Value
Constant Head (west) [m]	1
Constant Head (east) [m]	0
Constant Head (river) [m]	0
Error Head Measurements [m]	0.02
Error Flux Measurements [%]	10
Error TDEM Measurements [%]	ca. 3%; based on a real sounding

3.2 SHI/CHI – Geometric & Petrophysical Relationship

To perform the CHI and SHI we employ two types of constraints, a geometric and a petrophysical constraint. The geometric constraint applies to the elevation of the interface between the clay and the limestone in the groundwater model (thickness_clay) and the depth of the first layer in the TDEM model (t1). The petrophysical coupling constraint applies to the hydraulic conductivity of the upper layer of the groundwater model (K_{clay}) and the electrical resistivity of the first layer in the TDEM model (r1), employing a relationship between the logarithmic values of hydraulic conductivity and electrical resistivity [*Niwas and de Lima*, 2003; *Slater*, 2007]. This latter value was arbitrarily chosen, but implies a decreasing hydraulic conductivity for a decreasing electrical resistivity, as hydraulic conductivity and electrical resistivity decrease for increasing clay content. A typical hydraulic conductivity for clay is 10^{-5} m/s [*Fetter,* 1994] and 10^{1} Ωm is a representative electrical resistivity [*Kirsch*, 2006], which results in an expected value of -6 for the petrophysical coupling constraint.

The SHI starts with a geophysical inversion for the TDEM data after which the estimated resistivity model is used as an observation in the calibration process of the groundwater model. The weights of these observations are equal to the posterior standard deviation of the geophysical parameters (e_s), calculated with a posterior covariance matrix obtained after performing the geophysical inversion. For the SHI, the second line in equation 19 becomes

$$\begin{bmatrix} 1 & 0 & \cdots & \cdots & 0 \\ 0 & 1 & 0 & \cdots & 0 \end{bmatrix} \begin{bmatrix} thickness\_clay \\ \log 10(K_{clay}) \\ \vdots \\ \gamma_{M_h} \end{bmatrix} = \begin{pmatrix} t1 \\ \log 10(r1) - 6 \end{pmatrix} + e_s \qquad (30)$$

For the CHI we use the same type of coupling constraints involving the same geophysical and hydrologic parameters. However, now the geophysical

parameters are also part of the inversion and equation 24 is used for the coupling constraints. In this case equation 24 becomes

$$\begin{bmatrix} 1 & 0 & \cdots & 0 & -1 & 0 & \cdots & \cdots & 0 \\ 0 & 1 & 0 & \cdots & 0 & -1 & 0 & \cdots & 0 \end{bmatrix} \begin{bmatrix} thickness\_clay \\ \log 10(K_{clay}) \\ \vdots \\ \gamma_{M_h} \\ t1 \\ \log 10(r1) \\ \vdots \\ \pi_{M_g} \end{bmatrix} = \begin{pmatrix} 0 \\ -6 \end{pmatrix} + e_c \quad (31)$$

where the expected value for the geometric constraint is 0, whereas the petrophysical relationship is -6. The CHI is undertaken for varying values of e_c, ranging from 10 to 0.01 for both constraints.

3.4 Results

We first performed a separate inversion for both the groundwater and the geophysical model for 50 observation realizations together with different starting parameters. In the last column of Table 2 the results are shown for the separate inversion, which represent the average parameter estimate, standard deviation, data fit and model calls for the 50 realizations. The thickness of the clay is not well determined in the groundwater model, showing a posterior standard deviation of ca. 15% with respect to the estimate. In the geophysical model the estimate of the first layer thickness has a standard deviation of about 8%.

Table 2 Results of CHI, SHI and a separate inversion. Results of the CHI are given for an e_c of 0.01.

Inversion result	[CHI]	[SHI]	[Separate_Inversion]
Log10 K_{clay} [m/s]	-5.00 ± 0.3%	-5.00 ± 0.4%	-5.00 ± 1.1%
Log10 K_{lime} [m/s]	-3.00 ± 1.7%	-3.00 ± 1.5%	-3.00 ± 1.8%
Thickness_clay [m]	25.03 ± 6.9%	25.03 ± 7.1%	25.24 ± 15.1%
Log10 r1 [Ωm]	1.00 ± 1.6%	1.00 ± 1.8%	1.00 ± 1.8%
Log10 r2 [Ωm]	2.01 ± 2.1%	2.02 ± 2.2%	2.02 ± 2.2%
t1[m]	25.03 ± 6.9%	24.91 ± 8.0%	24.91 ± 8.0%
Average groundwater model runs	95	49	51
Average geophysical model runs	95	33	33
Misfit geophysics ϕ_g	0.77	0.79	0.77
Misfit hydrogeology ϕ_h	0.71	0.81	0.81

The third column in Table 2 shows the results for the SHI, which indicate an improvement in the estimation of the groundwater model parameters compared with the separate inversion. The geophysical model parameters are the same as is the computational burden for both approaches. The parameter estimate for parameter thickness_clay clearly improves compared to the separate inversion as does the standard deviation which is now roughly equal to the uncertainty associated with the geophysical parameter t1. The posterior parameter standard deviations of the other parameters are also reduced, but not as significant as the hydrogeological parameters that were subjected to the coupling constraints.

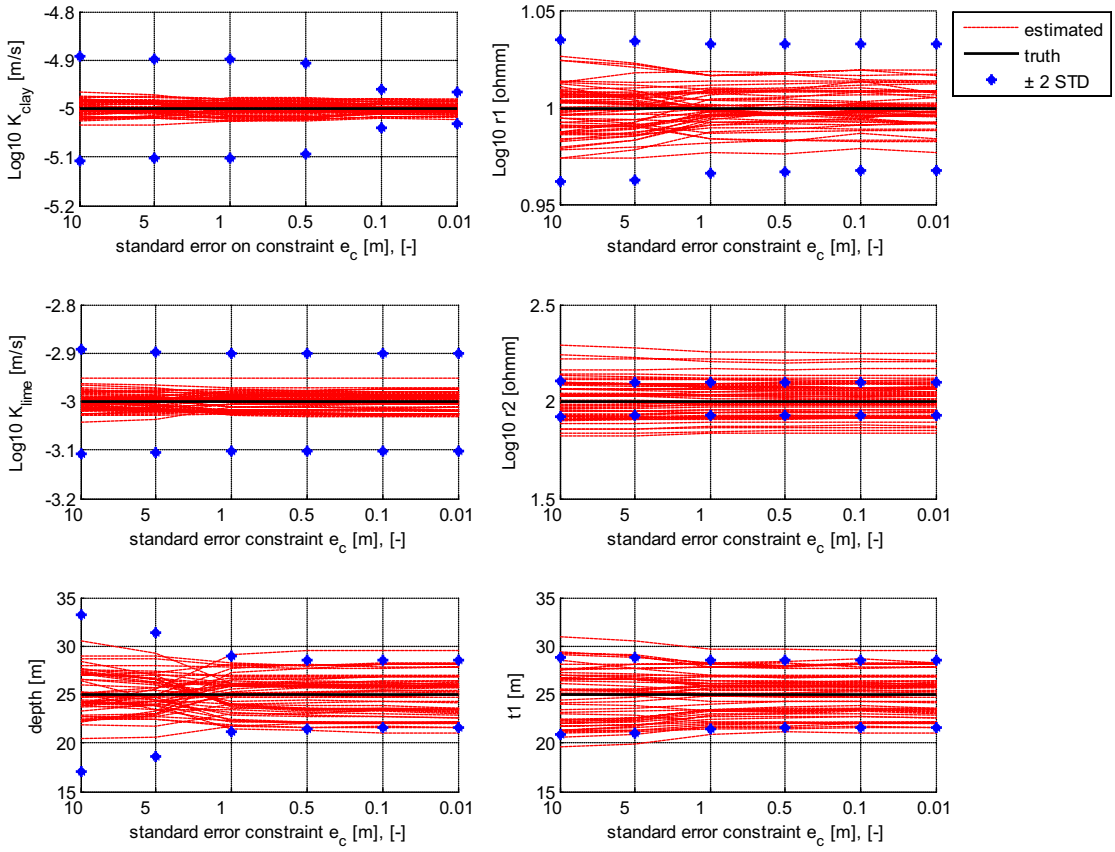

Figure 3 Parameter estimates (dashed red lines) for the synthetic example using a CHI with different e_c values for 50 realizations. Groundwater model parameters are shown in the left column of figures, geophysical parameters on the right. The straight black line marks the truth and the blued dots ± 2 standard deviations associated with the estimate. The x-axis shows the standard deviation of the two types of coupling constraints that were used, the geometrical constraint [m] between thickness clay and t1 and the petrophysical constraint between log10 K_{clay} and log10 r1 [-].

Figure 3 shows the estimated geophysical and groundwater model parameter values for 50 observation realizations, where the black line indicates the true parameter value and the dots ± 2 standard deviations of the estimated parameters. These are shown for different values of e_c used in the CHI. The differences between the estimated parameter values for each of these realization was caused by the different sets of measurement error that were added to the model-generated observations. The estimated groundwater model parameters, especially K_{clay} and thickness_clay, show a big improvement in terms of reducing their uncertainty when the coupling constraint is given more weight (i.e. smaller e_c). The estimated value also approximates the truth better, marked by some of the outliers in Figure 3. The geophysical model is less affected by the coupling procedure, but also shows an improvement. This is made clearer by the fourth column in Table 2. The benefit of the CHI is the reduction in parameter uncertainty (reflected by the posterior standard deviations) for both the geophysical and the hydrogeological models. It is important to note that the value for parameters thickness_clay and t1 now approximate its true value better. In the SHI a geophysical parameter estimate is imposed on the hydrogeological model that deviated from its true value by using t1 without any chance of feedback based on the hydrologic observations. This problem is resolved by using the CHI.

The computational burden associated with the CHI increased from 82 (49+33) model calls to 95. In the CHI, note that for the calculation of the Jacobian-entries in G' that are associated with the geophysical parameters and observations, only the geophysical model needs to be called; the same applies to the entries associated with the groundwater model parameters an hydrogeological observations. The increase in the computational burden for the CHI is caused by the number of optimization iterations, in which the geophysical and groundwater model parameters are updated, being the same, which is not the case if a separate inversion or SHI is conducted.

4. Example 2: Case study Risby landfill

As second example we consider a steady-state, real-world groundwater model for Risby landfill located in Denmark, to which we refer as the Risby model. This model was developed by *Christensen and Balicki* [2010] to characterize the hydrogeological interaction between a landfill, a local stream and a regional aquifer that is used for water supply. [*Christensen and Balicki*, 2010] provide a thorough description and discussion of the assumptions underlying the setup of this model and its results.

For this particular case, we investigate the application of a SHI and CHI to inform the groundwater model with Electrical Resistivity Tomography (ERT) data that was collected near Risby landfill (Figure 4). For this purpose, we first list the basic properties of the Risby area and the Risby groundwater model, after which we conduct a simple linear sensitivity analysis for the different hydrogeological parameters in the groundwater model, followed by the application of a SHI and CHI to inform the groundwater model with the ERT data.

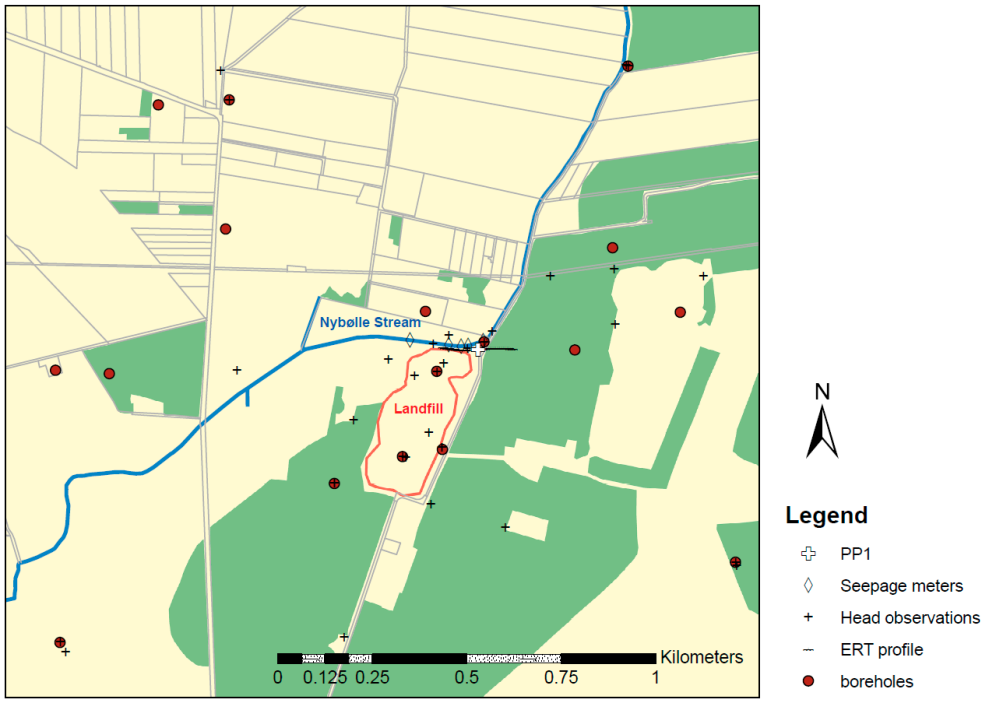

Figure 4 An aerial overview of Risby landfill, the ERT profile, parameter PP1 and available boreholes and hydrogeological observation data at Risby landfill.

4.1 Description of Risby Landfill

An extensive historical overview of Risby landfill was provided by [*Thomsen et al.*, 2011]. Figure 4a lists the key features of the study area, which are a landfill and a small brook called Nybølle stream. The geological setting of Risby landfill [*Gazoty et al.*, 2011, *Frederiksen et al.*, 2003; *Højbjerg et al.*, 2008, *Carl Bro A/S*, 1988] comprises pre-Quaternary limestone bedrock overlain by Quaternary glacial deposits. The pre-Quaternary limestone surface is located between -10 and +5 mamsl, corresponding to 20-30 m below the natural terrain surface. The Quaternary glacial deposits mainly consist of clay till, but intercalated sand lenses and sand layers are common. The sandy deposits range in thickness from a few centimeters to several meters.

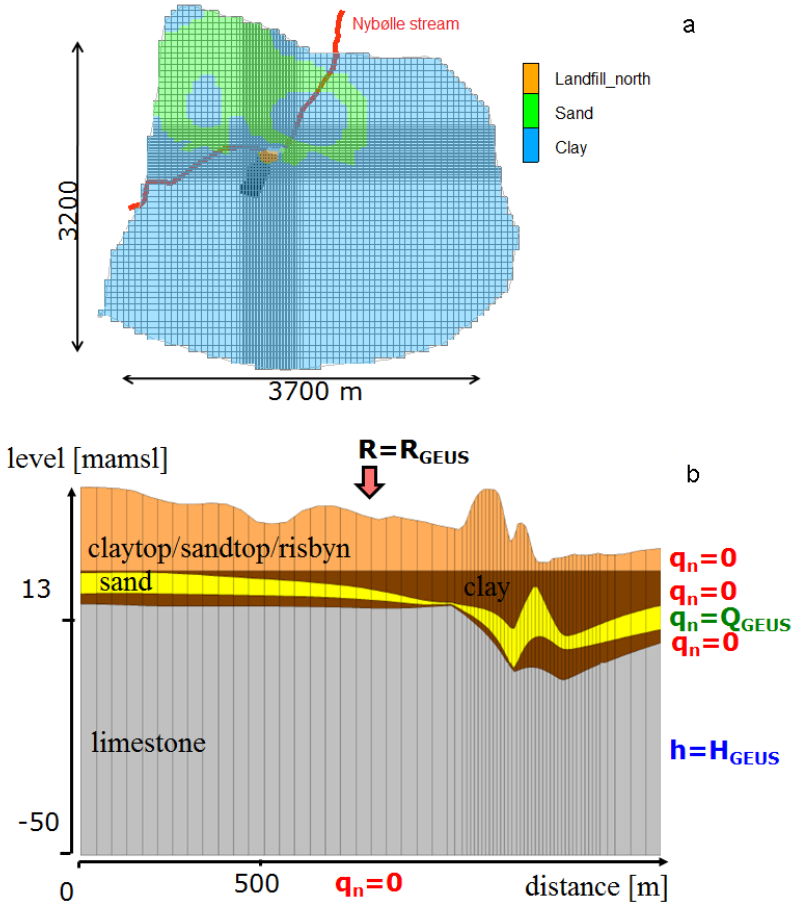

Figure 5 Horizontal discretization of the Risby groundwater model and zonation of layer 1 (a) and the geological setup and boundary conditions used (b).

4.1.1 Groundwater Model

Figure 5a shows the horizontal grid discretization that was used to simulate groundwater levels near Risby landfill. The grid cell size is 50 m further away from the landfill and 12.5 m near the landfill. For the geological setup, 5 continuous layers where chosen, where the 4 upper layers represent the glacial clay till and the latter layer the limestone aquifer. The top layer of the model, with its bottom elevation fixed at +15 mamsl was subdivided in three zones, which represent the extent of the upper sandy and clayey deposits together with the delineation of the northern part of the landfill (Figure 5a).

Boundary conditions applied in the Risby model are shown in Figure 5b and consist of constant heads, derived from a commonly used regional groundwater model, referred to as the GEUS-model [*Højbjerg et al.*, 2008]. The limestone was assumed to be impermeable at level -50 mamsl and a no flow boundary was

therefore assigned. The boundaries for the top layer and the remaining two clay layers were also set as no flow boundaries. q_n and h in Figure 5b represent the assigned flux and potential at the boundary. q_{GEUS}, h_{GEUS} and r_{GEUS} indicate that the specified flux, constant head values and recharge were extracted from the regional GEUS-model. Boundaries for the limestone were set as constant head boundaries with a potential equal to 14.9 m. The isopotential used, was the average simulated head in the limestone for the period 2001-2005 [*Højberg et al.*, 2008]. Boundaries for the sand-layer were prescribed flux boundaries. A flux of $7.2 \cdot 10^{-6}$ m3/s was applied for all cells along the boundary.

In [*Christensen and Balicki*, 2010] the Risby model has been calibrated using 6 parameters listed in Table 3, representing a uniform hydraulic conductivity for every geological layer, except for the uppermost layer which consist of three separate zones. The observation data consisted of 34 head measurements and 4 flux measurements, the locations of which are shown in Figure 4.

4.1.2 ERT Data

The landfill and its surroundings were mapped using various geo-electrical profiles for which ERT and induced polarization data were collected in order to delineate the landfill, sand pockets and the thickness of the glacial deposits overlying the limestone aquifer [*Gazoty et al.*, in prep.]. To demonstrate the SHI and CHI, we used the data associated with one of these ERT profiles north of the landfill; the location of the profile is shown in Figure 4.

Figure 6a shows the inverted resistivity model for the ERT profile using a few layer laterally constrained inversion approach as discussed in paragraph 2.1. This ERT profile consists of 38 1D resistivity models with 3 layers. The parameters estimated for each of the 38 resistivity models (5 m spaced) comprise 3 layer resistivities (r1, r2 and r3) and 2 layer thicknesses (t1 and t2). Lateral constraints were used with a factor of 1.2 for the layer depths (C_{Rh}) and a factor of 1.2 for the resistivities between neighboring resistivity models. At the location of the ERT profile, boreholes showed a depression in the limestone surface of ca. -10 mamsl. This depression has been interpreted as a buried Paleo-valley in the pre-Quaternary landscape and its shape is not well captured with the available boreholes. Another characteristic are relatively thick sand layers at the eastern part of Risby landfill.

In Figure 6a the limestone shows up as a bottom layer of relatively resistive material of ca. 100 -150 Ωm, which dips down towards the east. Sandy deposits

are more abundant at the eastern part of the landfill as evidenced by the relatively high electrical resistivities of about 50 -80 Ωm recorded at the eastern part of the profile. The top layer with a resistivity of ca. 10 Ωm is more pronounced at the western part of the profile, indicating predominantly clayey deposits. The presence of the landfill and the associated leachate plume might slightly affect this estimated resistivity. This component is disregarded in this paper as the scale of the inverted resistivity model is beyond the scale of the landfill and its contamination plumes, which have a typical layer thickness of 0.5 m, embedded within the top five meters of the glacial clay deposits at the western part of the profile [*Gazoty et al., 2011, Milošević et al., 2011*]. Figure 6c shows the uncertainty associated with the parameters that are estimated in the ERT model, expressed by their standard deviation as a percentage of the parameter estimate. This analysis included all the information provided by the data and parameter constraints. Note light colours in Figure 6c indicate relatively poorly resolved parameters, e.g. r1, r2 and t1 at the western part of the profile.

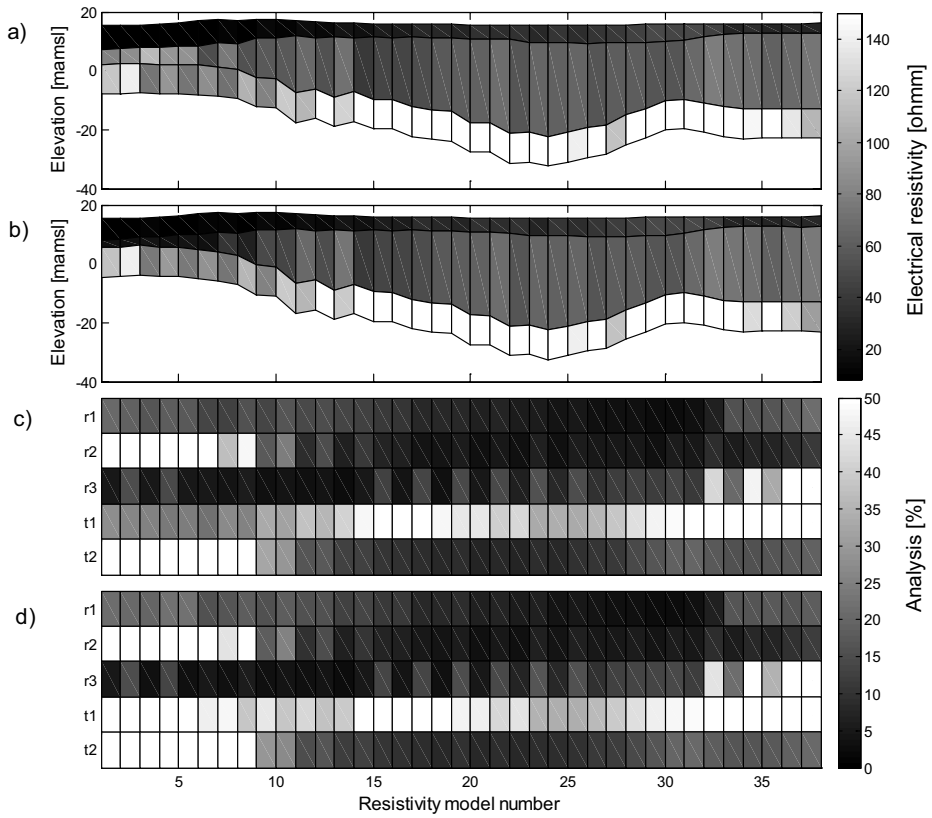

Figure 6 Inverted ERT model obtained after a separate geophysical inversion (a) and using the CHI with e_c=0.2 (b) together with a parameter uncertainty analysis expressed by their standard deviation relative to the parameter estimate. A gray scale marks well (dark coloured) and undetermined parameters (light coloured) for the separate geophysical inversion (c) and a CHI with e_c=0.2 (d).

4.2 Informing the Risby model with ERT data

In order to conduct a SHI and CHI, we first assess whether the interpretation of the estimated ERT model in the previous section is related to any of the variables and parameters that are used in the Risby groundwater model. As mentioned before, 6 parameters were estimated in the original Risby model [*Christensen and Balicki*, 2010], that are listed in Table 3. For these parameters we conducted a local, linear sensitivity analysis (Figure 7). This analysis showed that the hydraulic conductivity pertaining to the clay-layer (K_{clay}) is the most sensitive parameter.

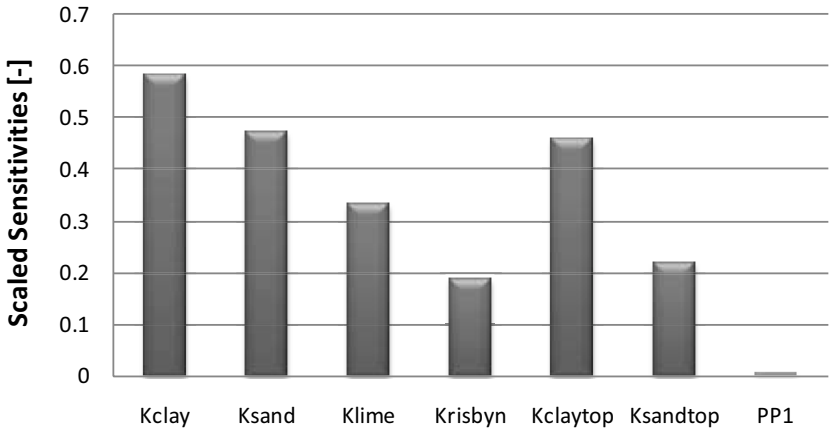

Figure 7 Scaled Sensitivities for the parameters of the Risby model.

To improve the estimate of K_{clay} we apply a petrophysical relationship described by Equation 19 with the use of an expected value of -9, as clay till has an approximate hydraulic conductivity of 10^{-8} m/d [*Fredericia*, 1990; *Carlbro A/S*, 1988] and an electrical resistivity of about 10 Ωm [*Kirsch*, 2006]. This relationship implies higher electrical resistivity is accompanied by a smaller clay content, which again results in a higher hydraulic conductivity. r1 and r2 in resistivity model number 1 to 10 are coupled to the estimation of K_{clay}, as the area east of the ERT profile contained large sandy deposits embedded in the clay. As we are only using a 3 layer resistivity model the average electrical resistivity in this part of the domain would not reflect the resistivity of the clay appropriately.

As the ERT model also informs us about the depth to the limestone, we introduce an additional parameter (PP_1) in the groundwater model representing the top elevation of the limestone. PP_1 represents a single pilot point [*Certes and de Marsily*, 1991] used to interpolate the elevation of the limestone surface together with the available borehole information. As expected, the sensitivity of this

parameter is very small with respect to the hydrogeological observations (Figure 7). To demonstrate the effect of geometric coupling we use parameter PP_1 in the inversion process. Parameters t1 and t2 in model number 14, 15 and 16 are coupled to the estimation of PP_1.

4.3 SHI

The SHI starts with the estimated geophysical model shown in Figure 6a. The scale of the individual 1D resistivity models comprised by the ERT model is rather small (electrode spacing of 5m) compared to the grid cell size of 12.5 m in the groundwater model. For this purpose we have chosen to use the geophysical parameter estimates of several resistivity models to constrain the groundwater parameters. To constrain K_{clay} we use the average estimate for r1 and r2 pertaining to resistivity model numbers 1 to 10. To constrain the estimation of PP_1 we use the average sum of t1 and t2 pertaining to resistivity model number 14, 15 and16. The weights associated with the constraints were based on the standard deviations of the geophysical parameter estimates calculated using equation 13.

4.4 CHI – Geometric Coupling & Petrophysical Relationship

We apply a CHI for the Risby model to find a well balanced estimate for r1 and r2 and K_{clay} using the petrophysical relationship described in paragraph 4.2, which is consistent with the hydrogeological interpretation of the ERT model. The same applies for the estimation of the depth to the limestone by introducing a geometric coupling constraint between parameters PP_1, t1 and t2. The petrophysical coupling constraint is used for resistivity models 1 to 10, the geometric constraint for resistivity model 14, 15 and 16.

4.5 Results

The last column in Table 3 shows the parameter estimation results of a separate inversion for both the geophysical and the groundwater model. Most of the parameters in the groundwater model are estimated with a standard deviation of 10%. When performing a SHI (Table 3, column 2), parameter uncertainty decrease for most of the parameters, except for $K_{claytop}$, $K_{sandtop}$ and PP_1, but parameter estimates remain similar. One of the causes is the high standard deviation associated with the geophysical parameters that are coupled. In Figure 6c these parameters also showed a relatively high standard deviation. As we used

this standard deviation to determine the weight of the constraints in the SHI, the constraint might be too weak to affect the estimation of the groundwater model parameters significantly.

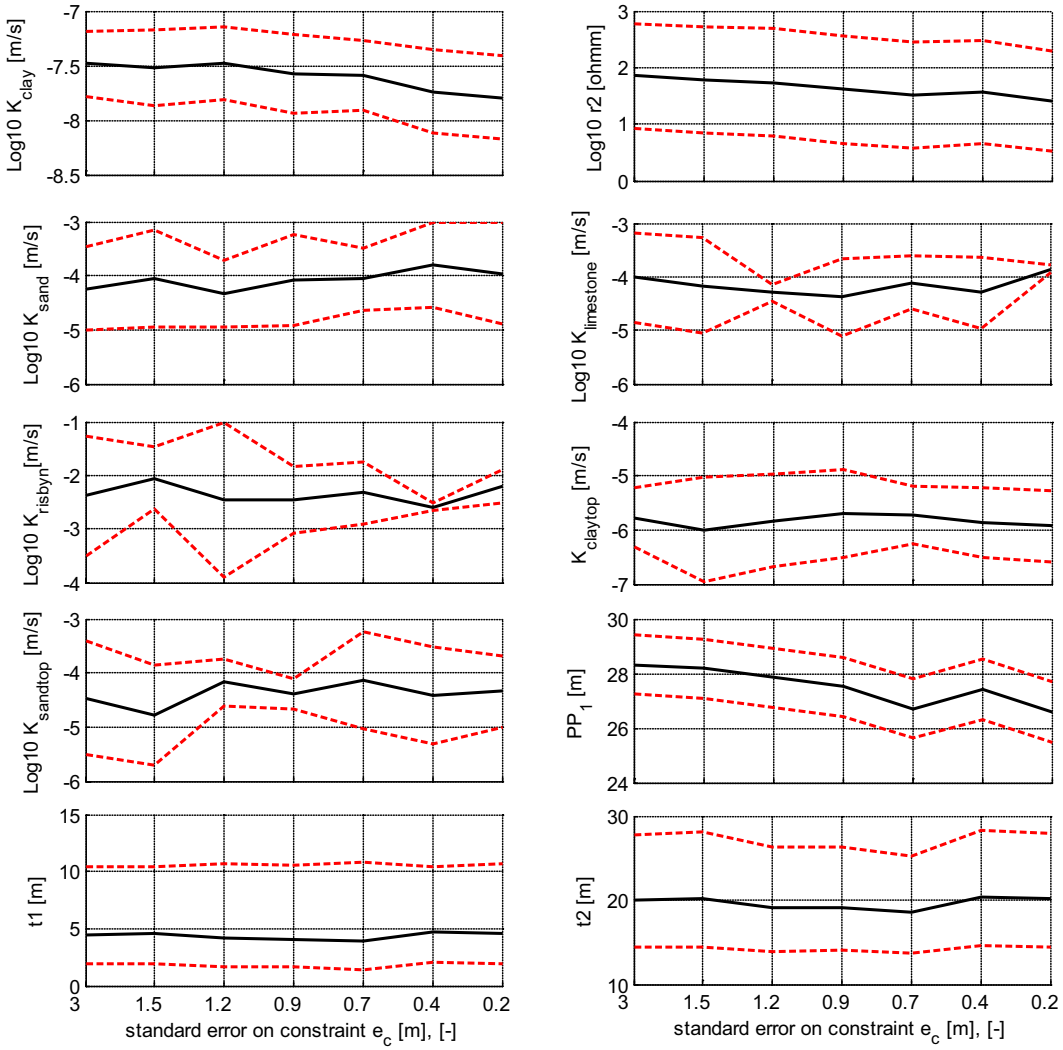

Figure 8 Parameter estimates (black straight line) and confidence bounds (red dashed lines) for different values of e_c when performing a CHI using a petrophysical relationship between K_{clay}, r1 and r2 and a geometrical constraint between parameters PP1 and t1 and t2. The confidence bounds represent the parameter estimate ± 2 standard deviations.

Figure 8 shows the result of the CHI. The parameter estimates for K_{clay} and r2 are affected when the weight of the petrophysical relationship is increased by setting the acceptable error e_c to a smaller value. The geometrical constraint between PP_1, t1 and t2 does not have a big impact on the geophysical parameters. However the estimate of PP_1 does approximate the geophysical model better when the constraint is given more weight. The average depth to the limestone in the ERT model is about 25 m (t1+t2). In the groundwater model this depth is estimated to be 28.26 m ± 2% and 28.04 m ± 4% using a separate inversion and a

SHI, respectively. In the CHI this estimate becomes ca. 26.58 m ± 2%. Table 3 shows that standard deviations of the groundwater model parameters for the CHI are almost equivalent compared to the SHI, but smaller compared with a separate inversion.

Figure 6b shows the inverted ERT model using the CHI with an e_c of 0.2. Compared with the result of a separate geophysical inversion in Figure 6a, the estimated resistivity of layer 2 decreased significantly from an average of 75 Ωm to ca. 30 Ωm for the first 10 resistivity models. Those were the models for which the r1 and r2 were coupled to the estimation of K_{clay} in the groundwater model. Figure 6d shows the standard deviations associated with the estimated geophysical model obtained with the CHI. The parameter standard deviation of r2 indicates this parameter is not well-determined using the CHI as was the case in the separate geophysical inversion. r1 is determined with an approximate standard deviation of 10%. However, Figure 6d shows t1 is less well resolved for those model numbers where the petrophysical relationship was applied. The geometric coupling constraint does not show any effect on the estimated geophysical models in Figure 6.

Table 3 Inversion results CHI and SHI for Risby landfill.

Inversion result	CHI(e_c=0.2)	SHI	Separate_Inversion
Log10 K_clay [m/d]	-7.79 ± 2%	-7.54 ± 2%	-7.52 ± 3%
Log10 K_sand [m/d]	-3.96 ± 12%	-4.26 ± 9%	-4.25 ± 10%
Log10 K_lime [m/d]	-3.85 ± 1%	-3.96 ± 3%	-3.99± 16%
Log10 K_risbyn [m/d]	-2.20 ± 7%	-2.33 ± 1%	-2.39 ± 26%
Log10 K_claytop [m/d]	-5.93 ± 6%	-5.81 ± 6%	-5.80 ± 4%
Log10 K_sandtop [m/d]	-4.35 ± 8%	-4.43 ± 7%	-4.42 ± 2%
PP_1 [m]	26.58 ± 2%	28.03 ± 4%	28.26 ± 2%
Average t1, model 14-16 [m]	4.53 ± 68%	4.55 ± 65%	4.55 ± 65%
Average t2, model 14-16 [m]	20.16 ± 20%	20.22 ± 20%	20.22 ± 20%
Average Log10 r1, model 1-10 [Ωm]	1.02 ± 9%	1.01 ± 8%	1.01 ± 8%
Average Log10 r2, model 1-10 [Ωm]	1.44 ± 32%	1.88 ± 29%	1.88 ± 29%
Groundwater model runs	210	63	91
Geophysical model runs	3230	1520	1520
Misfit geophysics ϕ_g	0.80	0.79	0.79
Misfit hydrogeology ϕ_h	0.76	0.70	0.65

Table 3 also lists the RMSE with respect to the geophysical and hydrogeological observations (respectively ϕ_g and ϕ_h), which was smaller than 1 for all simulations. No significant increase in data fit was noted, except a slightly higher ϕ_h for the CHI. When the imposed coupling constraints get more and more

strength (by decreasing e_c) or when a larger number of coupling constraints is applied, this will ultimately result in an increase in both ϕ_g and ϕ_h.

The last entry in Table 3 is the amount of model calls to perform the different kinds of inversion. The SHI was slightly more efficient compared to the separate inversion, as the calibration of the groundwater model was subjected to additional constraints. On the other hand, when a separate inversion is performed you do not used the geophysical model to inform the groundwater model with, so for this situation the 1520 geophysical model runs are not needed. The CHI required about twice as many geophysical and groundwater model runs compared to the separate inversion and ca. 3 times as many groundwater model runs compared with the SHI.

5. Discussion and conclusions

Most studies about coupled hydrogeophysical inversion (CHI) are performed by translating simulated hydrological state variables to geophysical parameter distributions. In contrast to these "state coupling" approaches, we developed a new method to perform a CHI for groundwater models with TDEM and ERT data, in which geophysical and hydrogeological parameters are coupled using geometric and petrophysical parameter coupling constraints. For a synthetic study the CHI resulted in improved parameter estimates and a reduction in parameter uncertainty for both the groundwater model and the geophysical model compared with a SHI and separate inversion. For another study, considering a real-world groundwater model and an ERT section, a local sensitivity analysis for the groundwater model parameters showed that the use of petrophysical coupling constraints is likely to be of more importance compared to the use of geometric coupling constraints in order to improve groundwater model parameter estimates through a CHI. For this second study, parameter uncertainty could not be reduced as well compared to a SHI and the computational burden associated with the CHI increased with a factor of ca. 2-3. However, the CHI clearly impacted the parameter estimates in both the groundwater model and geophysical model, resulting in consistent parameter estimates between the groundwater model and the geophysical model according to the hydrogeological interpretation of the geophysical model. This addresses the main advantage stated in *Hinnell et al.* [2010] of performing a CHI. *Hinnell et al.* [2010] point out that the formulation of a consistent framework for inference and solution between the geophysical model and hydrologic model is essential when performing a CHI. We believe our method would greatly increase the flexibility of defining such a framework, as 1)

a geophysical model does not necessarily relate completely to a relevant hydrologic process or property, 2) confidence associated with the hydrologic interpretation of a geophysical model can be tuned using different weights for the employed coupling constraints and 3) scale issues can be overcome by coupling several geophysical parameters to hydrologic parameters and vice versa. A similar CHI framework can be used with other types of optimization (e.g. Markov Chain Monte Carlo methods) by simply adding an additional coupling constraint component to the objective function that is minimized. To conclude, we would like to suggest some standard terminology for the types of CHI as was done for subdividing hydrogeophysical inversion in *Ferré et al* [2009]. A clear distinction should be made between state coupling and parameter coupling methods, whether time-lapse or static geophysical data has been used and to define the nature of the coupling (e.g. petrophysical coupling, geometric coupling).

Acknowledgements

This work was supported by the Danish Agency for Science Technology and Innovation funded project RiskPoint - Assessing the risks posed by point source contamination to groundwater and surface water resources under grant number 09-063216.

References

Archie,G.E., 1942. The electrical resistivity log as an aid in determining some reservoir characteristics. Transactions of the American Institute of Mining and Metallurgical Engineers, 146 54-61.

Auken,E. and Christiansen,A.V., 2004. Layered and laterally constrained 2D inversion of resistivity data. Geophysics, 69 (3): 752-761.

Binley,A., Winship,P., Middleton,R., Pokar,M., and West,J., 2001. High-resolution characterization of vadose zone dynamics using cross-borehole radar. Water Resources Research, 37 (11): 2639-2652.

Carl Bro A/S, 1988. Afsluttende fase 2 - undersøgelse på Risby Losseplads, Københavns Amtskommune, Copenhagen, Denmark.

Cassiani,G., Bohm,G., Vesnaver,A., and Nicolich,R., 1998. A geostatistical framework for incorporating seismic tomography auxiliary data into hydraulic conductivity. Journal of Hydrology, 206 (1-2): 58-74.

Cassiani,G., Bruno,V., Villa,A., Fusi,N., and Binley,A.M., 2006. A saline trace test monitored via time-lapse surface electrical resistivity tomography. Journal of Applied Geophysics, 59 (3): 244-259.

Certes,C. and Demarsily,G., 1991. Application of the Pilot Point Method to the Identification of Aquifer Transmissivities. Advances in Water Resources, 14 (5): 284-300.

Chen,J., Hubbard,S., Peterson,J., Williams,K., Fienen,M., Jardine,P., and Watson,D., 2006. Development of a joint hydrogeophysical inversion approach and application to a contaminated fractured aquifer. Water Resources Research, 42 (6).

Chen,J.S., Hubbard,S., Rubin,Y., Murray,C., Roden,E., and Majer,E., 2004. Geochemical characterization using geophysical data and Markov Chain Monte Carlo methods: A case study at the South Oyster bacterial transport site in Virginia. Water Resources Research, 40 (12).

Christensen, M. and M. Balicki., 2010. Hydrogeological characterization and numerical modeling of groundwater-surface water interaction at Risby landfill, Master's Thesis, DTU, Lyngby, Denmark.

Christiansen,L., Binning,P., Rosbjerg,D., Andersen,O., and Bauer-Gottwein,P., 2011. Using time-lapse gravity for groundwater model calibration: An application to alluvial aquifer storage. Water Resources Research, 47.

Dam,D. and Christensen,S., 2003. Including geophysical data in ground water model inverse calibration. Ground Water, 41 (2): 178-189.

Day-Lewis,F.D., Lane,J.W., Harris,J.M., and Gorelick,S.M., 2003. Time-lapse imaging of saline-tracer transport in fractured rock using difference-attenuation radar tomography. Water Resources Research, 39 (10).

Day-Lewis,F.D., Singha,K., and Binley,A.M., 2005. Applying petrophysical models to radar travel time and electrical resistivity tomograms: Resolution-dependent limitations. Journal of Geophysical Research-Solid Earth, 110 (B8).

Doherty, J., 2010. PEST: Model-independent parameter estimation, *Watermark Numer. Comput.*, Brisbane, Queensl., Australia. [Available at http:/www.pesthomepage.org]

Efferso,F., Auken,E., and Sorensen,K.I., 1999. Inversion of band-limited TEM responses. Geophysical Prospecting, 47 (4): 551-564.

Ferré, T., L. Bentley, A. Binley, N. Linde, A. Kemna, K. Singha, K. Holliger, J. A., Huisman, B. Minsley, 2009. Critical steps for the continuing advancement of hydrogeophysics. *EOS*, *90* (23), 200–201.

Fetter, C. W., 1994. Applied Hydrogeology. Prentice-Hall; New Jersey, USA. 3rd edition, ISBN: 0-02-336490-4.

Fitterman,D.V. and Anderson,W.L., 1987. Effect of Transmitter Turn-Off Time on Transient Soundings. Geoexploration, 24 (2): 131-146.

Fredericia,J., 1990. Saturated Hydraulic Conductivity of Clayey Tills and the Role of Fractures. Nordic Hydrology, 21 (2): 119-132.

Gazoty. A., Behroozmand, A., Fiandaca, G. and E. Auken, 2011. Landfill characterization with geophysical methods: the Risby case study, Applied Geophysics, In preparation.

Harbaugh, A. W., E. R. Banta, M. C. Hill, and M. G. McDonald, 2000. MODFLOW-2000, U.S. Geological Survey Modular Ground-Water Model - User Guide to Modularization Concepts and the Ground-Water Flow Process. Open-File Report 00-92. USGS; Virginia, USA.

Herckenrath, D., Auken, E., Christiansen, L., Behroozmand, A. and P. Bauer-Gottwein, 2011. Coupled hydrogeophysical inversion using time-lapse magnetic resonance sounding and time-lapse gravity data for hydraulic aquifer testing: Will it work in practice?, Water Resources Research, In Review.

HGG, 2008. Manual for the inversion program em1dinv, version 5.2, Department of Earth Sciences, University of Aarhus, Denmark. [Available at http://geofysiksamarbejdet.au.dk]

Hill, M. C., 1998. Methods and guidelines for effective model calibration, US Geological Survey water resources investigations report 98-4005.

Hinnell,A., Ferre,T., Vrugt,J., Huisman,J., Moysey,S., Rings,J., and Kowalsky,M., 2010. Improved extraction of hydrologic information from geophysical data through coupled hydrogeophysical inversion. Water Resources Research, 46.

Højberg, A. L., L. Troldborg, P. Nyegaard, M. Ondracek, S. Stisen, B. S. B. Christensen, and A. Nørgaard, 2008. National Vandressource Model - Sjælland, Lolland, Falster og Møn - Opdatering januar 2008, GEUS, Copenhagen, Denmark.

Hubbard,S.S., Rubin,Y., and Majer,E., 1999. Spatial correlation structure estimation using geophysical and hydrogeological data. Water Resources Research, 35 (6): 1809-1825.

Huisman,J., Hubbard,S., Redman,J., and Annan,A., 2003. Measuring Soil Water Content with Ground Penetrating Radar: A Review. Vadose Zone Journal, 2 (4): 476-491.

Hyndman,D.W. and Gorelick,S.M., 1996. Estimating lithologic and transport properties in three dimensions using seismic and tracer data: The Kesterson aquifer. Water Resources Research, 32 (9): 2659-2670.

Kemna,A., Vanderborght,J., Kulessa,B., and Vereecken,H., 2002. Imaging and characterisation of subsurface solute transport using electrical resistivity tomography (ERT) and equivalent transport models. Journal of Hydrology, 267 (3-4): 125-146.

Kirsch, R., 2006. Petrophysical properties of permeable and low-permeable rocks, Groundwater Geophysics, Springer Berlin Heidelberg, ISBN: 978-3-540-29387-3.

Knight,R., 2001. Ground penetrating radar for environmental applications. Annual Review of Earth and Planetary Sciences, 29 229-255.

Kowalsky,M.B., Finsterle,S., Peterson,J., Hubbard,S., Rubin,Y., Majer,E., Ward,A., and Gee,G., 2005. Estimation of field-scale soil hydraulic and dielectric parameters through joint inversion of GPR and hydrological data. Water Resources Research, 41 (11).

Lambot,S., Antoine,M., van den Bosch,I., Slob,E.C., and Vanclooster,M., 2004. Electromagnetic inversion of GPR signals and subsequent hydrodynamic inversion to estimate effective vadose zone hydraulic properties. Vadose Zone Journal, 3 (4): 1072-1081.

Lambot,S., Slob,E., Vanclooster,M., and Vereecken,H., 2006. Closed loop GPR data inversion for soil hydraulic and electric property determination. Geophysical Research Letters, 33 (21).

Lambot,S., Slob,E., Rhebergen,J., Lopera,O., Jadoon,K.Z., and Vereecken,H., 2009. Remote Estimation of the Hydraulic Properties of a Sand Using Full-Waveform Integrated Hydrogeophysical Inversion of Time-Lapse, Off-Ground GPR Data. Vadose Zone Journal, 8 (3): 743-754.

Linde,N., Finsterle,S., and Hubbard,S., 2006. Inversion of tracer test data using tomographic constraints. Water Resources Research, 42 (4).

Linde,N., Binley,A., Tryggvason,A., Pedersen,L.B., and Revil,A., 2006. Improved hydrogeophysical characterization using joint inversion of cross-hole electrical resistance and ground-penetrating radar traveltime data. Water Resources Research, 42 (12).

Looms,M.C., Jensen,K.H., Binley,A., and Nielsen,L., 2008. Monitoring unsaturated flow and transport using cross-borehole geophysical methods. Vadose Zone Journal, 7 (1): 227-237.

Menke, W., 1984. Geophysical Data Analysis: Discrete Inverse Theory, Elsevier, New York.

Milošević, N., Thomsen, N.I., Juhler, R. K., Albrechtsen, H. J. and P.L. Bjerg, 2011. Identification of discharge zones and quantification of contaminant mass discharges into a local stream from a landfill in a heterogeneous geologic setting, Journal of Hydrology, Submitted.

Niwas,S. and de Lima,O.A.L., 2003. Aquifer parameter estimation from surface resistivity data. Ground Water, 41 (1): 94-99.

Pollock,D. and Cirpka,O.A., 2010. Fully coupled hydrogeophysical inversion of synthetic salt tracer experiments. Water Resources Research, 46.

Purvance,D.T. and Andricevic,R., 2000. On the electrical-hydraulic conductivity correlation in aquifers. Water Resources Research, 36 (10): 2905-2913.

Refsgaard,J.C., van der Sluijs,J.P., Brown,J., and van der Keur,P., 2006. A framework for dealing with uncertainty due to model structure error. Advances in Water Resources, 29 (11): 1586-1597.

Slater,L., 2007. Near surface electrical characterization of hydraulic conductivity: From petrophysical properties to aquifer geometries - A review. Surveys in Geophysics, 28 (2-3): 169-197.

Tarantola,A. and Valette,B., 1982. Generalized Non-Linear Inverse Problems Solved Using the Least-Squares Criterion. Reviews of Geophysics, 20 (2): 219-232.

Tarantola, A., 2005. Inverse Problem Theory and Model Parameter Estimation, SIAM.

Thomsen, N., Milosevic, N. and P. L. Bjerg, 2011. Application of a mass balance method at an old landfill to assess the impact on surrounding water resources, Waste Management.

Topp,G.C., Davis,J.L., and Annan,A.P., 1980. Electromagnetic Determination of Soil-Water Content - Measurements in Coaxial Transmission-Lines. Water Resources Research, 16 (3): 574-582.

Vanderborght,J., Kemna,A., Hardelauf,H., and Vereecken,H., 2005. Potential of electrical resistivity tomography to infer aquifer transport characteristics from tracer studies: A synthetic case study. Water Resources Research, 41 (6).

Vereecken,H., Binley,A., Cassiani,G., Revil,A., and Titov,K., 2006. Applied hydrogeophysics. Applied Hydrogeophysics, 71 1-8.

Vozoff,K. and Jupp,D.L.B., 1975. Joint Inversion of Geophysical Data. Geophysical Journal of the Royal Astronomical Society, 42 (3): 977-991.

Vrugt,J.A., ter Braak,C., Diks,C., Robinson,B.A., Hyman,J.M., and Higdon,D., 2009. Accelerating Markov Chain Monte Carlo Simulation by Differential Evolution with Self-Adaptive Randomized Subspace Sampling. International Journal of Nonlinear Sciences and Numerical Simulation, 10 (3): 273-290.

Ward S.H. and G.W. Hohmann G.W., 1988. Electromagnetic theory for geophysical applications, Electromagnetic Methods in Applied Geophysics (ed. M.N. Nabighian), Vol. 1(4), 131–311. Society of Exploration Geophysicists.

Winsauer,W.O. and Mccardell,W.M., 1953. Ionic Double-Layer Conductivity in Reservoir Rock. Transactions of the American Institute of Mining and Metallurgical Engineers, 198 129-134.

Yeh,T.C.J., Liu,S., Glass,R.J., Baker,K., Brainard,J.R., Alumbaugh,D., and LaBrecque,D., 2002. A geostatistically based inverse model for electrical resistivity surveys and its applications to vadose zone hydrology. Water Resources Research, 38 (12).

II

Calibrating salt water intrusion models with Time-Domain Electromagnetic Data

Herckenrath, D., Odlum, N., Nenna, V., Auken, E., and P. Bauer-Gottwein

Ground Water, submitted

Calibrating a salt water intrusion model with Time Domain Electromagnetic data

Daan Herckenrath[1], Nick Odlum[3], Vanessa Nenna[3], Esben Auken[2] and Peter Bauer-Gottwein[1]

1 Department of Environmental Engineering, Technical University of Denmark, Miljøvej, Building 113, DK-2800, Kgs. Lyngby, Denmark
2 Department of Geoscience, Aarhus University, Høegh-Guldbergs Gade 2, 8000 Aarhus C, Denmark
3 Department of Geophysics, Stanford University, Panama Mall 397, 8000 Stanford, USA

** Corresponding author: daah@env.dtu.dk*

Abstract

Salt water intrusion models are commonly used to support groundwater resource management in coastal aquifers. Concentration data used for model calibration is often sparse and limited in spatial extent. With airborne and ground-based electromagnetic surveys, electrical resistivity models can be obtained to provide high resolution three-dimensional models of subsurface resistivity variations that can be related to geology and salt concentrations on a regional scale. Several previous studies have calibrated salt water intrusion models with geophysical data. These approaches, however, are normally limited to the use of the inverted electrical resistivity models only, without considering the measured geophysical data directly. This induces a number of errors related to inconsistent scales between the geophysical and hydrologic models and the applied regularization constraints. To overcome these errors and to apply a more consistent integration approach, we perform a coupled hydrogeophysical inversion (CHI) in which we estimate a small number of parameters for a salt water intrusion model using the raw geophysical measurement data. We refer to this methodology as CHI-S, in which simulated hydrologic state variables are transformed to a geophysical model, after which a geophysical forward response is calculated and compared with the collected measurement data. In addition to existing applications of CHI-S, our inversion framework allows for the estimation of some geophysical model parameters separately to take into account geophysical parameters that cannot be interpreted by the hydrologic model. This approach was applied for a semi-synthetic example, based on a field site in Santa Cruz County, California, and a time-domain electromagnetic (TDEM) data set that was collected at this location, comprising 14 TDEM soundings. For this area we developed a 2D cross-sectional salt water intrusion model, for which we estimated five uniform aquifer properties (diffusion, dispersion, hydraulic conductivity, anisotropy and porosity). In addition to the hydrologic parameters, one petrophysical shape parameter and one geophysical parameter were estimated. These seven parameters could be resolved well by fitting more than 300 apparent resistivities that were comprised by the TDEM dataset. Except for four soundings all the TDEM data could be fitted close to an RMSE of 1. Two possible explanations for the poor fit of these four soundings, which are located close to the coast, are the assumption of spatial uniformity and neglecting 3D effects for generating the TDEM forward responses due to lateral concentration gradients and the presence of cliffs.

1. Introduction

Salt water intrusion models are commonly used to quantify the impact of groundwater withdrawals and sea level rise on coastal freshwater resources [*Lebbe et al.*, 2008; *Giambastiani et al.*, 2007; *Zhang et al.*, 2004]. Many coastal regions are densely populated, and there are growing concerns about the over-exploitation of the available freshwater resources due to increasing water demands for domestic, agricultural and industrial use. Complex geological structures and the limited amount of information about the current level of saltwater intrusion are typical features complicating groundwater management. Past studies have demonstrated the ability of electromagnetic (EM) data to determine the extent of saltwater intrusion at many sites in the world [e.g. *Fitterman and Stewart*, 1986; *Frohlich et al.*, 1997; *Adepelumi et al.*, 2005; *Goldman et al.*, 1991]. *Levi et al.* [2008] use Time Domain Electromagnetic (TDEM) data to differentiate between fresh, brackish, and saline water at sites in the Judea Desert, Israel. Other studies have combined EM data with structural information derived from other geophysical methods to map saltwater intrusion in aquifers in Spain [*Duque et al.*, 2008], or to track the rate of saltwater intrusion in Oman [*Abdalla et al.*, 2010]. EM methods have also been used to image hydrogeological structure for use in conjunction with hydrologic models [*Fitterman and Stewart*, 1986; *Auken et al.*, 2006; *Koukadaki et al.*, 2007]. These datasets are very appealing to hydrogeologists because of their high spatial resolution and the scale they represent. Applications of airborne EM surveys in coastal aquifers include salt water intrusion mapping in Florida [*Langevin et al.*, 2003], mapping of buried valleys [*Auken et al.*, 2008] and mapping of a partially saltwater filled a cave system in Mexico [*Supper et al.*, 2009].

Similar to *Nenna et al.* [2007], this paper is focused on the use of EM data for supporting water managers in coastal urban areas in Santa Cruz and Monterey Counties, California. In *Nenna et al.* [2007] EM methods are evaluated to act as non-invasive alternatives for the use of sentinel wells to monitor saltwater intrusion in coastal aquifer systems and to characterize the continuity of important confining units. In this paper we present a new framework, based on *Pollock and Cirpka* [2010], *Kowalsky et al.* [2005], *Hinnel et al.* [2010] and *Lambot et al.* [2009], to integrate EM data into salt water intrusion models using a coupled hydrogeophysical inversion approach in order to provide one integral tool to quantify and map saltwater intrusion that can be updated in real-time using EM and concentration data.

Currently a growing number of studies are devoted to the integration of geophysical data into hydrologic models [*Vereecken et al.*, 2004]. *Ferre et al.* [2009] provide an overview of different integration techniques, which are more thoroughly discussed in *Hinnel et al.* [2010]. In this study we highlight two of these approaches which are a Sequential Hydrogeophysical Inversion (SHI) approach and a Coupled Hydrogeophysical Inversion (CHI) approach. In a SHI a geophysical inversion is performed after which a hydrologic model is calibrated using the estimated geophysical parameters as additional observations. [*Hinnell et al.*, 2010] discusses a CHI framework in which a geophysical inversion is undertaken using a hydrological model as interpretation framework. This procedure can be subdivided in three distinct components, a hydrologic model, a geophysical model and a petrophysical relationship. In this approach a hydrologic model is used to simulate a hydrologic state variable (e.g. moisture content, solute concentration), which is subsequently translated into a geophysical parameter distribution using a petrophysical relationship [e.g. *Topp et al.,* 1980; *Archie*, 1942] to simulate a geophysical forward response (e.g. apparent resistivity, electromagnetic wave velocity). We refer to this methodology as Coupled Hydrogeophysical Inversion-State (CHI-S).

CHI-S has been successfully applied for estimating water content and solute concentrations with Ground Penetrating Radar (GPR) and Electrical Resistivity Tomography (ERT) data in *Pollock and Cirpka* [2010], *Kowalsky et al.* [2005], *Hinnel et al.* [2010] and *Lambot et al.* [2009]. In *Bauer-Gottwein et al.* [2009] a CHI-S approach is used for a salt water intrusion model and Time Domain Electromagnetic (TDEM) data, but this study was primarily focused on the limitation of standard 1D TDEM forward models to interpret the three-dimensional nature of subsurface anomalies caused by seawater intrusion and salt transport phenomena.

This paper will primarily focus on the benefits of a CHI-S for TDEM datasets and salt water intrusion models. A limitation of existing CHI-S approaches is that these methods only include the estimation of hydrologic model parameters and petrophysical relationship parameters. This implies that the complete geophysical model is calculated from the simulations with the hydrologic model. In some cases the geophysical model includes parameters which cannot be estimated from the hydrologic model and need to be estimated separately to fit the geophysical measurement data satisfactorily.

This paper starts with a description of the theory and implementation associated with our CHI-S approach. Then an overview is given for the field site for which we apply the CHI-S, after which a description is provided with regards to the TDEM data, the salt water intrusion model and the setup for this specific application of CHI-S.

2. Methodology

2.1 Hydrologic Inversion

To explain the CHI-S we start from the traditional approach to calibrate a hydrologic model. Consider a dataset of hydrologic observations, vector d_h

$$d_h = \left(h_1, h_2, ..., h_{N_h}\right)^T \tag{1}$$

Subscript N_h indicates the number of hydrologic observations represented by h, which can include for instance hydraulic head, water fluxes and concentration measurements. Next we consider the hydrologic parameters that need to be estimated, assembled in vector

$$\gamma = (\gamma_1, \gamma_2, ..., \gamma_{M_h})^T \tag{2}$$

where M_h represents the number of hydrologic parameters; in this paper the parameters represent uniform aquifer properties such as hydraulic conductivity and porosity.

To estimate the hydrologic parameters we follow a well established iterative least-squares inversion approach [*Tarantola and Valette*, 1982; *Menke*, 1984), using a linearized approximation with the first term of the Taylor expansion, to obtain

$$d_h + e_h \cong g_h(\gamma_{prior}) + G_h(\gamma_{true} - \gamma_{prior}) \tag{3}$$

for a hydrologic forward model g_h with an initial combination of hydrogeological parameters γ_{prior} that is sufficiently close to the true parameter values γ_{true} for the linear approximation to be good. In short we write

$$\Delta d_h = G_h \Delta\gamma + e_h \tag{4}$$

where Δd_h represents the difference between the simulated hydrologic forward response and the observed data, $\Delta\gamma$ symbolizes the hydrologic parameter update and Jacobian G_h contains all partial derivatives of the hydrologic forward mapping for every i^{th} observation in d_h with respect to each j^{th} parameter in γ.

$$G_h(i,j) = \frac{\partial d_{hi}}{\partial \gamma_j} \tag{5}$$

In addition to the observations, the hydrologic inversion can be constrained by prior constraints and a variety of regularization constraints (e.g. smoothness). The implementation and derivation of such constraints can be found in *Tarantola and Valette* [2003], *Auken and Christiansen* [2004] and *Doherty* [2008]. The inversion problem can be written as

$$\begin{bmatrix} G_h \\ I \\ R_h \end{bmatrix} \cdot \Delta\gamma = \begin{bmatrix} \Delta d_h \\ \Delta\gamma_{prior} \\ \Delta r_h \end{bmatrix} + \begin{bmatrix} e_h \\ e_{prior} \\ e_r \end{bmatrix} \tag{6}$$

where operator I is the identity matrix and R_h is associated with the regularization constraints. $\Delta\gamma_{prior}$ and Δr_h represent the deviation from the expected value for the prior parameter constraints and regularization constraints. e_{prior} and e_r are the errors associated with these constraints. More compact, equation 6 is

$$G_h' \cdot \Delta\gamma = \Delta d_h' + e_h' \tag{7}$$

The covariance matrix C_h' of the joint observation error e_h' is expressed as

$$C_h' = \begin{bmatrix} C_h & 0 & 0 \\ 0 & C_{prior} & 0 \\ 0 & 0 & C_r \end{bmatrix} \tag{8}$$

The hydrogeological model estimate γ_{est} is updated as given in equation 9

$$\Delta\gamma_{est} = \left[G_h'^T C_h'^{-1} G_h'\right]^{-1} G_h'^T C_h'^{-1} \Delta d_h' \tag{9}$$

by minimizing the following objective function:

$$\phi_h = \left(\sum_{i=1}^{N_h + N_{prior} + N_r} \Delta d_h'^T \cdot C_h^{-1} \cdot \Delta d_h'^T \right)^{\frac{1}{2}} \tag{10}$$

In equation 10, N_{prior} is the number of prior parameter constraints and N_r the number of regularization constraints. The posterior standard deviation of the estimated hydrogeological parameters is calculated based on a post-calibrated parameter covariance matrix, defined as

$$C_{hest} = \left[G_h'^T C_h'^{-1} G_h'\right]^{-1} \tag{11}$$

To indicate the confidence with which parameters are estimated posterior parameter standard deviation are calculated as the square root of the diagonal elements of C_{hest} using

$$STD(\gamma_s) = \sqrt{C_{hest}(s,s)} \tag{12}$$

2.2 Coupled Hydrogeophysical Inversion – State (CHI-S)

In the CHI-S approach of *Pollock and Cirpka* [*2010*], *Kowalsky et al.* [*2005*], *Hinnel et al.* [*2010*] and *Lambot et al.* [*2009*] a complete geophysical model is generated based on the simulations of a hydrologic model. In this study, we also consider geophysical parameters that have to be estimated separately. For this purpose we subdivide the geophysical parameters into groups π_u and π_c, where π_c are the geophysical input parameters that are calculated from the simulations made with the hydrologic model and where π_u represents the geophysical parameters that are directly estimated. To perform a CHI-S, we consider another dataset containing geophysical observations

$$d_g = \left(\rho_{a1}, \rho_{a2}, ..., \rho_{aN_g}\right)^T \tag{13}$$

N_g indicates the number of geophysical observations represented by ρ_a, which typically includes apparent resistivities for geo-electric and electromagnetic methods. In addition to the hydrologic parameters in γ, we consider 2 additional groups of parameters

$$\pi_u = (\pi_{u1}, \pi_{u2}, ..., \pi_{uM_g})^T \tag{14}$$

$$p = (p_1, p_2, ..., p_{M_p})^T \tag{15}$$

M_g is the number of parameters in π_u, which includes the geophysical parameters that are not coupled with the hydrologic model and p lists a number (M_p) of petrophysical parameters used to transform hydrologic state variables to a geophysical parameter. γ, π_u and p can be assembled in one parameter vector, named x.

$$x = (\gamma, \pi_u, p)^T \tag{16}$$

The operator G_h in equation 4 only describes the relationship between the hydrologic input parameters γ and the hydrologic data in d_h. An additional operator is required that describes the relationship between hydrologic input parameters and the geophysical data. This relationship comprises the use of a petrophysical relationship and a geophysical forward model to transform hydrologic states to geophysical parameter distributions. The petrophysical relationship can be described as following

$$\pi_c = Ps \tag{17}$$

where P symbolizes the petrophysical relationship and s a hydrologic state as hydraulic head or solute concentration. Subsequently a geophysical forward mapping is undertaken based on the parameters in π_u and π_c which describe the complete geophysical model π.

$$d_g = G_g \pi \tag{18}$$

In equation 18, G_g describes the geophysical forward model. Including the geophysical data into the inversion problem described in equation 6, we can formulate the CHI-S by

$$\begin{bmatrix} G_h \\ G_c \\ I \\ R_h \end{bmatrix} \cdot \Delta x = \begin{bmatrix} \Delta d_h \\ \Delta d_g \\ \Delta x_{prior} \\ \Delta r_h \end{bmatrix} + \begin{bmatrix} e_h \\ e_g \\ e_{prior} \\ e_r \end{bmatrix} \tag{19}$$

where G_c represents an operator to generate the hydrologic and geophysical forward response based on the parameters in x. Note that this operator is different for the various groups of parameters in x. For example, to calculate the partial derivatives for the geophysical parameters in π_u with respect to the geophysical observations, the hydrologic mapping operator G_h and the petrophysical relationship P will not play any role in contrast to the calculation of the partial derivatives of the geophysical observations with respect to the hydrologic parameters.

2.3 Implementation

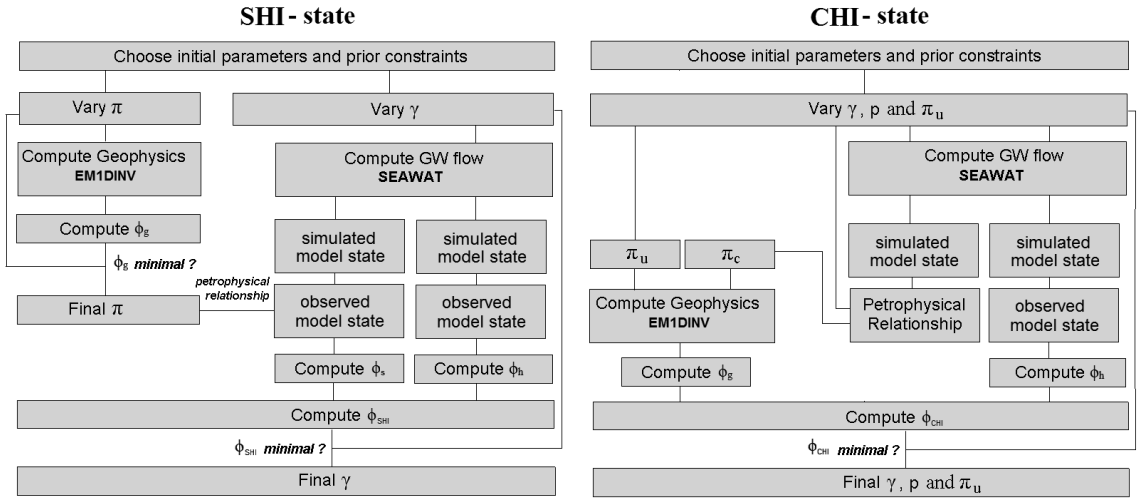

Figure 1 Inversion framework for a salt water intrusion model and TDEM data using a sequential (left) and coupled hydrogeophysical inversion approach (right).

The left panel of Figure 1 provides a visual description of a sequential hydrogeophysical inversion (SHI-S) framework and its implementation for a salt water intrusion model, which is investigated in previous studies [*Langevin et al.*, 2003; *Macaulay and Mullen*, 2007]. A SHI-S consists of three steps, in which first a geophysical inversion is performed, which yields an estimated distribution of geophysical parameters (e.g. electrical resistivities). The estimated geophysical parameters can act as observations for the salt water intrusion model by applying a petrophysical relationship between the estimated geophysical parameters and the simulated salt concentrations. The final step is to perform a hydrologic inversion in which the input parameters of a hydrologic model are estimated using the estimated geophysical parameters as observation data.

The coupled hydrogeophysical inversion approach (CHI-S) begins with the calculation of the salt water intrusion model, after which the simulated salt concentrations are translated to a geophysical parameter distribution using a petrophysical relationship in order to generate a geophysical forward response that can be compared with the geophysical measurement data. Note that the geophysical parameter distributions include parameters, which are estimated directly in the CHI-S (π_u). The CHI-S was implemented using the optimization software PEST [*Doherty*, 2010], which employs a Levenberg-Marquardt gradient-search algorithm. The SEAWAT computer program [*Langevin and Guo*, 2006; *Langevin et al.*, 2008] was used for simulating groundwater flow and salt concentrations.

In this paper we use simulated salt concentrations to generate the parameter distributions for the TDEM model. For this purpose we employ Archie's law [*Archie*, 1942].

$$\rho = \rho_{gw}\varphi^{-m}S^{-n} = \rho_{gw}FS^{-n} \tag{20}$$

where m is a cementation factor, which typically ranges between 1.3 for unconsolidated sands and 2 for consolidated sandstones. Archie's law also includes the water saturation S, but as we consider saturated groundwater flow only we assume S-n is 1. n is a factor that takes into account the large increase in electrical resistivity with decreasing saturation and has a value close to 2. As Archie's law implicitly assumes that total porosity is equal to the effective porosity of the medium [*Lesmes and Friedman*, 2005], φ can be replaced by the saturated water content θs. θs-m is equal to the formation factor F. [*Lesmes and Friedman*, 2005] provide a thorough discussion about Archie's law and more

complex alternatives to include for example surface conductivity as in [*Winsauer and McCardell*, 1953].

To generate TDEM forward responses, we used the EM1DINV software developed by Aarhus University [*HGG*, 2011]. The forward modeling algorithm used in EM1DINV is based on *Ward and Hohmann* [1988] and includes the modeling of low-pass filters according to *Effersø et al.* [1999] and the turn-on and turn-off ramps described by *Fitterman and Anderson* [1987].

3. Semi-synthetic case study: School

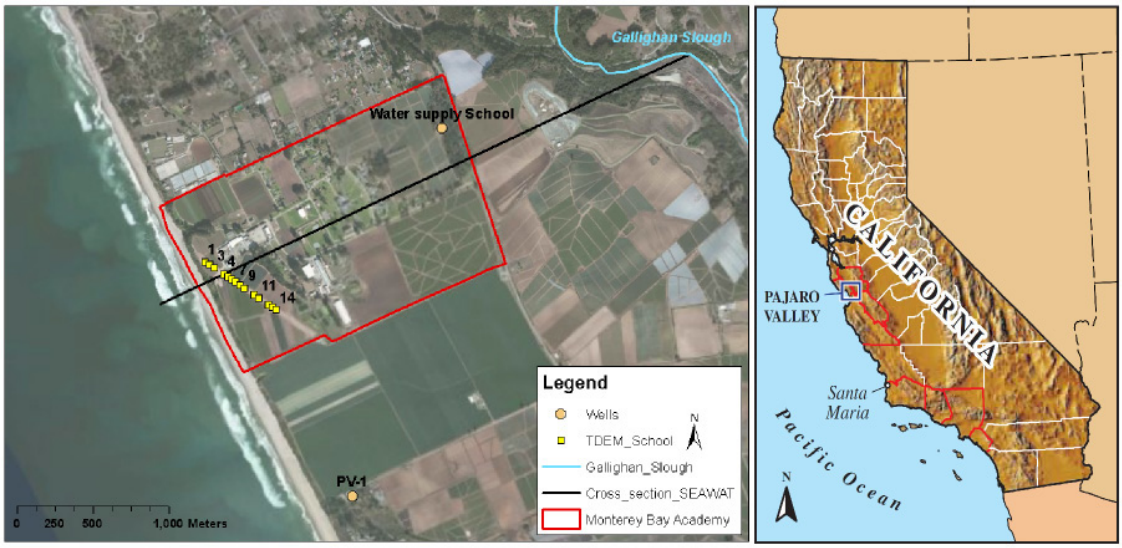

Figure 2 Aerial map of the School-site (left), providing an overview of the TDEM sounding locations, boreholes and the cross-section for which the SEAWAT simulations are performed**.**

For this research we study a field site located within the Pajaro Valley, a coastal watershed of 160 square miles located adjacent to the Pacific Ocean in Santa Cruz County, California. A map of the site is given in Figure 2, showing its main properties and the location of the TDEM soundings that were collected in this area. Pajaro Valley has been predominantly developed for agriculture since the late 1800s. About 84 percent of the water is used for agriculture and 16 percent is used for industrial and municipal water supply; almost all of the demand is supplied by ground water [*Hanson*, 2003].

3.1 Hydrogeology

At the School-site three major geological units can be distinguished that are relevant for groundwater flow. These geological units reside on top of relatively impermeable granite basement rock from the Cretaceous. From bottom to top

these three units are the Purisima Formation (poorly consolidated Miocene-Pliocene marine deposits), the Aromas Sand (unconsolidated Pleistocene deposits) and the shallow Alluvium (unconsolidated Holocene dune deposits). In addition, the Aromas Sand can be subdivided into an upper and lower portion on the basis of lithology and geophysical characteristics [*Hanson*, 2003]. The aquifer system of Pajaro Valley consists of three principal aquifers: a deep aquifer at ca. - 90 mamsl comprised of the Lower Aromas Sand and Purisma Formation, a primary aquifer in the Upper Aromas Sands, and a water table aquifer comprised of the same unit [*Bond and Bredehoeft*, 1987; *Hanson*, 2003]. In this research we will only focus on the water table aquifer, comprised of the Upper Aromas Sand deposits and the shallow Alluvium.

The Upper Aromas deposits are layered marine and terrestrial coarse-grained deposits separated by extensive fine-grained deposits that potentially restrict vertical movement of ground water and seawater intrusion. Lowered groundwater levels caused by overdraft in the coastal areas have resulted in widespread seawater intrusion in the Aromas Sands, starting as early as 1947 [*Mann*, 1988]. Since many of the wells in the coastal and inland sub-regions are screened at depths of 200 to 400 feet below land surface, a direct avenue is provided for seawater intrusion through the coarse-grained deposits of the shallower alluvium and Aromas Sand. Geophysical logs from monitoring wells indicate discrete zones of saline water that are related to seawater intrusion in the aquifer of the shallow Alluvium and the Upper Aromas Sand, but also indicate salt water intrusion in the deep aquifer system of the Lower Aromas Sand.

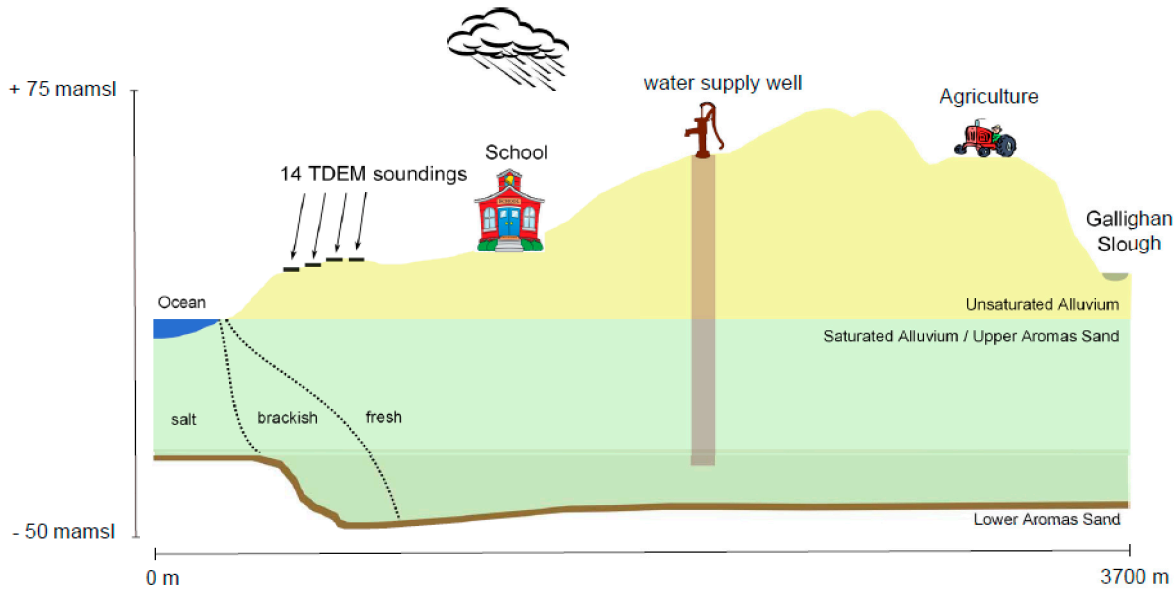

Figure 3 Hydrogeological schematization of the School-site.

3.2 TDEM data

At the School-site 19 TDEM soundings were collected on an old airstrip to obtain a transect of TDEM soundings which can be used for a 2D resistivity model representing electrical resistivity variations perpendicular to the coast. We will refer to the individual soundings as TDEM 1, TDEM 2, etc., where the increasing sounding number represents soundings respectively further away from the coast. TDEM data was collected using a Geonics ProTEM 47. For the measurements a 20-m double-turn transmitter-loop was used due to the limited width of the airstrip. Data was collected at ultra-high and very-high frequencies employing 20 time-gates for each frequency mode. Both offset and center-loop receiver configurations were used, but in this research we only use the center-loop data as the offset receiver geometry produced more noisy data.

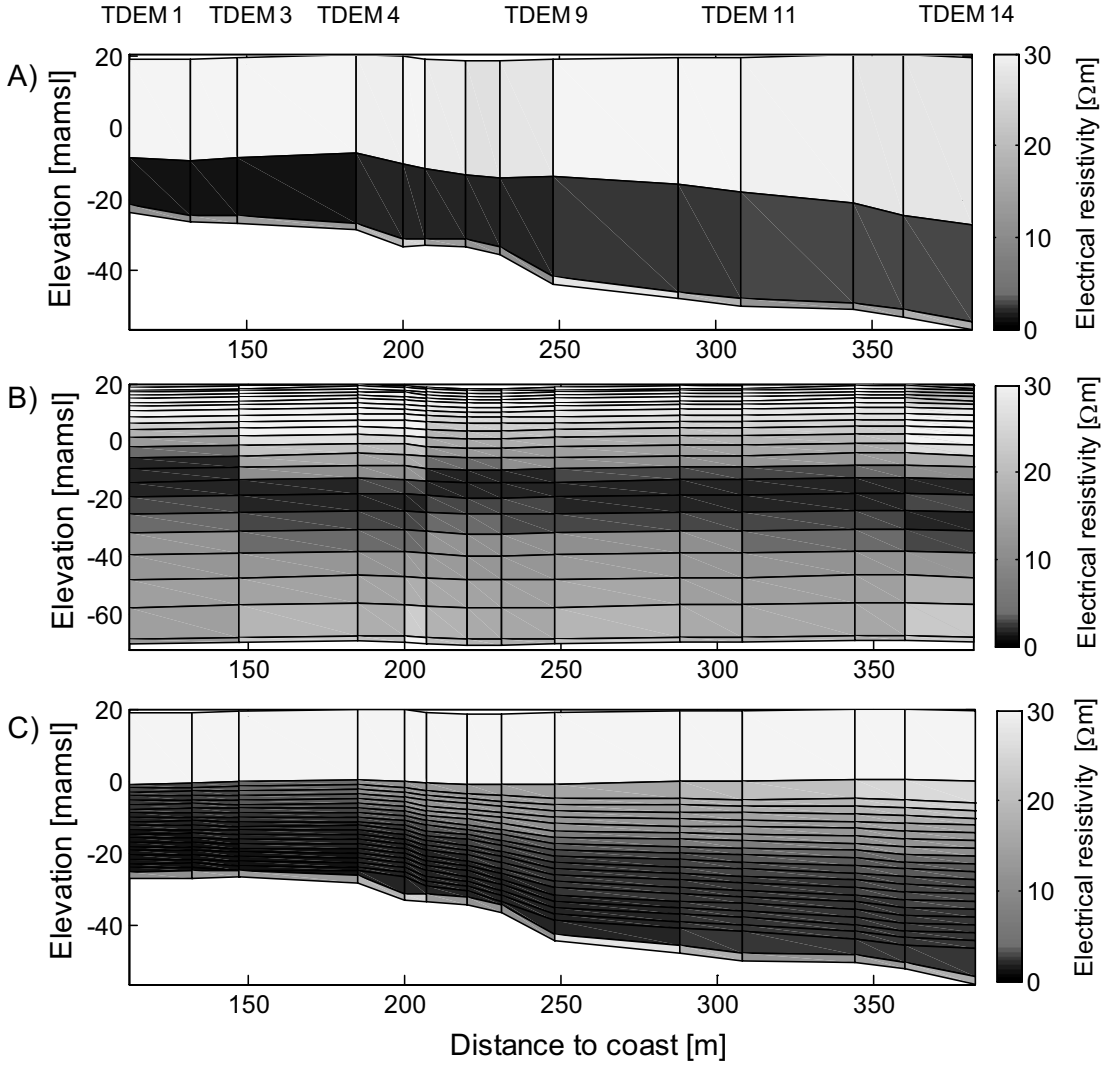

Figure 4 Inversion results of the 14 TDEM soundings using A) a 3-layer electrical resistivity model, B) 25-layer smooth inversion and C) CHI-S inversion.

To process the TDEM data, we used the Sitem-software (*HGG*, 2011) and 2 different methods to perform an initial inversion for the TDEM data. An overview of different approaches for the inversion and modeling of TDEM data can be found in *Oldenburg* [1990]. We applied a few-layer inversion in which a small number of layer thicknesses and layer conductivities were estimated for each sounding location. The second inversion method we used was a 25-layer smooth inversion using the EM1DTM code, in which layer thicknesses are fixed prior to inversion, after which EM1DTM estimates the electrical resistivity of each layer by minimizing both the data misfit and a number of smoothness constraints [*Farquharson and Oldenburg*, 1993]. The noise in the data was estimated to be 5% to take in account errors that result from neglecting 3D effects and imperfect instrument specifications (e.g. filters, wave form of the applied pulses) in addition to the standard deviations of measured field data.

TDEM sounding 15-19 did not yield data of satisfactory quality, which can be attributed to environmental noise sources. Such noise sources can include buried debris and cables, but at the School-site the noise was primarily attributed to the presence of metal irrigation pipes. Figure 4a presents the inverted 3-layer resistivity models for TDEM sounding 1-14 as a function of the distance with respect to the coast. All electrical resistivity models show a first layer with a high resistivity, a second layer with a very low electrical resistivity and a third layer with a higher resistivity compared to the second layer.

At the site we have an unsaturated zone of approximately 20 m thickness, consisting of dry sandy deposits, which typically have a high electrical resistivity of more than 100 Ωm [*Kirsch*, 2006]. Groundwater levels are expected to be close to ocean level. As the bottom of the first layer in Figure 4a occurs around -10 mamsl, this first layer can be interpreted as a layer comprising both the dry deposits and the freshwater saturated aquifer. Furthermore we can distinguish a second layer with a very low electrical resistivity of less than 1 Ωm. Given the setting of a coastal aquifer, this can only be interpreted as salt water saturated sediments. The final third layer in Figure 4a is remarkable as it shows an increased electrical resistivity compared with the layer above. As freshwater has a smaller density compared to salt water, this third TDEM layer must represent a geological unit with different hydrogeological properties preventing the salt water from going down in the deeper aquifer system. The electrical resistivity values indicate this third layer is likely to represent a freshwater saturated clay deposit. Note the 3-layer electrical resistivity model in Figure 4a assumes an infinite extension of the third layer, so no thickness can be derived for this clay

deposit. In Figure 4a we assigned an arbitrary thickness of 2m to this layer for visualization purposes. A gamma log at a nearby site (borehole PV-1 in *Hanson* [2003]) indicated clayey sand deposits with a thickness of ca. 5 m at an elevation of approximately -15 mamsl. In the geophysical inversion the electrical resistivity of this layer cannot be well resolved due to the overlying layer of seawater which is a very good electrical conductor blurring the signal pertaining to layers underneath. Moreover, this layer may be highly heterogeneous. As *Nenna et al.* [2011] show, the detection of this confining layer with TDEM is very powerful for risk assessment with regards to saltwater intrusion in coastal aquifers adjacent to Monterey Bay. In Figure 4a a dip can be seen associated with the clay layer. As the TDEM soundings are neither oriented perpendicular nor parallel to the coast, we do not know in which direction the dip is most significant. Based on the gamma log in PV-1 and the dipping rate of the Lower Aromas Sand documented in *Hanson* [2003] the dip in Figure 4a is likely to be oriented perpendicular to the coast. In this research we will only consider the water table aquifer and use the elevation of the third TDEM layer to represent the bottom boundary of this aquifer. Figure 4b shows the inversion result for the 25-layer smooth model. The pattern is consistent with 4a, showing both the clay layer and the salt water saturated layer. Figure 4c will be discussed at a later stage, as it marks the result for the CHI-S.

3.3 Salt water intrusion model

The main purpose for the investigations at the School-site is to evaluate whether we can successfully retrieve the hydrogeological properties of this site using TDEM data only. For the School-site we developed a vertical 2D cross-sectional saltwater intrusion model to simulate saltwater intrusion due to the pumping activities near the Monterey Bay Academy and obtain a range of values for the key hydrogeological properties of the Upper Aromas Sand at this location.

The model has a length of ca. 3700 m and a width equivalent to the width of the school property highlighted in Figure 2 corresponding to ca. 915 m. The assumption of a cross-sectional model with these dimensions implies the neglecting of groundwater flow parallel to the coast and the influences that are caused by groundwater pumping at locations close to the School site. For example, the land use around the School site comprises a lot of agriculture [*Hanson*, 2003], which uses groundwater for crop irrigation. For the salt water intrusion model we use the ocean as a west boundary for which we assume hydrostatic seawater conditions with a constant concentration C_s of 35 kg/m3 and

a hydraulic head of 0 mamsl. To control the water flux at the east boundary we apply a drain, which represents Gallighan Slough, set at a level of + 3 mamsl. The groundwater recharge rate applied on top of the model was equal to 0.35 ft/d which corresponds to 107 mm/yr. This value was based on earlier investigations by [*CH2M/HILL*, 2005]. No-flow conditions are specified for the bottom of the model. *Bond and Bredehoeft* [1987] indicated a marginal flow from the water table aquifer towards the deeper aquifer system but this process was disregarded in this research. The elevation of the bottom of the model was derived based on the inversion results of the TDEM soundings and one borehole at the School-site. The aquifer properties are represented by a uniform hydraulic conductivity, anisotropy, porosity, specific yield, dispersivity and diffusion value. These will be estimated in the CHI-S and will be elaborated more on in the next section.

Table 1 Variables and input parameters for the SEAWAT-simulations

Input Variables		**Numerical solution parameters**	
Recharge [mm/yr]	107	Number columns	500
Extraction rate School [m^3/d]	950	Number layers	50
ρs [kg/m^3]	1025	Column size, dx	7 m
ρf [kg/m^3]	1000	Layer size, dz	ca. 1-2 m
Cs [kg/m^3]	35		
α_L,α_T [m]	0	Solver flow	PCG
Estimated Parameters & Starting Values		Head stop criterion	10^{-2} m
K_h [m/d]	20	Flow stop criterion	10^{-2} m3 /d
K_z /K_h [-]	0.1		
S_y [-]	0.285	Solver advective transport	finite difference
α_L,α_T/ α_L [-]	10, 0.1	Concentration stop criterion	10^{-4} kg/m3
D_m [m^{-2}/d]	10^{-4}		
θ_s, θ_{res} [-]	0.33, 0.045	Solver dispersion and source terms	implicit finite difference
m [-]	1.3	Time step length	20 d

For this study, we did not possess much information about the exact pumping history at and near the School site. For the SEAWAT-model, we assume one single water supply well positioned at 1900 m from the coast, which corresponds approximately with one of the water supply wells at the School site. Figure 8 in *Bond and Bredehoeft* [1987], shows a pumping rate between 7 and 28 L/s at this location. Recent daily extraction rates at the School site amount to ca. 445.4 m^3/d. However, using a cross-sectional model implies that the applied pumping rate is uniformly distributed along the coastline. The extraction rate should therefore not be seen as the exact pumping rate for the supply wells at the School

site, but as the average value of groundwater extraction per unit length of the coast. Note our model extends further inland as the length of the School site; about twice the length of the School site. Furthermore many other pumping wells are present around the School site [*Hanson*, 2003], which influence is not directly taken in account using the 2D model. In addition, we do not know the development of groundwater extraction over time. Based on the available data, we assumed a pumping rate of an equivalent line sink parallel to the coast of 900 m^3/d. This estimate is considered to be acceptable for this study as we use the School-site primarily for demonstrating the use of CHI-S for salt water intrusion models.

Two stress periods were used for the simulations. The length of the first stress period was 4 x 10^4 days, this being sufficient to allow the concentration field to reach equilibrium for the natural situation. The second stress period had a length of 67 years, equivalent to the period between the establishment of Camp McQuaid in 1943 [*U.S Army Corps of Engineers*, 1997] and the time the TDEM data was collected, in which we apply a uniform pumping rate of 950 m^3/d.

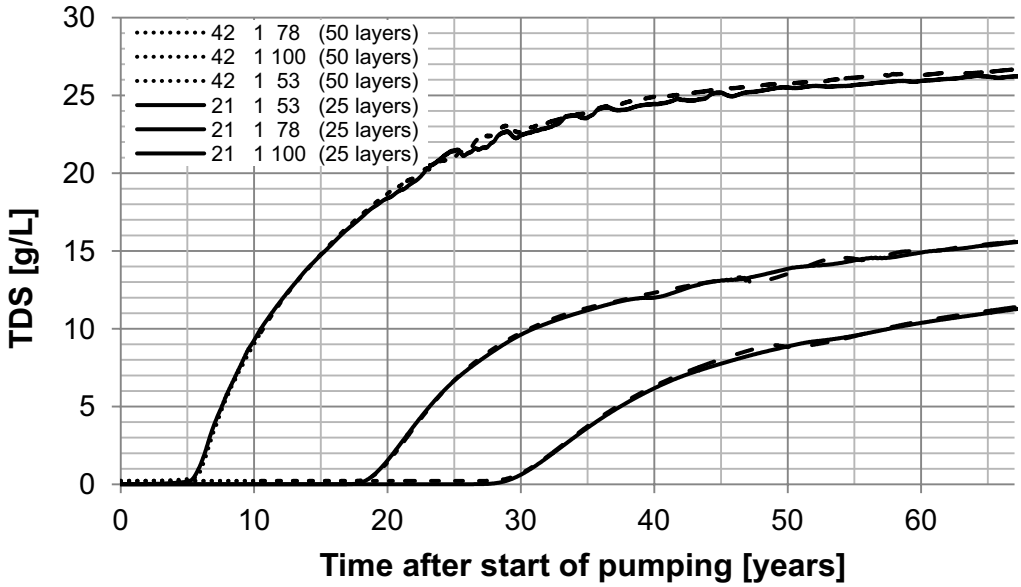

Figure 5 Concentration time series for a model with 50 (dashed) and 25 layers (solid), showing no significant signs of numerical dispersion due to a limited vertical discretization. For the SEAWAT-simulations we will therefore continue to use 25 layers.

The model was discretized with 500 columns and 25 layers resulting in a cell size of 7 by 1-2 m. The transport equation was solved using an implicit finite-difference scheme with upstream weighting. The lengths of transport steps were fixed at 20 days. To investigate the effect of numerical dispersion in our model

due to the grid discretization, we compared the simulations of the 25-layer model with a model using 50 layers. These simulations were performed for the parameter values listed in Table 1. The results of the comparison are plotted in Figure 5, showing only a marginal difference between both models. The reduction of the amount of layers was important to save computational time associated with the saltwater intrusion model and to simplify the generation of the TDEM forward responses. Based on Figure 5 we use 25 model layers for the SEAWAT simulations in this paper.

3.4 Parameterization

For the CHI-S we estimate three groups of parameters, parameters pertaining to the saltwater intrusion model (γ), the TDEM model (π_u) and parameters associated with the petrophysical relationship described in equation 20 (p). In Table 3 these parameters are listed together with their starting values and the group they belong to. The parameters for the salt water intrusion model are the following: hydraulic conductivity K_h [m/d], anisotropy K_z/K_h [-], specific yield S_y [-], porosity θ_s [-], longitudinal dispersivity α_L [m] and molecular diffusion D_m [m^2/d].

The hydraulic conductivity for sand has a large range. *Freeze and Cherry* [1979] for example provide a range of 10^3 - 10^5 m/yr and *Carsell and Parrish* [1988] list an average of 29.70 ± 15.60 cm/hr. Translated to meters per day these ranges are 2.7 – 274 m/d and 7.1 ± 3.7 m/d, respectively. Aquifer pumping tests by *Harding Lawson Associates* [1994] at Ford Ord, located 30 km south of the School-site, recorded estimated hydraulic conductivities of ca. 200-300 ft/d or 60-90 m/d for the Upper 180- foot aquifer, which is hydrostratigraphically similar to the water table aquifer at the School-site. As a starting value we will therefore choose a value of 20 m/d which is in between the average provided by *Carsell and Parrish* [1988] and the estimates by Harding Lawson Associates. K_z/K_h was set initially to 0.1 and is also an estimable parameter.

Parameters θ_s and the S_y are estimated using the following relationship

$$S_y = \theta_s - \theta_{res} \qquad (21)$$

where θ_{res} is the residual water content that is not drainable. We assumed a constant value for this parameter according to Table 3 in *Carsell and Parrish* [1988], who derive an average value of 0.045 for sandy soils based on 246 samples collected at various sites. For the porosity we use a starting parameter value of 0.33, which yields a starting parameter value of 0.285 for S_y. The

dispersion was separated into longitudinal α_L and transversal dispersivity α_T. α_T was set constant to 10% of the longitudinal dispersivity, which was set initially to a starting value of 10 m. The starting value for molecular diffusion was set to 10^{-4} m^2/d.

Subsurface resistivities were generated from simulated concentration using the petrophysical relationship. However, the resistivity of the unsaturated zone and the resistivity of the freshwater-saturated clay layer were not linked to the simulated hydrologic model states. Instead they were included in π_u or based on the geophysical inversion results in Figure 4a. However these properties cannot be based upon the results of the hydrologic model. Table 2 lists in which way the electrical resistivity model is built up to generate a TDEM forward response during the CHI-S.

Table 2 TDEM model configuration for CHI-S at the School-site. The last column shows whether the geophysical parameters are generated from the SEAWAT-model (π_c), separately estimated (π_u) or based on the prior geophysical inversion results.

TDEM layer 1	unsaturated zone	π_u
TDEM layer 2	concentration layer 5	π_c
TDEM layer 3	concentration layer 6	π_c
|	|	π_c
TDEM layer 22	concentration layer 25	π_c
TDEM layer 23	clay	not estimated, based on geophysical inversion

TDEM layer 1 represents the unsaturated zone, whose thickness is calculated based on the hydraulic heads simulated in SEAWAT at the TDEM locations. The electrical resistivity of this layer is unknown and will be estimated during the CHI-S. Due to dry cells in the upper 3-4 layers in the SEAWAT-model, the concentration of layer 5 in the SEAWAT-model was used to obtain an electrical resistivity for TDEM layer 2 by employing Archie's law. The bottom elevation of TDEM layer 2 corresponded to the bottom of SEAWAT-layer 5. This was subsequently done for TDEM layers 3 – 22 using the salt concentrations of the SEAWAT-model at the sounding locations. The thickness of all these TDEM layers was fixed according to the vertical discretization of the SEAWAT-model. TDEM layer 23 was used to take into account the presence of the clay, but its electrical resistivity was not an estimable parameter in the CHI-S. The electrical resistivity and top elevation of layer 23 were based upon the geophysical inversion results (Figure 4a). We considered these results to provide a proper estimate for the electrical resistivity of the clay as the SEAWAT-model does not

provide information about this parameter and the inclusion of this parameter in the CHI-S would increase the computational burden.

The final parameter that was estimated was the cementation factor m, used in Archie's law to calculate the formation factor together with the porosity (note that porosity is also an estimable parameter) for which we used a starting value of 1.3.

4 Results

In Table 3 the parameter estimates are shown for applying the CHI-S for the TDEM soundings and the SEAWAT-model associated with the School-site. All parameters could be resolved fairly well marked by posterior parameter standard deviations of around 10 % with respect to the parameter estimates, except for the anisotropy and the electrical resistivity of the unsaturated zone. In the inversion both parameters were not very sensitive with respect to the geophysical observations.

Table 3 Overview of estimated parameters used in the CHI-S for the School site

Parameter	Group	Starting Value	Estimated Value
K_h [m/s]	γ	20	19.64 ± 10 %
K_z/K_h [-]	γ	0.1	0.19 ± 22 %
S_y [-]	γ	0.285	0.32 ± 6 %
α_L [m]	γ	10	8.23 ± 7 %
D_m [m^2/d]	γ	10^{-4}	7.98E-03 ± 11 %
θ_s [-]	γ	0.33	0.36 ± 6 %
m [-]	p	1.3	1.12 ± 5 %
Resistivity unsaturated zone [Ωm]	π_u	200	195.69 ± 37 %
Resistivity clay layer [Ωm]	Not estimated	-	-

Hydraulic conductivity was expected to have slightly higher values, based on the aquifer pumping test results by *Harding Lawson Associates* [1994], but its value is well within the range provided by Freeze and Cherry. Anisotropy was expected to have a value of much less than 1, but we cannot judge whether 0.2 is too high or too low. Other studies in this area used anisotropy values of around 0.01 [e.g. *Hydrometrics*, 2009], but these studies are representative for larger scales and the deep aquifer system, where clay layers in the Aromas and Purisma Formation are represented using a larger vertical anisotropy. Porosity and specific yield (which was tied to the porosity through a fixed residual water content) fall within the range provided by *Carsell and Parrish* [1988]. This parameter was one of the

most sensitive parameters in this application. This makes sense as porosity not only controls how far the freshwater/saltwater interface moved inland but also has a major influence converting concentrations into electrical resistivities as it is part of the petrophysical relationship. Longitudinal dispersivity was estimated to be around 8 m. *Gelhar and Axness* [1953] provide an indication of around 10% of the scale of the model, which would be around 5 meter using the depth of the aquifer as a representative scale. The estimated dispersivity is also larger compared to the gridcell sizes, the scale at which scale numerical dispersion acts. Diffusion was estimated around 810^{-3} m^2/d. This process is often neglected as a contribution to the total dispersive flux [*Bond and Bredehoeft*, 1987]. The estimated value for Archie's cementation factor is rather low, as a value for clean sand would be 1.3. The electrical resistivity of the unsaturated zone should be well above 100 Ωm, which is the case according to Table 3.

Figure 6 shows the fit between simulated and measured apparent resistivities for every sounding. As our model is highly simplified we do not expect to fit the data perfectly. The bottom right plot in Figure 6 shows the RMSE for each of the TDEM soundings, which should have a value of around 1. For sounding 1- 3 and sounding 14 the RMSE is significantly larger. The large misfit of sounding 1-3 suggests a structural error in either the TDEM model or the saltwater intrusion model as the apparent resistivities at the first 6-7 time gates are consistently underestimated. This means the electrical resistivity of the upper part of the subsurface is underestimated at these particular soundings. Explanations are likely related to the assumption of uniform aquifer properties and a uniform electrical resistivity for the unsaturated zone.

Furthermore we did not take into account 3D effects when generating the TDEM responses, as we used a 1D electrical resistivity model for each sounding, which does not take in account the lateral variations in electrical resistivity that fall within the footprint of the instrument. For soundings 1-3 these lateral variations might be important due to the shape of the saltwater/freshwater interface. Another factor which was not taken into account by the 1D TDEM models is the close position (less than 30 m from the TDEM-receiver) of TDEM sounding 1-3 with respect to the cliffs that were present along the coast line. The presence of these cliffs (note their height is around +20 mamsl,) can be important as the resistivity of air is infinitely large. However, based on a number of undocumented TDEM forward responses, the assumption of uniform aquifer properties and the neglecting of 3D effects most likely caused the poor data fit

for TDEM sounding 1-3. The large RMSE for sounding 14 can be explained by poor data quality (note TDEM sounding 15-19 were not used for this reason).

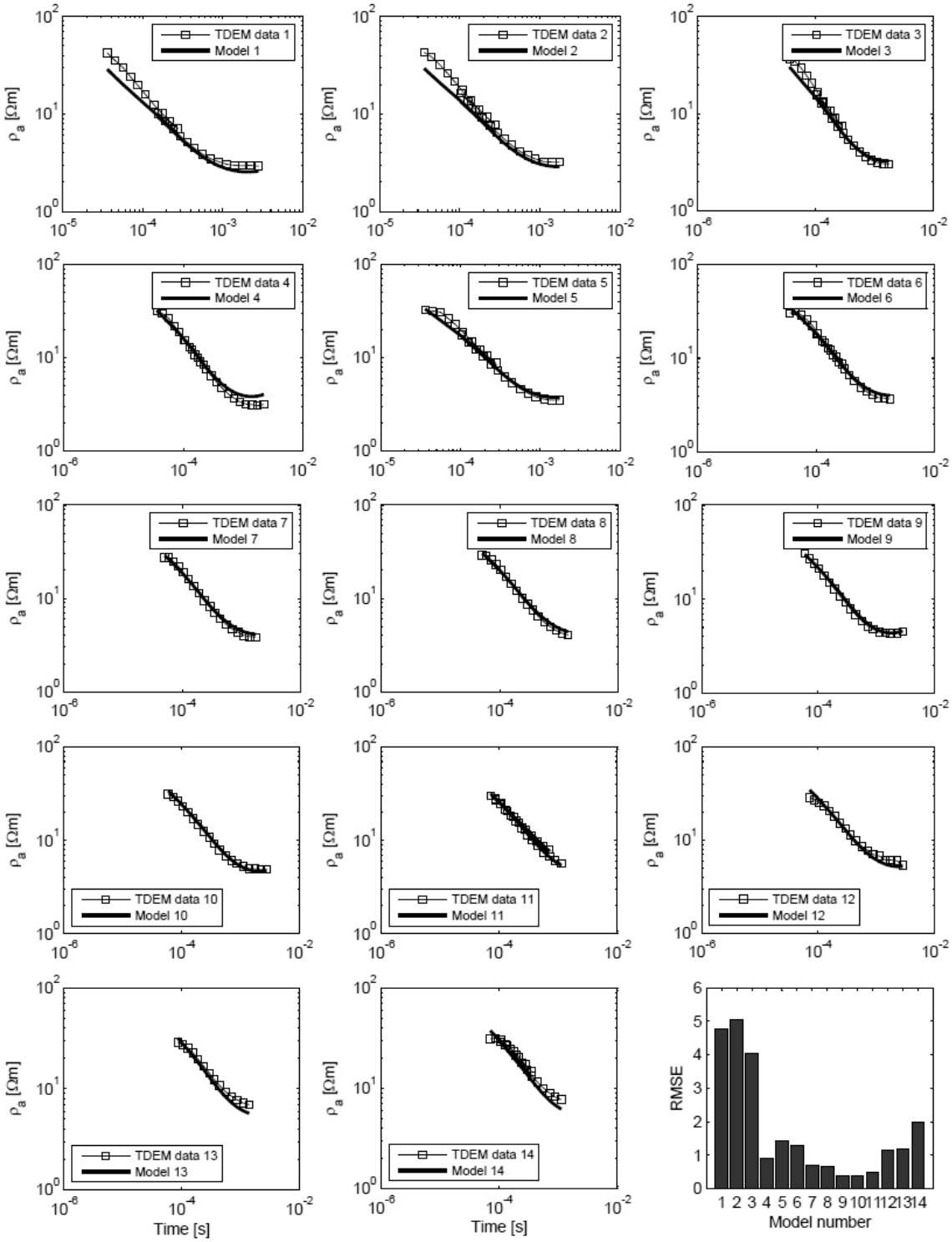

Figure 6 Simulated (solid) and observed (squares) apparent resistivities ρ_a for the 14 TDEM soundings. The bottom right figure indicates the residuals per TDEM sounding location in terms of the RMSE.

Figure 4c shows a similar plot as Figure 4a, in which the electrical resistivity models are plotted as a profile with respect to the coast. The bottom layer is the same in both figures, which represent the clay layer that is present at the site. The second commonality is the high resistivity of the top layer. However the amount of detail for the electrical resistivity in the aquifer is much higher. Also the electrical resistivity model resulting from the 25-layer smooth inversion showed a much less consistent pattern about the distribution of salt and fresh water in the aquifer. Of course this can be due to spatial heterogeneity, but also due to the definition of the smoothness constraints in the geophysical model. Given the simple SEAWAT-model, the data fit and the small amount of parameters which could be resolved well (Table 3), obviously the hydrologic model provided a well defined regularization framework for inverting the TDEM data.

In Figure 7 we plotted the result of the SEAWAT-simulations for the calibrated model, representing the salt concentration distribution of the water table aquifer after 67 years of pumping at the School-site.

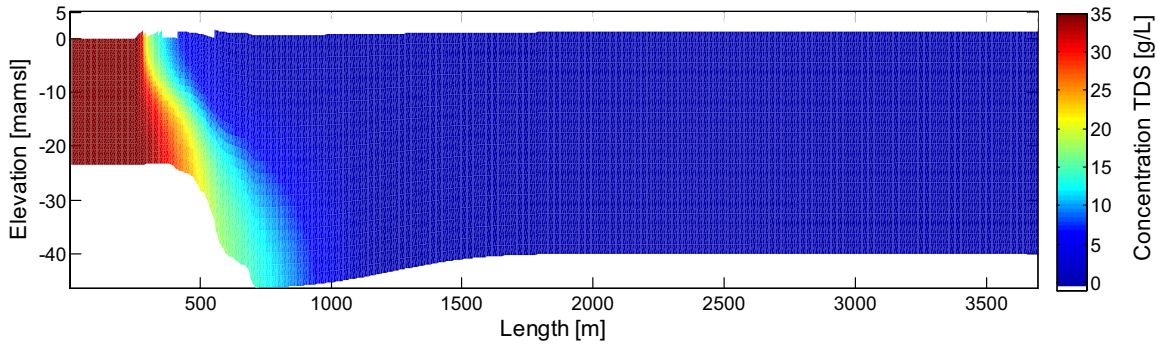

Figure 7 Concentration distribution after 67 years of pumping (950 m^3/d) at the School-site for the SEAWAT-model calibrated with the TDEM data using a CHI.

6. Conclusion

In this paper we investigated the application of a coupled hydrogeophysical inversion approach to estimate the hydraulic properties of a saltwater intrusion model with Time-Domain Electromagnetic (TDEM) data. In many areas TDEM data have been used to map salt-water intrusion in coastal aquifers. In some studies TDEM data is used for the calibration of saltwater intrusion models, but for most cases only the estimated electrical resistivity models are used as observed data. This introduces a number of errors, including the inconsistency of scales between the geophysical and hydrologic model and improper geophysical regularization constraints. For this purpose we used the coupled

hydrogeophysical inversion approach of *Pollock and Cirpka* [*2010*], *Kowalsky et al.* [*2005*]*, Hinnel et al.* [*2010*] and *Lambot et al.* [*2009*], which great strength is to perform a geophysical inversion given a certain hydrogeological interpretation of the geophysical model. We refer to this methodology as Coupled Hydrogeophysical Inversion – State (CHI-S) as these models translate simulated hydrologic state variables to a geophysical model. We modified these existing CHI-S frameworks as these methods do not include the direct estimation of geophysical model parameters that cannot be computed from a set of hydrologic simulations. However, these parameters might be essential to fit the geophysical data satisfactory.

We employed our CHI-S approach for a field site in Santa Cruz County, California. In this region salt water intrusion has been occurring [*Hanson*, 2003] as a result of groundwater extraction. For this site we collected 19 TDEM soundings and developed a cross-sectional saltwater intrusion model in SEAWAT, representing the upper aquifer system. Based on a separate geophysical inversion of the TDEM data we could detect a confining geological unit, marking the hydrologic base of the upper aquifer. With the CHI-S we could successfully estimate parameter values for the main hydraulic properties of the aquifer, using the data of 14 TDEM soundings that comprised more than 300 apparent resistivities.

For most TDEM soundings the level of data fit was acceptable, however, a structural underestimation of apparent resistivities was found for the early time-gates pertaining to three soundings located closest to the ocean. Explanations for this underestimation could be the assumption of uniform aquifer properties in the SEAWAT-model and the assumption of a 1D layered earth model for generating a geophysical forward response, which neglects lateral variations in electrical resistivity due to the presence of topography (e.g. cliffs) and the shape of the freshwater/saltwater interface. 3D approaches are available to generate a TDEM forward response [e.g. *Bauer-Gottwein et al*., 2009, *Commer and Newman*, 2004; *Newman et al.*, 1986; *Wang and Hohmann*, 1993], but these often require an impractically large computational burden. The electrical resistivity models that resulted from the CHI-S provided a huge improvement in spatial resolution, which would be very difficult to obtain with a traditional geophysical inversion as the complex spatial correlation between geophysical parameters cannot be captured with standard regularization constraints.

To summarize the efforts of this research, we think our CHI-S approach provides a promising method to extract hydrogeological information that might be contained within existing and future TDEM datasets with which salt water intrusion models can be constrained. This could not only be important to simulate the past system state of a coastal aquifer, but also provides an opportunity to use TDEM data and salt water intrusion models consistently as a real-time monitoring tool to support current groundwater management. The CHI-S approach we developed in this paper could be simultaneously used with the CHI-P approach that was developed in *Herckenrath et al.* [2011], in which geophysical parameters (P) are coupled with hydrologic model parameters (e.g. hydraulic conductivities) instead of the simulated hydrologic state variables. Both the CHI-S and CHI-P could offer a flexible tool to fully exploit the hydrogeological information contained within geophysical measurement data.

Acknowledgements

This work was supported by the Danish Agency for Science Technology and Innovation funded project RiskPoint - Assessing the risks posed by point source contamination to groundwater and surface water resources under grant number 09-063216. We would like to thank Professor Rosemary Knight for providing guidance in framing this study. The costs of the field work at Monterey Bay were covered by a grant from the S. D. Bechtel, Jr. Foundation to B. Thompson (P.I.), J. Christensen, P. Kitanidis, R. Knight, and F. Wolak, Stanford University.

References

Archie, G. E. 1942. The electrical resistivity log as an aid in determining some reservoir characteristics. *Transactions of the American Institute of Mining and Metallurgical Engineers* 146:54-61.

Adepelumi, A.A., B.D. Ako, T.R. Ajayi, O. Afolabi, and E.J. Omotoso (2009), Delineation of saltwater intrusion into the freshwater aquifer of Lekki Peninsula, Lagos, Nigeria, Environmental Geology, 56, 927:933.

Auken, E. and A. V. Christiansen. 2004. Layered and laterally constrained 2D inversion of resistivity data. *Geophysics* 69, no. 3:752-761.

Auken, E., A. V. Christiansen, L. H. Jacobsen, and K. I. Sorensen. 2008. A resolution study of buried valleys using laterally constrained inversion of TEM data. *Journal of Applied Geophysics* 65, no. 1:10-20.

Bauer-Gottwein, P., B. N. Gondwe, L. Christiansen, D. Herckenrath, L. Kgotlhang and S. Zimmermann. 2009. Hydrogeophysical exploration of three-dimensional salinity anomalies with the the time-domain electromagnetic method (TDEM), *Journal of Hydrology*.

Bond, L. D. and J. D. Bredehoeft. 1987. Origins of Seawater Intrusion in A Coastal Aquifer - A Case-Study of the Pajaro Valley, California. *Journal of Hydrology* 92, no. 3-4:363-388.

Cassiani, G., V. Bruno, A. Villa, N. Fusi, and A. M. Binley. 2006. A saline trace test monitored via time-lapse surface electrical resistivity tomography. *Journal of Applied Geophysics* 59, no. 3:244-259.

Christiansen, L., P. Binning, D. Rosbjerg, O. Andersen, and P. Bauer-Gottwein. 2011. Using time-lapse gravity for groundwater model calibration: An application to alluvial aquifer storage. *Water Resources Research* 47.

CH2M/Hill, 2005. Hydrogeologic assessment of the Seaside groundwater basin: Report prepared for Somach, Simmons & Dunn and California American Water Co.

Commer,M. and Newman,G. 2004. A parallel finite-difference approach for 3D transient electromagnetic modeling with galvanic sources. *Geophysics*, 69 (5): 1192-1202.

Day-Lewis, F. D., K. Singha, and A. M. Binley. 2005. Applying petrophysical models to radar travel time and electrical resistivity tomograms: Resolution-dependent limitations. *Journal of Geophysical Research-Solid Earth* 110, no. B8.

Doherty, J. 2003. Ground water model calibration using pilot points and regularization. *Ground Water* 41, no. 2:170-177.

Doherty, J. 2010. PEST: Model-independent parameter estimation, Watermark Numer. Comput., Brisbane, Queensl., Australia. [Available at http:/www.pesthomepage.org]

Duque, C., M. L. Calvache, A. Pedrera, W. Martin-Rosales, and M. Lopez-Chicano. 2008. Combined time domain electromagnetic soundings and gravimetry to determine marine intrusion in a detrital coastal aquifer (Southern Spain). *Journal of Hydrology* 349, no. 3-4:536-547.

Efferso, F., E. Auken, and K. I. Sorensen. 1999. Inversion of band-limited TEM responses. *Geophysical Prospecting* 47, no. 4:551-564.

Farquharson, C.G. and D.W. Oldenburg (1993), Inversion of time-domain electromagnetic data for a layered Earth, Geophys. J. Int., 114, 433-442.

Ferré, T., L. Bentley, A. Binley, N. Linde, A. Kemna, K. Singha, K. Holliger, J. A., Huisman, B. Minsley. 2009. Critical steps for the continuing advancement of hydrogeophysics. EOS, 90 (23), 200–201.

Fitterman, D. V. and M. T. Stewart, Transient Electromagnetic Sounding for Groundwater, Geophysics, 51(4), 995-1005, 1986.

Fitterman, D. V. and W. L. Anderson. 1987. Effect of Transmitter Turn-Off Time on Transient Soundings. *Geoexploration* 24, no. 2:131-146.

Freeze, A. R. and J. A. Cherry. 1979. Groundwater. Prentice Hall, Inc..

Frohlich, R.K., D.W. Urish, J. Fuller, and M. O'Reilly (1994), Use of geoelectrical methods in groundwater pollution surveys in a coastal environment, Journal of Applied Geophysics, 32, 139-154.

Gelhar, L. W. and C. L. Axness. 1983. 3-Dimensional stochastic-analysis of macrodispersion in aquifers. *Water Resources Research* 19(1).

Giambastiani, B. M., M. Antonellini, G. H. Essink, and R. J. Stuurman. 2007. Saltwater intrusion in the unconfined coastal aquifer of Ravenna (Italy): A numerical model. *Journal of Hydrology* 340, no. 1-2:91-104.

Goldman, M., D. Gilad, A. Ronen and A. Melloul, Mapping of Seawater Intrusion Into the Coastal Aquifer of Israel by the Time Domain Electromagnetic Method, Geoexploration, 28(2), 153-174, 1991.

Harding Lawson Associates, 1994. Basewide remedial investigation/ Feasibility study Fort Ord, California, Appendix E: Aquifer test results.

Hanson, T. H.. 2003. Geohydrologic Framework of Recharge and Seawater Intrusion in the Pajaro Valley, Santa Cruz and Monterey Counties, California. U.S. Geological Survey, Water-Resources Investigations Report 03-4096.

Herckenrath, D., A. Gazoty, G. Fiandaca, E. Auken, M. Christensen, M. Balicki and P. Bauer-Gottwein, 2011. Sequential and Coupled Hydrogeophysical Inversion of a Groundwater Model using Geoelectric and Transient Electromagnetic Data. Journal of Hydrology, Submitted.

HGG, 2011. Getting started with SiTEM and Semdi, Department of Earth Sciences, University of Aarhus, Denmark. Download from (http://geofysiksamarbejdet.au.dk).

Hinnell, A., T. Ferre, J. Vrugt, J. Huisman, S. Moysey, J. Rings, and M. Kowalsky. 2010. Improved extraction of hydrologic information from geophysical data through coupled hydrogeophysical inversion. *Water Resources Research* 46.

Hubbard, S. S., Y. Rubin, and E. Majer. 1999. Spatial correlation structure estimation using geophysical and hydrogeological data. *Water Resources Research* 35, no. 6:1809-1825.

Hydrometrics LLC. 2009. Seaside groundwater basin modeling and protective groundwater elevations. Report prepared for Seaside Basin Watermaster.

Kemna, A., J. Vanderborght, B. Kulessa, and H. Vereecken. 2002. Imaging and characterisation of subsurface solute transport using electrical resistivity tomography (ERT) and equivalent transport models. *Journal of Hydrology* 267, no. 3-4:125-146.

Kirsch, R., 2006. Petrophysical properties of permeable and low-permeable rocks, Groundwater Geophysics, Springer Berlin Heidelberg, ISBN: 978-3-540-29387-3.

Kowalsky, M. B., S. Finsterle, J. Peterson, S. Hubbard, Y. Rubin, E. Majer, A. Ward, and G. Gee. 2005. Estimation of field-scale soil hydraulic and dielectric parameters through joint inversion of GPR and hydrological data. *Water Resources Research* 41, no. 11.

Lambot, S., E. Slob, J. Rhebergen, O. Lopera, K. Z. Jadoon, and H. Vereecken. 2009. Remote Estimation of the Hydraulic Properties of a Sand Using Full-Waveform Integrated Hydrogeophysical Inversion of Time-Lapse, Off-Ground GPR Data. *Vadose Zone Journal* 8, no. 3:743-754.

Langevin, C. D., D. Fitterman and M. Deszcz-Pan. 2003. Calibration of a Variable-Density Groundwater Flow Model Using Detailed Airborne Geophysical Data. Second International Conference on Saltwater Intrusion and Coastal Aquifers— Monitoring, Modeling and Management. Merida, Mexico.

Langevin, C. D. and W. X. Guo. 2006. MODFLOW/MT3DMS-based simulation of variable-density ground water flow and transport. *Ground Water* 44, no. 3:339-351.

Lebbe, L., N. Van Meir and P. Viaene. 2008. Potential implications of sea-level rise for Belgium. *Journal of Coastal Research* 24, no. 2:358-366.

Lesmes, D. P. and S. P. Friedman. 2005. Relationships between the Electrical and Hydrogeological Properties of Rocks and Soils, Water Science and Technology Library, Volume 50, Part 2, 87-128.

Macaulay, S. and I. Mullen. 2007. Predicting salinity impacts of land-use change: Groundwater modelling with airborne electromagnetics and field data, SE Queensland, Australia. *International Journal of Applied Earth Observation and Geoinformation* 9, no. 2:124-129.

Mann, J.F. 1988, Regarding overdraft and seawater intrusion: Letter to General Manager of Pajaro Valley Water Management Agency, January 1988, 8 p.

Menke, W., 1984. Geophysical Data Analysis: Discrete Inverse Theory, Elsevier, New York.

Mullen, I., K. Wilkinson, R. Cresswell, and J. Kellett. 2007. Three-dimensional mapping of salt stores in the Murra-Darling Basin, Australia - 2. Calculating landscape salt loads from airborne electromagnetic and laboratory data. *International Journal of Applied Earth Observation and Geoinformation* 9, no. 2:103-115.

Nenna, V., D. Herckenrath, N. Odlum and R. Knight. 2011. Sentinel geophysics for coastal aquifers in northern California: Application and evaluation of electromagnetic methods, Journal of Applied Geophysics, Submitted.

Newman,G.A., Hohmann,G.W., and Anderson,W.L. 1986. Transient Electromagnetic Response of A 3-Dimensional Body in A Layered Earth. Geophysics, 51 (8): 1608-1627.

Niwas, S. and O. A. L. de Lima. 2003. Aquifer parameter estimation from surface resistivity data. *Ground Water* 41, no. 1:94-99.

Oldenburg, D. W.. 1990. Inversion of electromagnetic data: An overview of new techniques: Surveys in Geophysics, 11, 231–270.

Paine, J. G. 2003. Determining salinization extent, identifying salinity sources, and estimating chloride mass using surface, borehole, and airborne electromagnetic induction methods. *Water Resources Research* 39, no. 3.

Pollock, D. and O. A. Cirpka. 2010. Fully coupled hydrogeophysical inversion of synthetic salt tracer experiments. *Water Resources Research* 46.

Supper, Robert, Klaus Motschka, Andreas Ahl, Peter Bauer-Gottwein, Bibi Gondwe, Gonzalo Merediz Alonso, Alexander Roemer, David Ottowitz, and Wolfgang Kinzelbach. 2009. Spatial mapping of submerged cave systems by means of airborne electromagnetics: an emerging technology to support protection of endangered karst aquifers. *Near Surface Geophysics* 7, no. 5-6:613-627.

Tan, K., H. Apps, L. Halas, D. Gibson, and K. Lawrie. 2005. Utilizing Airborne Electromagnetic Data To Model The Subsurface Salt Load In A Catchment, Bland Basin, NSW. *Modsim 2005: International Congress on Modelling and Simulation: Advances and Applications for Management and Decision Making: Advances and Applications for Management and Decision Making*:1478-1484.

Tarantola, A. and B. Valette. 1982. Generalized Non-Linear Inverse Problems Solved Using the Least-Squares Criterion. *Reviews of Geophysics* 20, no. 2:219-232.

Topp, G. C., J. L. Davis, and A. P. Annan. 1980. Electromagnetic Determination of Soil-Water Content - Measurements in Coaxial Transmission-Lines. *Water Resources Research* 16, no. 3:574-582.

U.S Army Corps of Engineers. 1997. Preliminary Assessment Camp McQuaide. Santa Cruz County, California.

Vereecken, H., A. Binley, G. Cassiani, A. Revil, and K. Titov. 2006. Applied hydrogeophysics. *Applied Hydrogeophysics* 71:1-8.

Vozoff, K. and D. L. B. Jupp. 1975. Joint Inversion of Geophysical Data. *Geophysical Journal of the Royal Astronomical Society* 42, no. 3:977-991.

Wang,T. and Hohmann,G.W. 1993. A Finite-Difference, Time-Domain Solution for 3-Dimensional Electromagnetic Modeling. Geophysics, 58 (6): 797-809.

Winsauer, W. O. and W. M. Mccardell. 1953. Ionic Double-Layer Conductivity in Reservoir Rock. *Transactions of the American Institute of Mining and Metallurgical Engineers* 198:129-134.

Zhang, Q., R. E. Volker, and D. A. Lockington. 2004. Numerical investigation of seawater intrusion at Gooburrum, Bundaberg, Queensland, Australia. Hydrogeology Journal 12, no. 6:674-687.

III

Coupled hydrogeophysical inversion using time-lapse magnetic resonance sounding and time-lapse gravity data for hydraulic aquifer testing: potential and limitations

Herckenrath, D., Behroozmand, A., Christiansen, L., Auken, E., and P. Bauer-Gottwein

Water Resources Research, in review

Coupled hydrogeophysical inversion using time-lapse magnetic resonance sounding and time-lapse gravity data for hydraulic aquifer testing: Will it work in practice?

Daan Herckenrath[1], Esben Auken[2], Lars Christiansen[1], Ahmad A. Behroozmand[2] and Peter Bauer-Gottwein[1]

1 Department of Environmental Engineering, Technical Univeristy of Denmark, Kgs. Lyngby, Denmark
2 Department of Geoscience, Aarhus University, Aarhus, Denmark

* *Corresponding author: daah@env.dtu.dk*

Abstract

Temporal changes in water content can be directly related to the time-lapse signals retrieved using magnetic resonance sounding (TL-MRS) and relative gravimetry (TL-RG). Previous studies suggest that TL-RG measurements can potentially provide accurate estimates of aquifer characteristics in an aquifer pumping test experiment when used in a coupled hydrogeophysical inversion approach. However, these studies considered highly idealized conditions. The aim of this paper is twofold: 1) we investigate three major issues which likely limit the practical utility of TL-RG for pumping test monitoring: partially penetrating pumping wells in anisotropic aquifers, delayed drainage effects and typical data errors for TL-RG, 2) we introduce TL-MRS in a similar coupled hydrogeophysical inversion framework and compare the performance of TL-MRS and TL-RG for pumping test monitoring. For this purpose we consider a virtual pumping test, for which we generate synthetic drawdown, TL-MRS and TL-RG observations and subsequently determine the aquifer parameters in an inverse parameter estimation approach. The inclusion of TL-RG and TL-MRS data did slightly improve parameter estimates for the specific yield and hydraulic conductivity when considering a fully penetrating well and minimal data error. Using more conservative TL-RG and TL-MRS data error estimates according our own field experience strongly limited the informative value of the TL-RG data; TL-MRS data was less affected by this. For a partially penetrating well under anisotropic conditions parameter uncertainty could be reduced more effectively compared to a fully penetrating well. Delayed drainage effects did not limit the ability of the TL-MRS and TL-RG data to reduce parameter uncertainty significantly. The incorporation of representative measurement error correlation in the TL-RG data neither affected its informative value. A local sensitivity analysis showed that observations were most sensitive to the pumping rate and the thickness, specific yield and hydraulic conductivity of the aquifer. The inclusion of TL-MRS data proved to be more effective to constrain the aquifer parameters compared with TL-RG. The inclusion of both TL-RG and TL-MRS had limited added value compared to TL-MRS only. We conclude that this particular application of coupled hydrogeophysical inversion has a limited potential for TL-RG, while TL-MRS appears to be a more promising method.

1. Introduction

The application of geophysical techniques in combination with hydrologic models has gained much interest in recent years to map subsurface structures and to estimate hydrologic properties [*Vereecken et al.*, 2006]. *Hinnell et al.* [2010] and *Ferré et al.* [2009] discuss the different types of (hydro)geophysical inversion approaches that are used. *Hinnell et al.* [2010] provides an extended list of references to case study applications using different types of coupling approaches. For example, geostatistical techniques can be employed to estimate hydrologic properties using the parameter correlation structure of geophysical models [*Cassiani et al.*, 1998; *Hubbard et al.*, 1999; *Yeh et al.*, 2002; *Chen et al.*, 2004]. [*Hyndman and Gorelick*, 1996], [*Chen et al.*, 2006] and [*Linde et al.*, 2006] are examples of studies were hydrologic parameters are estimated using both hydrologic and geophysical data. In many other studies geo-electrical [*Kemna et al.*, 2002; *Vanderborght et al.*, 2005; *Cassiani et al.*, 2006] and electromagnetic data [*Binley et al.*, 2001; *Day-Lewis et al.*, 2003; *Lambot et al.*, 2004; *Looms et al.*, 2008b, *Knight*, 2001; *Huisman et al.*, 2003] are used to monitor temporal changes in water content or solute concentrations.

Hinnell et al. [2010], *Ferré et al.* [2009], *Kowalsky et al.* [2005], *Pollock and Cirpka* [2010] and *Lambot et al.* [2006, 2009] describe a fully coupled hydrogeophysical inversion approach, in which a hydrological model is part of the geophysical inversion process and a single objective function is minimized which comprises both a geophysical and hydrological component. In other words, both the geophysical and the hydrologic model and their associated observations are used to constrain one another.

An important hydrologic state variable that can be estimated using one of the above inversion approaches is soil water content. As soil water content is difficult to measure, an increasing number of techniques have been suggested to estimate water content and changes in water storage. The strength of most geophysical methods that have been proposed, are their non-invasive character and their ability to provide data with a high spatial resolution. Current employed techniques are predominantly geo-electric methods which estimate the electrical resistivity of the subsurface, e.g. electrical resistivity tomography (ERT), and methods which estimate the relative electrical permittivity of the subsurface based on the measured speed of propagated electromagnetic waves, e.g. ground penetrating radar (GPR). Geo-electric and wave propagation methods, however, do not measure water storage directly, as a petrophysical relationship [*Archie*,

1942; *Topp et al.*, 1980] is needed to convert electrical resistivity and relative permittivity to soil water content. Furthermore, GPR can only be used in high resistivity sediments.

Recently, Magnetic Resonance Sounding (MRS) and relative gravimetry (RG) have emerged as promising methods to map hydrogeological properties. RG is a well-established method to characterize geological structures as locating paleochannels and the delineation of buried bedrock [*Carmichael and Henry*, 1977; *Zawila et al.*, 1997]. Time-lapse RG (TL-RG) surveys have been performed to estimate regional water storage changes and specific yield [*Montgomery*, 1971; *Pool and Eychaner*, 1995, *Jacob et al.*, 2009, *Pool*, 2008], record changes in land-surface elevation [*Wessells and Strange*, 1985], map properties of geothermal fields [*Hunt*, 1970; 1977] and monitor a natural gas reservoir [*van Gelderen et al.*, 1999]. Furthermore, *Poeter* [1990] proposed gravity surveying during an aquifer pumping test to map heterogeneities in aquifer properties around the pumping well.

MRS is well-known for its application in hospitals, where MRI (Magnetic Resonance Imaging) has been used for imaging and medical diagnosis [*Bushong*, 2003; *Körver et al.*, 2010]. Furthermore, MRS has been applied to characterize porosity and fluid properties of oil wells [*Coates et al.*, 1999; Dunn et al., 2002]. For hydrogeological characterization purposes, MRS has been applied to estimate water content, hydraulic conductivity and transmissivity [*Legchenko et al.*, 2002; *Vouillamoz et al.*, 2002; *Wyns et al.*, 2004; *Lachassagne et al.*, 2005], providing information about aquifer boundaries, specific yield and the pore-size characteristics of the subsurface, which can be used to estimate hydraulic conductivity [*Boucher et al.*, 2009; *Chalikakis et al.*, 2008; *Ezersky et al.*, 2010; *Guerin et al.*, 2009]. As suggested by *Lubczynski and Roy* [2003], time-lapse MRS (TL-MRS), can be used as a monitoring tool, which has been applied by *Descloitres et al.* [2008] to monitor groundwater level fluctuations at the discharge point of a watershed in Southern India. In this paper we will use TL-MRS by directly inverting for the change in MRS signal between two soundings at the same location for different times, rather than inverting for the collected MRS data at each separate sounding time.

In contrast to GPR and geo-electrical methods, data retrieved with TL-MRS and TL-RG can directly be related to temporal changes in soil water content without the use of an empirical relationship like Archie's law [*Archie*, 1942] and the Topp equation [*Topp et al.*, 1980]. Both techniques could offer a cost-effective

alternative for monitoring wells to augment aquifer pumping tests in unconfined aquifers [*Poeter*, 1990; *Damiata and Lee*, 2006]. A major advantage of using a non-invasive geophysical method would be the higher flexibility with which water table drawdown can be measured (indirectly) at various locations around the pumping well.

Two recent papers, *Damiata and Lee* [2006] and *Blainey et al.* [2007] demonstrate with synthetic datasets that water table drawdown during aquifer testing with a fully penetrating well could possibly be monitored with TL-RG measurements. In *Damiata and Lee* [2006] the signal-to noise ratios are investigated for such a virtual aquifer pumping test, given instrument accuracy of approximately 1 μGal with portable gravimeters and 0.01 to 0.1 μGal for fixed-station (absolute) gravimeters. In *Blainey et al.* [2007] a coupled hydrogeophysical inversion was subsequently performed for the same synthetic example to complement the drawdown data and obtain better estimates for the specific yield and hydraulic conductivity. For their synthetic example a fully penetrating well was considered and the aquifer was assumed to be homogeneous and isotropic.

In this study, we address three major issues that can significantly limit the practical use of TL-RG data to improve the determination of aquifer properties during pumping tests as described in *Damiata and Lee* [2006] and *Blainey et al.* [2007]: (1) partially penetrating pumping wells in anisotropic aquifers, (2) delayed drainage effects and (3) data error on the geophysical data. Moreover, we extend the coupled inversion approach described by *Blainey et al.* [2007] to assess the potential of TL-MRS data in this framework.

Most pumping tests use a partially penetrating well in an anisotropic aquifer showing delayed drainage. One important reason for using only partially penetrating wells for thick unconfined aquifers is that the cost of screening their full thickness is significant. A second reason for only screening the bottom few meters of the borehole is to protect the well from contamination. In many cases, the aquifer consists of sedimentary deposits, which have an anisotropic hydraulic conductivity tensor [*Boulton*, 1970] where the horizontal hydraulic conductivity is much higher compared to the vertical. When aquifer tests are conducted under the conditions of a partially penetrating well in an anisotropic aquifer (we do not consider horizontal anisotropy [*Ferre and Thomasson,* 2010]), measured drawdown of the free water table can be significantly smaller compared with the drawdown of the piezometric head at the well screen. This will result in much

smaller TL-MRS and TL-RG signals and thus likely limit the applicability of both data types to estimate aquifer properties.

Delayed drainage denotes non-instantaneous release of water from the unsaturated zone during the pumping test. *Narasimhan and Zhu* [1993] showed the importance of including effects of a time-dependent drainage from the unsaturated zone in models of flow to a well in unconfined aquifers and concluded that the rate at which water is released from the unsaturated zone has a similar time-scale at which pumping tests are conducted. This process will result in residual water content above the lowered water table, which influences the magnitude of the signal changes measured by TL-RG and TL-MRS.

In the previous studies of *Damiata and Lee* [2006] and *Blainey et al.* [2007] the instrument precisions were used as the standard errors on synthetic data instead of typical data error levels as seen when measuring real data. In this study, we use typical data errors associated with TL-RG and TL-MRS measurements that can be obtained during field surveys with state of the art equipment. In this paper "measurement error" or "data error" refers to the standard deviation of the errors associated with the hydrogeological and the geophysical data. Recently, *Christiansen et al.* [2011a] and *Jacob et al.* [2009] published results of TL-RG surveys indicating with which accuracy TL-RG data can be collected. These studies indicate measurement errors in the order of 2-4 μGal. A survey by *Chalikakis et al.* [2008] showed MRS data can be obtained with measurement error of approximately 10 nV.

To understand whether TL-MRS and TL-RG data have potential to estimate aquifer properties during unconfined pumping tests, we start with the reproduction of the modeling and inversion results shown in *Blainey et al.* [2007]. Subsequently a coupled hydrogeophysical inversion is performed for 16 realizations of synthetic head, TL-RG and TL-MRS data. Then scenarios are analyzed in which we consider each of the three, previously mentioned practical issues, i.e. partially penetrating well, delayed yield and data error. One additional scenario is used to quantify the combined effect of these limiting factors, while a final scenario takes correlated measurement error for TL-RG data into account. Results are discussed in terms of objective function plots, parameter cross-correlation and parameter uncertainty reduction. Finally, a sensitivity analysis is performed, to identify the impact of the pumping test design variables (and aquifer properties) on the magnitude of the geophysical signals.

2. Methods

2.1 Virtual pumping Test

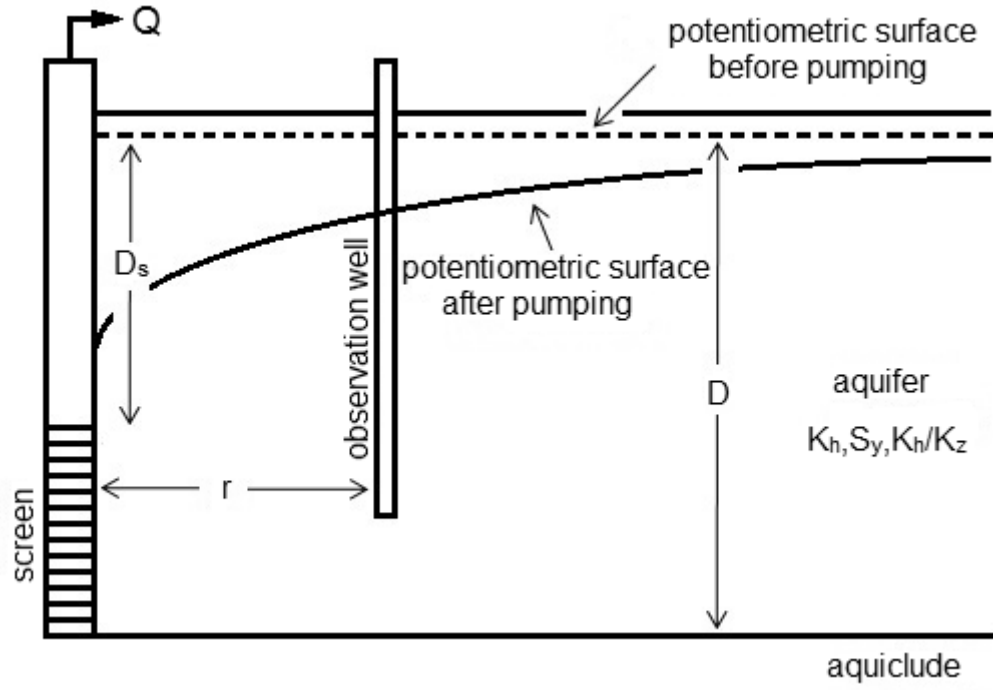

Figure 1 Design of a pumping test (modified from [*Duffield*, 2002]). Parameters are defined in Table 1.

Figure 1 shows a schematic overview of the pumping test configuration that was used for the analysis and Table 1 lists the design parameters for the different scenarios investigated in this paper. Scenario "Fully Penetrating" is the same as the scenario used in *Blainey et al.* [2007] and *Damiata and Lee* [2006]. The water table drawdown is modeled using an analytical expression derived by *Moench* [1997], implemented in the well-documented, widely used software WTAQ [*Barlow and Moench*, 1999]. Under the assumption of instantaneous release of water from storage in the unsaturated zone (instantaneous drainage), this model is equivalent to the solution by *Neuman* [1972, 1973].

Delayed drainage effects were modeled with the approach by *Boulton* [1970] and *Moench* [1997]. In this approach, the decrease in water content in the unsaturated zone $\Delta\theta$ [-] is modeled as an exponential function, using t [d] as the elapsed time since the time of drainage t_d [d]:

$$\Delta\theta(x,y,z,t,t_d) = S_y\left(1 - e^{-(t-t_d(x,y,z))\frac{1}{\alpha_d}}\right) \quad (1)$$

In Equation 1, the delay index $1/\alpha_d$ [-] (listed in Table 1) specifies the rate of an exponential release of water from the unsaturated zone above the water table, with a maximum amount of drainable water content equal to the specific yield S_y [-]. $\Delta\theta$ equals to S_y when instantaneous drainage is assumed. Values for $1/\alpha_d$ have an approximate range of 0.5-2 days and mainly depend on the aquifer material [*Moench*, 1997; *Rajesh et al.*, 2010; *Boulton*, 1970].

Table 1 Parameter values and parameters used for the coupled hydrogeophysical inversion.

Property	Scenario					
	Fully Penetrating	*High Noise*	*Partially Penetrating*	*Delayed Yield*	*Partially Penetrating & Delayed Yield & High Noise*	*Correlated Noise Gravity*
Thickness of aquifer (D), m	50					
Depth to initial water level (hi), m	25					
Hydraulic conductivity (Kh), m/s	10^{-4}					
Anisotropy Kh/Kz	1	1	10	1	10	1
Specific yield (Sy)	0.25					
Radius of borehole, m	0.1					
Well type	Fully Penetrating	Fully Penetrating	Partially Penetrating	Fully Penetrating	Partially Penetrating	Fully Penetrating
Screen interval, m below initial water level	0-50	0-50	40-50	0-50	40-50	0-50
Density of groundwater, kg/m3	1000					
Flow rate (Q), m3/s	0.06309					
Duration of pumping, d	7					
Locations observation wells, m from pumping well	5, 8.3, 13.9, 23.2, 38.7, 64.6, 107.8, 179.8, 300					
Locations RG observations, m from pumping well	5, 8.3, 13.9, 23.2, 38.7, 64.6, 107.8, 179.8, 300					
Locations MRS observations, m from pumping well	5, 179.8					
Measurement error drawdown, cm	5					
Measurement error TL-RG, µGal	2	4	2	2	4	4
Measurement error TL-MRS, nV	10	20	10	10	20	-
Delay index $1/\alpha_d$ [Boulton, 1970], d	0	0	0	2	2	0

2.2 Time-Lapse Relative Gravity

2.2.1 Modeling TL-RG signals caused by water table drawdown

During a survey with a relative gravimeter the vertical component of the gravitational acceleration is measured, which is defined as

$$g = \int_{-\infty}^{\infty}\int_{-\infty}^{\infty}\int_{-\infty}^{\infty}\left[G\frac{\rho(x,y,z)}{r^2}\cos\alpha\right]dxdydz \qquad (2)$$

where $G = 6.673\cdot10^{-11}\mathrm{m^3kg^{-1}s^{-2}}$ is the universal gravitational constant, r [m] is the distance from the instrument to the volume element of density ρ [kg/m^3] and α the angle between the orientation of r and the vertical direction. In this paper, ρ changes due to removal of water during pumping. If storage effects due to the compressibility of water and the aquifer matrix are neglected, the subsurface density will only change between the initial and the pumped water table. Under these assumptions the change in gravity signal Δg [µGal] is given by [*Leirião et al.*, 2009]

$$\Delta g(x,y) = \rho_w G \int_{-\infty}^{\infty}\int_{-\infty}^{\infty}\int_{h_i(x,y)}^{h_f(x,y)} \Delta\theta(x,y,z)\frac{z - z_g}{\left[(x-x_g)^2 + (y-y_g)^2 + (z-z_g)^2\right]^{\frac{3}{2}}} dz dx dy \quad (3)$$

This forward model is valid under the assumption of an unconfined aquifer, where the subsurface density change is equal to the density of water times the change in water content $\Delta\theta$ of the aquifer [*Leirião et al.*, 2009]. As discussed earlier $\Delta\theta$ depends on the specific yield, which has a typical value between 0.01 and 0.3 for unconfined aquifers. h_i is the initial water table [m], h_f the final water table [m], which is computed with the hydraulic model, and provides the integration bounds in the vertical direction. Subscript g denotes the x, y and z coordinate of the gravity instrument and ρ_w the density of water [kg/m^3]. We use an arbitrary radius of 500 m (based on an instrument footprint analysis) as horizontal integration boundaries for Equation 3. A numerical integration was performed for Equation 3 using an adaptive recursive Simpson's rule algorithm (function dblquad in MATLAB). The final water table h_f is location-dependent and is calculated using WTAQ.

2.2.2 RG Instrument

As a Scintrex CG-5 relative gravimeter is commonly used for measuring TL-RG signals, we use the specifications of this instrument to generate synthetic test data. The Scintrex CG-5 uses a fused quartz spring mechanism that reacts to changes in gravitational force. *Merlet* [2008] documents an instrument accuracy of ca. 1 μGal for the Scintrex CG-5 relative gravimeter.

Leirião et al. [2009] characterize the footprint of the relative gravimeter as a function of the depth to the target. At the reference station drawdown should be zero within the footprint of the instrument. For example, when the initial water table is at 20 m depth, approximately 90% of the gravity signal comes from a circular area with a radius of approximately 200 m.

Christiansen et al. [2011a] provides a thorough discussion of various important corrections and precautions that need to be made when doing surveys with a relative gravimeter. For example, each time a measuring station is reoccupied, instrument heights should be the same. When the height of a gravimeter has changed only a few millimeters in between the station occupations, this will introduce an error which is comparable with the instrument resolution of 1 μGal. Furthermore corrections have to be made to account for e.g. instrument tilt, ocean loading, air pressure, tidal corrections and ground movement. However, the

magnitude of these processes still affects the accuracy with which the gravity signal is measured, as these corrections are not perfect.

The measurements of relative gravimeters are also influenced by instrument drift, i.e. the zero position of the spring does not remain constant with time. Instrument drift effects are time dependent and are caused by the instrument properties. Drift effects cannot be identified separately and are typically approximated with a linear drift coefficient for time periods of a few hours. This coefficient has a value in the order of 20 μGal/hr. Contributions to this total drift can be subdivided into two groups: spring aging drift and transport drift, which are discussed more thoroughly in *Christiansen et al.* [2011a]. Assuming the drift to be linear can result in correlated measurement errors induced by imperfect corrections for e.g. ocean loading, as is depicted in Figure 4 in *Christiansen et al.* [2011a].

When measuring temporal changes in gravity signal Δg, typically a gravity network is repeatedly measured. During such a survey, a reference station is selected where the change in gravity signal is assumed to be unaffected by mass changes induced by the pumping test. At the reference station the gravity value is usually set to zero. Gravity differences δg_{obs} are recorded with the gravimeter between the different stations of the gravity network. To calculate separate gravity values for each network station (or gravity observation point) we have to perform a network adjustment by solving Equation 4, in which gravity signals g_{est} [μGal] are estimated for the different network stations together with a linear instrument drift coefficient c [μGal/hr]. This is done by a least-squares fit of the differences in gravimeter readings δg_{obs} [μGal] between the stations and the use of a design matrix [a_{ij}] associated with the specific network configuration. The design matrix includes values of +1 or -1, 0 or the time difference [hr] between two gravity measurements, where n indicates the number of gravity differences that are measured and where m marks the number of gravity stations that is occupied.

$$\begin{pmatrix} \delta g_{obs,1} \\ \delta g_{obs,2} \\ \vdots \\ \delta g_{obs,n} \end{pmatrix} = \begin{pmatrix} a_{11} & a_{12} & \cdots & a_{1m} \\ a_{21} & \ddots & & \vdots \\ \vdots & & & \vdots \\ a_{n1} & \cdots & \cdots & a_{nm} \end{pmatrix} \begin{pmatrix} c \\ g_{est,1} \\ \vdots \\ g_{est,m} \end{pmatrix} + \varepsilon \qquad (4)$$

After this least squares-adjustment a posteriori measurement error $\sigma_{g_{est}}$ [µGal] (referred to as σ_{GRAV} [µGal] throughout the rest of this paper) can be calculated, based on the residuals ε [µGal] and a weight matrix based on the measurement errors $\sigma_{g_{obs}}$ [µGal] associated with the individual gravimeter readings. To obtain the temporal change in gravity signal Δg (Equation 3) at each gravity observation location, the same network has to be measured again at a later time in order to determine the change in g_{est}.

Christiansen et al. [2011a] reported measurement errors σ_{GRAV} of 2-3 µGal. *Gehman et al.* [2009] reported a measurement error of 4.76 µGal, based on the cumulative error associated with an instrument precision of 3 µGal and the error resulting from uncertainties in instrument height and corrections for surface water and instrument drift. However, *Gehman et al.* [2009] did not propagate the a priori errors associated with the gravimeter readings through the network adjustment procedure. *Jacob et al.* [2009] used an approach in which the observed variance in gravimeter readings per network station were used to calculate the weight matrix associated with δg_{obs} and reported a σ_{GRAV} ranging between 1.2-2.4 µGal. Using the same methodology for a 2 year survey, *Jacob et al.* [2010] published values of 2.5-5 µGal.

To account for typical measurement errors in the analyses, we investigate uncorrelated gravity data with a measurement error σ_{GRAV} of 2 µGal and a more conservative estimate of 4µGal. In addition to that, we also perform an analysis with correlated measurement errors, in which we include one of the typical problems associated with the assumption of a linear instrument drift, by adding a diurnal varying drift component that could not be captured with the linear drift coefficient [*Christiansen et al*., 2011a].

2.3 Magnetic Resonance Sounding

2.3.1 Modeling TL-MRS signals caused by water table drawdown

With Magnetic Resonance Sounding (MRS) the spins of the hydrogen protons of water molecules in the subsurface are excited with an external magnetic field and the signal response resulting from precession of the protons is measured, after the external magnetic field is switched off. The quantum mechanical phenomenon of nuclear magnetic resonance can be described by the Bloch-equations on the macroscopic level. The Bloch equations are the basis for modeling the MRS

signal due to the water content distribution in the subsurface [e.g. *Legchenko and Valla*, 2002]

$$E(t) = -\int_{-\infty}^{\infty}\int_{-\infty}^{\infty}\int_{-\infty}^{\infty}\left[\begin{array}{l}\omega_0 M_0 \theta(x-x_{MRS}, y-y_{MRS}, z_{MRS}-z) b_{\perp}^{Rx}(x-x_{MRS}, y-y_{MRS}, z_{MRS}-z)\cdot \\ \sin(\frac{1}{2}\gamma b_{\perp}^{Tx}(x-x_{MRS}, y-y_{MRS}, z_{MRS}-z)q) e^{-\frac{t}{T_2^*(x-x_{MRS}, y-y_{MRS}, z_{MRS}-z)}}\end{array}\right] dzdxdy \quad (5)$$

where $\omega_0 = \gamma B_0$, is the angular Larmor frequency of the Earth's magnetic field B_0 [T] at which the external magnetic pulse is applied. q=I τ denotes the excitation pulse length, where I is the current amplitude in the transmitter loop [A] and τ [s] is the pulse duration. M_0 is the nuclear magnetization for protons in water at thermal equilibrium [A/m or J/T/m^3], γ and θ are the gyromagnetic ratio for the protons (0.2675 rad/s/nT) and the free water content of the subsurface [-]. Subscript MRS denotes the x, y and z coordinate of the MRS instrument, and $b_{\perp}^{Tx}$ represents the magnetic field that would be created by a unit current in the transmitting antenna. For a coincident circular loop configuration (transmitter and receiver loops are the same) with a radius of a [m], $b_{\perp}^{Rx} = b_{\perp}^{Tx} = \sqrt{(\cos(\delta)b_z + \sin(\delta)\sin(\varphi)b_r)^2 + (\cos(\varphi)b_r)^2}$, where b_r and b_z are the radial and vertical components of the magnetic induction field [T/A], respectively. Angles δ and φ represent the inclination and the azimuth angle of the Earth's magnetic field. In the following, we assume a resistive half-space. Finite subsurface resistivity can be taken into account when interpreting MRS data [*Legchenko*, 2004; *Braun and Yaramanci*, 2008]. However, for reasons of clarity and simplicity, we use the infinite resistivity earth model. Under this assumption, b_r and b_z can be expressed in terms of elliptic integrals [*Legchenko and Valla*, 2002], using a composite parameter

$$m(a,r,z) = \sqrt{\frac{4ar}{(a+r)^2 + z^2}} \quad (6)$$

where r and z are the distance and the depth with respect to the loop. The radial (b_r) and vertical components (b_z) of the magnetic induction field are:

$$b_r(a,r,z) = \frac{\mu}{2\pi\sqrt{(a+r)^2+z^2}}\left[\begin{array}{l}\frac{2\cdot a\cdot z}{(a-r)^2+z^2}E(m(a,r,z)) - \\ \frac{4\cdot a\cdot z}{(a+r)^2+z^2}F(m(a,r,z))\end{array}\right] \quad (7)$$

$$b_z(a,r,z) = \frac{\mu}{2\pi\sqrt{(a+r)^2+z^2}}\left[\frac{a^2-r^2-z^2}{(a-r)^2+z^2}E(m(a,r,z)) + L(m(a,r,z))\right] \quad (8)$$

with

$$L(m) = \int_0^{\pi/2} \frac{1}{\sqrt{1 - m^2(\sin(\psi))}} d\psi \tag{9}$$

$$E(m) = \int_0^{\pi/2} \sqrt{1 - m^2(\sin(\psi))} d\psi \tag{10}$$

$$F(m) = \frac{L(m) - E(m)}{m^2} \tag{11}$$

ψ is the horizontal angle with respect to the magnetic north and also calculated based on the Cartesian coordinates.. Equation 5 was modified to simulate the temporal change in initial amplitude of the signal ($E(t = 0)$), due to a change in water content $\Delta\theta$ which depends on the water table drawdown and specific yield of the aquifer, resulting in

$$\Delta E(q) = -\int_{-\infty}^{\infty}\int_{-\infty}^{\infty}\int_{h_i(x,y)}^{h_f(x,y)} \left[K(q, x - x_{MRS}, y - y_{MRS}, z_{MRS} - z)\Delta\theta(x, y, z)\right] dz dx dy \tag{12}$$

with integration kernel:

$$\begin{aligned} &K(q, x - x_{MRS}, y - y_{MRS}, z_{MRS} - z) = \omega_0 M_0 b_{\perp}^{Rx}(x - x_{MRS}, y - y_{MRS}, z_{MRS} - z) \cdot \\ &\sin\left(\frac{1}{2}\gamma b_{\perp}^{Tx}(x - x_{MRS}, y - y_{MRS}, z_{MRS} - z)q\right) \end{aligned} \tag{13}$$

In this paper we consider initial amplitude data *E*(t=0) only. An alternative approach is to invert for the relaxation constant T_2^*, which can be correlated with the hydraulic conductivity of the aquifer [e.g. *Mueller-Petke and Yaramanci*, 2010]. To calculate the TL-MRS-response, based on Equation 12, we use the same numerical integration method as was applied for the TL-RG forward model. During this numerical integral calculation, Equation 12 is evaluated for different combinations of x, y and z coordinates. When these coordinates are transformed to cylindrical coordinates, *K* can still be solved for in terms of elliptic integrals. The integration bounds for z are location dependent (x,y), as in our application the integration bounds for the depth are equal to the initial groundwater level (h_i) and the water table during pumping (h_f), which is calculated by the pumping test modeling software WTAQ. As we use temporal changes in MRS signal, Equation 12 is applied to account for the differences in MRS signal that are measured before and after pumping. We assume the change in TL-MRS signal is only caused by the amount of drained water that was stored between the initial and the pumped water table.

The MRS code was benchmarked against the analytical solutions presented in *Legchenko and Valla* [2002] for infinitely thin sheets of water with an infinite lateral extent at different depths. Figure 2 shows the values calculated with our numerical model together with the analytical solutions in *Legchenko and Valla* [2002], which are in good agreement. Major factors influencing the speed of our forward code were the integration bounds, the accuracy of the numerical integral evaluation and the depth at which the sheet of water is positioned. *Legchenko and Schushakov* [1998] provide the definition of proper integration bounds for the MRS forward model.

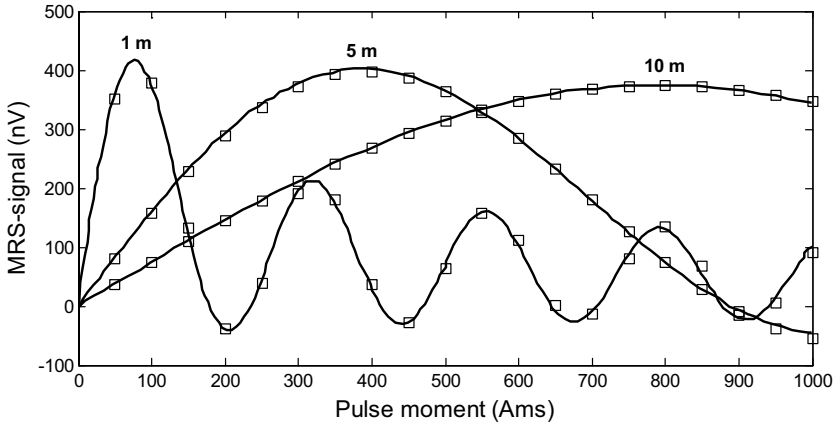

Figure 2 Validation of numerical MRS-code (squares) against infinite sheet solution (smooth lines) presented in *Legchenko and Valla* [2002] for an infinite sheet of water at 1, 5 and 10 m beneath the MRS instrument for a circular loop (a= 50m) over an infinitely resistive halfspace at a 90˚ magnetic inclination (B_0=60000 nT).

2.3.2 MRS Instrument

For generating the TL-MRS observations we consider the properties of a NUMIS^{plus} system. The NUMIS^{plus} device consists of an oscillating current generator, a receiver, a MRS signal detector, a transmitter/receiver loop and a microprocessor. The transmitter generates the reference frequency equal to the Larmor frequency. The signal is recorded by the receiver at a frequency of 10-20 kHz and from its envelope the parameters initial amplitude E(t=0) and relaxation time are estimated [*IRIS Instruments*, 2010]. The measured signals are affected by environmental noise sources caused by external electromagnetic interference such as electrical discharges in the atmosphere, magnetic storms, etc. Interference may also be due to the ambient noise produced by power lines and electric fences. Furthermore, the electrical resistivity of the subsurface induces attenuation of the signal as it also affects the calculation of the integration kernel (K) of Equation 12 [*Legchenko and Valla*, 2002; *IRIS Instruments*, 2010]. Note that this effect is not taken into account in our implementation as it is small for

moderate and high resistivities of the ground (> 100 Ohm.m). Measurements are often performed in the range of 0-4 s. For a sequence of pulse lengths (q), the noise, initial amplitude and relaxation time are measured. These pulse lenghts are often spaced denser for smaller values of q due to high spatial variation of the kernel function in the shallow parts. The parameters of the currently available NUMIS^{plus} system and other surface MRS equipments do not permit measurements of very short signals (earlier times than about 20 ms) corresponding to "bounded" water in the subsurface [*IRIS Instruments*, 2010]. As with RG, expected signal-to-noise ratios for MRS in a pumping test experiment are relatively small (compared to drawdown data). For MRS data errors were estimated from measurements in Denmark with a NUMIS^{plus} system presented by *Chalikakis et al.* [2008]. These results indicate that measurement errors of 10 nV can be achieved. However, in our field campaigns, we have experienced measurement errors of around 20 nV in good noise conditions. Figure 3 shows an example plot of a noise measurement during an MRS sounding in Denmark in terms of the mean amplitude of the MRS-signal. Note that the plot constitutes a single noise measurement (pre-stacked) and the two peaks represent the energizing pulses that are used to conduct the MRS-measurements. The pre-stacked standard deviation of the noise is around 27 nV which is a perfect condition for a MRS survey. When the measurements are repeated a number of times (stacked) a post-stacked measurement error of 20 nV can be obtained.

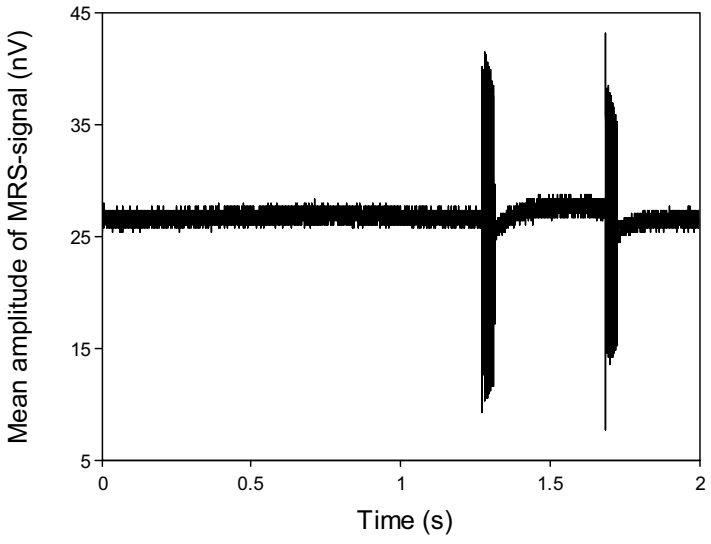

Figure 3 Noise measurements during an MRS sounding in Skive, Denmark. The pre-stacked standard deviation of the noise is around 27 nV, indicated by the mean amplitude of the retrieved MRS signal. Two peaks of 40 ms width represent the energizing pulses injected into the loop by the instrument (double-pulse measurement).

3. Coupled Hydrogeophysical Inversion

A coupled hydrogeophysical inversion was carried out to estimate the specific yield S_y [-] and the hydraulic conductivity K_h [m/s] based on drawdown data, TL-RG and TL-MRS data. This was done in order to evaluate the value of TL-RG and TL-MRS data for six different pumping test scenarios: (1) a fully penetrating well with low-noise geophysical data, (2) a fully penetrating well with high-noise geophysical data, (3) a partially penetrating well in an anisotropic aquifer, (4) a fully penetrating well in an aquifer showing delayed drainage effects, (5) a real-world scenario of a partially penetrating well in an anisotropic aquifer showing delayed yield in combination with high-noise geophysical data and (6) TL-RG data with correlated measurement errors. Table 1 summarizes the properties for the six pumping tests scenarios that were investigated. For each of these scenarios, we generated 16 different realizations of synthetic drawdown, TL-RG and TL-MRS measurements for subsequent parameter estimation.

3.1 Parameterization and Optimization Algorithm

The applied coupled hydrogeophysical inversion approach proceeds in the following steps: first water table drawdown is simulated with a pumping test model, with K_h and S_y as input parameters. The simulated drawdown and S_y are then used to determine, respectively, the integration bounds and the change in water content $\Delta\theta$ to calculate the change in the geophysical signals with the TL-MRS and TL-RG forward models.

The synthetic observations are subsequently perturbed with random data error, according to the expected measurement errors for each observation type. The gradient-search algorithm PEST [*Doherty*, 2010] was used to iteratively update specific yield and hydraulic conductivity until the optimal fit between the synthetic observations and simulated data is achieved. Parameter starting values were varied between 0.1 and 0.4 for S_y and -3.75 and -4.25 m/s for the log10 of K_h.

To be consistent with *Blainey et al.* [2007] we consider 9 observation points for drawdown and gravity measurements at 5.0, 8.3, 13.9, 23.2, 38.7, 64.6, 107.8, 179.8 and 300 m distance from the extraction well. Only two observation locations for the MRS-instrument are used, situated at 5 and 179 m from the pumping well. MRS data comprises initial amplitude data measured at 8 pulse lengths between 0.5-4.0 A·s, covering a similar range as measured by *Chalikakis*

et al. [2008] and example data in the NUMIS^{plus} manual [*IRIS Instruments*, 2010].

3.2 Observations and Measurement Error

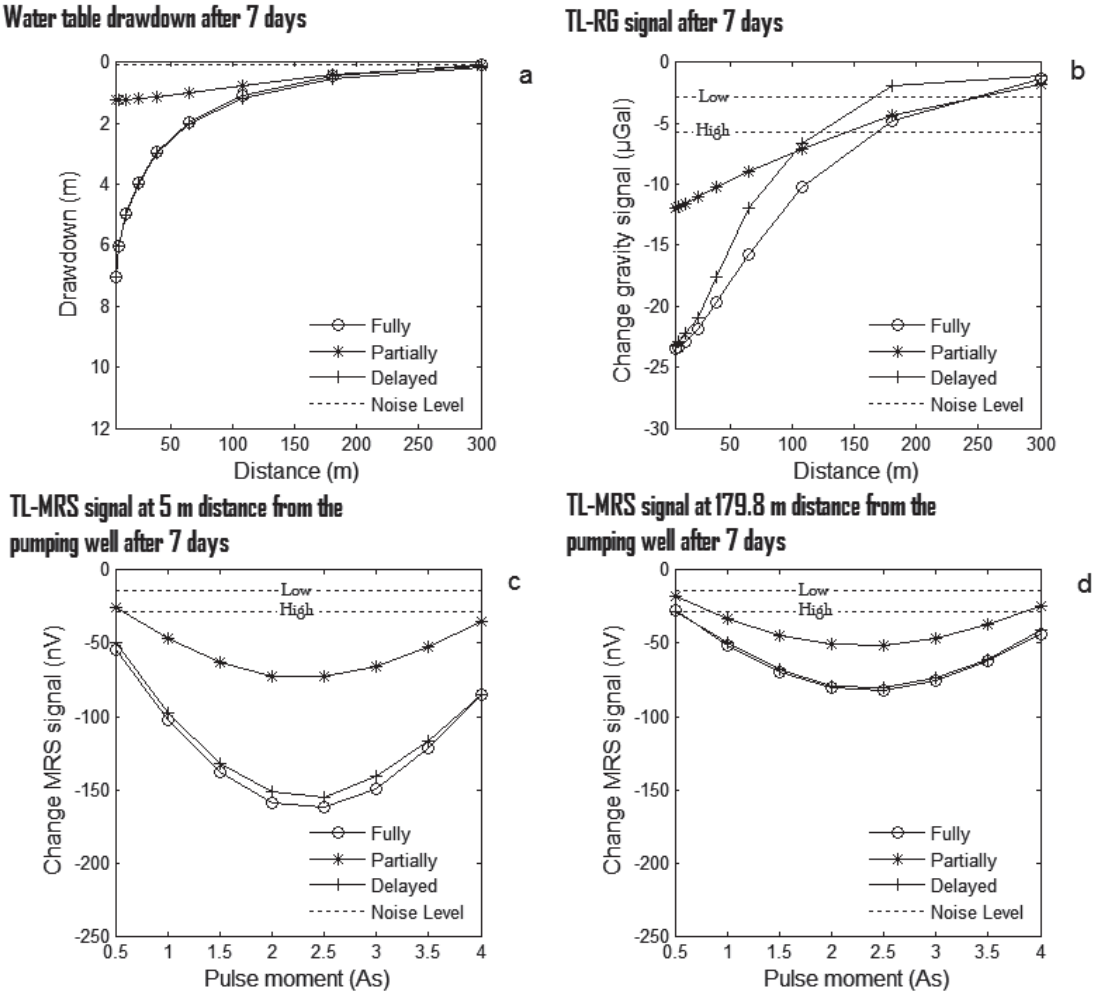

Figure 4 Water table drawdown (a) and simulated TL-RG data (b) after seven days of pumping for a fully and partially penetrating well and the inclusion of delayed yield. (c) and (d) show the TL-MRS signal at respectively 5.0 and 179.8 m from the extraction well. Note this figure shows the synthetic data without the added measurement errors. Indicated by the dashed lines are the standard deviations of the measurement errors ('Noise level') that were used to generate the synthetic TL-RG and TL-MRS observations.

3.2.1 Simulated Drawdown, TL-RG and TL-MRS signals for a pumping test

Figure 4a shows the water table drawdown at the nine observation points obtained after 7 days of pumping given $K_h=10^{-4}$m/s and $S_y=0.25$ for a fully penetrating well. Figure 4b visualizes the corresponding TL-RG response for all

measurement points (same as piezometers). Figures 4c and 4d show the TL-MRS signal obtained at respectively 5.0 m and 179.8 m from the pumping well. In the figures also the standard deviation of the added measurement errors are plotted ("Noise level"), which were used for the generation of the synthetic observations.

The plots for the partially penetrating well in Figure 4 show a significantly smaller decrease in TL-MRS and TL-RG signal. The TL-RG signals are reduced by more than a factor of two for measurements close to the pumping well. Near the pumping well gravity changes are in the order of 10 μGal. The range of the received TL-MRS signal at 5 meters from the pumping well is reduced from 50-150 nV to a range of 30-60 nV.

3.2.2 Generation of synthetic observations

To estimate S_y and K_h we generated 16 synthetic observation sets, including drawdown, TL-RG and TL-MRS data, to which random/uncorrelated measurement error was added. Table 1 lists the standard deviation of the applied data errors for the different observation types which were used per scenario. We assumed a measurement error of 5 cm for the drawdown data [*Blainey et al.*, 2007], 2-4 μGal for the TL-RG measurements and 10-20 nV for the TL-MRS measurements.

In the scenario "Correlated Noise Gravity" we added correlated measurement error to the TL-RG data. For this purpose we generated a set of gravimeter readings (g_{rel}) with a measurement error of 4 μGal to which we added a linear drift of 20 μGal/hr and a sinusoidal drift component with a period of 1 day and amplitude of 5 μGal. The sinusoidal drift is assumed to represent errors in the various corrections applied to the TL-RG data and is unknown for any specific field application. RG measurements in a "star"-network are assumed [*Christiansen et al.*, 2011a], where first a reference station "REF" is measured (not impacted by the pumping test), after which each of the 9 gravity observation locations G_i are occupied. The reference station is re-occupied after each station occupation (sequence REF-G_1-REF-G_2-…-G_9-REF). Between every occupation we assume a time interval of 10 minutes, i.e. a total measurement period of 190 minutes. For each of these network stations we estimate an individual gravity signal by solving Equation 4 (network adjustment), assuming a linear instrument drift. The unknown sinusoidal drift component results in correlated data errors. This procedure is executed for a time period before the pumping test starts and after 7 days of pumping. For the measurements after 7 days of pumping, we assume the sinusoidal drift component to have a 12-hour phase shift compared to

the pre-pumping survey. This numerical experiment results in one set of TL-RG observations with correlated errors. Note that error correlation in TL-RG surveys depends on the network configuration, the magnitude of the unknown drift components and the duration of the survey and will thus be different for every field experiment.

3.3 Objective Function & Parameter Uncertainty

For both the TL-RG and the TL-MRS we calculate the fit between the simulated and "observed" water table drawdown and geophysical data with the following objective function

$$\phi_{total} = (1 - w_{GRAV} - w_{MRS}) \cdot \left[\frac{1}{N_{HEADS}} \sum_{i=1}^{N_{HEADS}} \frac{\left(h_{meas,i} - h_{sim,i}\right)^2}{\sigma^2_{h_{meas},i}} \right]^{\frac{1}{2}} + w_{GRAV} \cdot \left[\frac{1}{N_{GRAV}} \sum_{i=1}^{N_{GRAV}} \frac{\left(GRAV_{meas,i} - GRAV_{sim,i}\right)^2}{\sigma^2_{GRAV_{meas},i}} \right]^{\frac{1}{2}} + w_{MRS} \cdot \left[\frac{1}{N_{MRS}} \sum_{i=1}^{N_{MRS}} \frac{\left(MRS_{meas,i} - MRS_{sim,i}\right)^2}{\sigma^2_{MRS_{meas},i}} \right]^{\frac{1}{2}} \quad (14)$$

where N_{HEADS} indicates the number of head data (9 in our case) and N_{GRAV} and N_{MRS} indicate the number of the different geophysical observations (9 for the TL-RG, 16 for the TL-MRS). h, GRAV and MRS indicates the simulated and observed head, TL-RG, and TL-MRS signals. σ_h, σ_{GRAV} and σ_{MRS} represent the standard deviation of the measurement error associated with the different observations. w_{GRAV} and w_{MRS} are subjective weights defining the trade-off between the geophysical and hydrological observation misfit, where $w_{HEADS} = 1 - w_{GRAV} - w_{MRS}$.

Determination of the optimal value for w_{GRAV} and w_{MRS} in reducing parameter uncertainty was not pursued in this research. In order to perform such a weight analysis, a Pareto method can be employed as described in *Christiansen et al.* [2011b] and *Moore et al.* [2010]. *Blainey et al.* [2007], using a similar model setup, report that parameter uncertainty is not very sensitive to different nonzero values of w_{GRAV}. However, they did observe a trend where larger values for w_{GRAV} result in more accurate specific yield estimates and less accurate hydraulic conductivity estimates. For this paper, we choose to use the same values for these subjective weights in order to respect their relative signal-to-noise ratios. For example, when TL-RG, TL-MRS and drawdown data are used, w_{GRAV} and w_{MRS} were assigned a value of 1/3. For more complex hydrological models the impact of w_{GRAV} can be of more significance. Still, the added measurement errors

could incorporate some degree of structural error, since the number of synthetically generated observations was small. This effect is reduced by performing the coupled hydrogeophysical inversion for 16 different observation realizations. Parameter uncertainty and parameter cross-correlations are subsequently estimated based on the posteriori covariance matrix for the calibrated parameter sets [*Doherty*, 2010].

Figure 5 shows 15 objective function plots pertaining to three different situations when no measurement errors are added to the synthetically generated measurements. The first column of plots in Figure 5 shows the individual objective function components associated with the drawdown, TL-RG and TL-MRS data and the combined objective function for a fully penetrating well when assuming unrealistically low data errors for the TL-RG and TL-MRS data (respectively 0.4 μGal and 2 nV) to illustrate how drawdown and geophysical data constrain one another. The plot associated with the drawdown component indicates that the hydraulic conductivity is well determined in contrast to the specific yield. Plots for the TL-RG and TL-MRS component show a nearly similar shape, illustrating that hydraulic conductivity and specific yield cannot be determined with MRS and RG data only. The combined objective function shows a clear improvement in the objective function surface highlighting a clear global minimum in comparison with the more stretched surfaces for the individual data types. The second column of plots in Figure 5 pertains to a fully penetrating well where we assume a measurement error of 5 cm for drawdown data and respectively 2 μGal and 10 nV for the gravity and MRS observations. The combined objective function surfaces do not vary significantly from the one associated with the drawdown objective function component as the signal-to-noise ratio for the geophysical data is much lower compared to the drawdown data. The third column of plots in Figure 5 applies to a partially penetrating well in anisotropic conditions. The plots for the TL-RG and TL-MRS data show a similar pattern compared with the fully penetrating well. The drawdown objective function plot shows that the hydraulic conductivity cannot be resolved as well as for the fully penetrating well. Combining the drawdown and geophysical data in this situation could potentially be very powerful as the objective function valleys associated with the geophysical data have a different orientation compared with the drawdown component, allowing for a well-defined global minimum. However, the information contained in the geophysical data is reduced, due to much smaller signal-to-noise ratios. This causes the combined objective functions in Figure 5 (column 3, row 4 and 5) to have a nearly similar shape as the drawdown objective function.

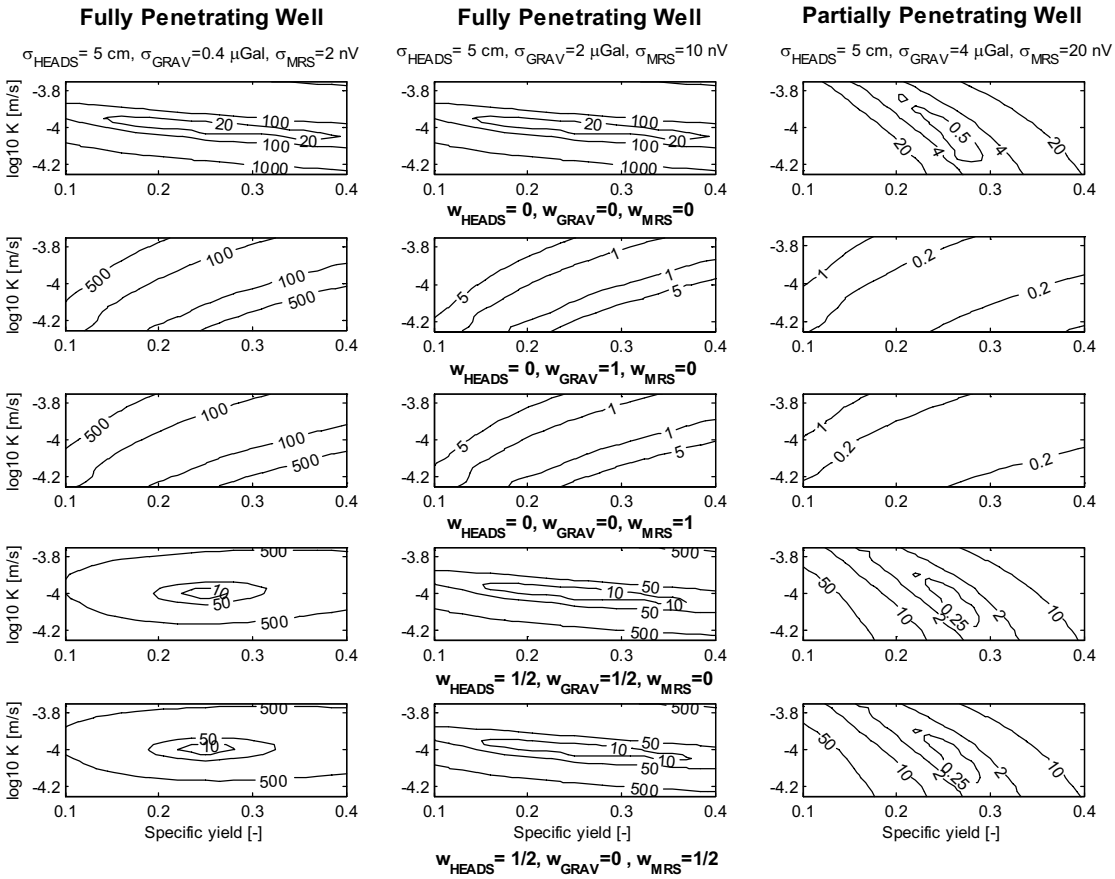

Figure 5 Objective function surfaces for the drawdown, gravity and MRS objective component together with the combined objective function surfaces for a fully and partially penetrating well with a S_y=0.25 and K_h=10^{-4} m/s. Weights for each data type that contribute to the objective function are plotted underneath. The first column of plots pertains to TL-MRS and TL-RG data with unrealistically small measurement errors (0.4 μGal, 2 nV). The second column represents a fully penetrating well in combination with typical signal-to-noise ratios (0.05 m, 2 μGal, 10 nV) for the different data types. The third column represents a partially penetrating well in combination with typical signal-to-noise ratios for the different data types, clearly showing a different orientation of the objective function surface pertaining to the drawdown and the geophysical data.

4. Inversion Results

4.1 Fully Penetrating Well

To assess to what extent the addition of the TL-MRS and TL-RG observations improve the estimation of the specific yield and hydraulic conductivity, cross-correlation values between the specific yield and hydraulic conductivity and their uncertainty are listed in Table 2 for each of the scenarios discussed in this paper. Note that the values listed in Table 2 are average values pertaining to the inversion results of 16 different observation realizations that were used to calculate each scenario listed in Table 1. For a fully penetrating well, parameter

cross-correlation indicates that both parameters can be identified separately, since its value is significantly smaller than 1.00. However, due to low sensitivity of the specific yield with respect to the drawdown measurements [*Blainey et al.*, 2007], the uncertainty range for this parameter is rather large. When introducing TL-MRS or TL-RG measurements in the inverse process, which are more sensitive to the specific yield of the aquifer, parameter cross-correlation drops from -0.86 to respectively -0.80 and -0.82. This also results in a decrease of the uncertainty ranges for the specific yield and hydraulic conductivity with approximately 30%; average parameter estimates do not change significantly for the different calibration datasets. Parameter uncertainty bounds, calculated based on the posteriori covariance matrix, show the "true" aquifer properties were captured within 2 standard deviations of the estimated parameter values.

Table 2 Inversion results showing data misfit, parameter cross-correlation, estimated values, uncertainty ranges and uncertainty reduction percentages for the hydraulic conductivity and specific yield for different observation data sets and each scenario described in Table 1.

Calibration dataset	RMSE[a]	Cr-Corr[b] Sy-Kh	Kh[c] (m/s)	Parameter uncertainty (%)[d]	Uncertainty reduction [%][e]	Sy[c] (-)	Parameter uncertainty (%)[d]	Uncertainty reduction [%][e]	Scenario
Truth	-	-	$1 \cdot 10^{-4}$	-	-	0.25	-	-	Truth
Heads	0.82	-0.86	$9.99 \cdot 10^{-5} \pm 2.35 \cdot 10^{-6}$	2%	-	0.251 ± 0.022	9%	-	Fully Penetrating
Gravity	0.77	1.00	$1.07 \cdot 10^{-4} \pm 2.60 \cdot 10^{2}$	>> 100 %	-	0.259 ± 2.248	>> 100 %	-	
MRS	0.86	0.99	$1.07 \cdot 10^{-4} \pm 1.96 \cdot 10^{-4}$	>> 100 %	-	0.278 ± 0.339	>> 100 %	-	
Heads & Gravity	0.86	-0.80	$1.00 \cdot 10^{-4} \pm 1.79 \cdot 10^{-6}$	2%	24%	0.250 ± 0.016	6%	27%	
Heads & MRS	0.92	-0.82	$9.98 \cdot 10^{-5} \pm 1.58 \cdot 10^{-6}$	2%	33%	0.252 ± 0.014	6%	34%	
Heads & Gravity & MRS	0.92	-0.77	$1.00 \cdot 10^{-4} \pm 1.45 \cdot 10^{-6}$	1%	38%	0.251 ± 0.013	5%	42%	
Heads	0.82	-0.86	$9.99 \cdot 10^{-5} \pm 2.35 \cdot 10^{-6}$	2%	-	0.251 ± 0.022	9%	-	High Noise
Heads & Gravity	0.93	-0.84	$9.99 \cdot 10^{-5} \pm 2.08 \cdot 10^{-6}$	2%	11%	0.252 ± 0.019	8%	12%	
Heads & MRS	0.95	-0.85	$1.00 \cdot 10^{-4} \pm 1.73 \cdot 10^{-6}$	2%	26%	0.250 ± 0.016	6%	28%	
Heads & Gravity & MRS	0.92	-0.84	$1.00 \cdot 10^{-4} \pm 1.74 \cdot 10^{-6}$	2%	26%	0.251 ± 0.016	6%	27%	
Heads	0.83	-0.87	$9.99 \cdot 10^{-5} \pm 2.43 \cdot 10^{-6}$	2%	-	0.251 ± 0.023	9%	-	Delayed yield
Heads & Gravity	0.86	-0.83	$1.00 \cdot 10^{-4} \pm 1.89 \cdot 10^{-6}$	2%	22%	0.250 ± 0.018	7%	24%	
Heads & MRS	0.93	-0.83	$9.98 \cdot 10^{-5} \pm 1.60 \cdot 10^{-6}$	2%	34%	0.252 ± 0.015	6%	35%	
Heads & Gravity & MRS	0.92	-0.79	$1.00 \cdot 10^{-4} \pm 1.49 \cdot 10^{-6}$	1%	39%	0.251 ± 0.014	5%	41%	
Heads	0.76	-0.97	$1.01 \cdot 10^{-4} \pm 5.91 \cdot 10^{-5}$	58%	-	0.250 ± 0.057	23%	-	Partially Penetrating
Heads & Gravity	0.83	-0.96	$1.04 \cdot 10^{-4} \pm 4.97 \cdot 10^{-5}$	33%	42%	0.247 ± 0.036	14%	38%	
Heads & MRS	0.90	-0.93	$9.74 \cdot 10^{-5} \pm 3.02 \cdot 10^{-5}$	31%	49%	0.254 ± 0.033	13%	43%	
Heads & Gravity & MRS	0.83	-0.92	$9.94 \cdot 10^{-5} \pm 2.91 \cdot 10^{-5}$	29%	51%	0.251 ± 0.032	13%	44%	
Heads	0.77	-0.98	$1.02 \cdot 10^{-4} \pm 4.46 \cdot 10^{-5}$	44%	-	0.250 ± 0.061	25%	-	Partially Penetrating & High Noise & Delayed yield
Heads & Gravity	0.92	-0.97	$1.00 \cdot 10^{-4} \pm 3.61 \cdot 10^{-5}$	36%	19%	0.250 ± 0.052	21%	15%	
Heads & MRS	0.92	-0.97	$1.00 \cdot 10^{-4} \pm 2.81 \cdot 10^{-5}$	27%	37%	0.249 ± 0.041	16%	34%	
Heads & Gravity & MRS	0.96	-0.97	$1.00 \cdot 10^{-4} \pm 2.76 \cdot 10^{-5}$	27%	38%	0.251 ± 0.040	16%	34%	
Heads & Gravity	0.84	-0.84	$1.00 \cdot 10^{-4} \pm 1.97 \cdot 10^{-6}$	2%	16%	0.250 ± 0.018	7%	17%	Correlated Noise Gravity

[a] Root Mean Square Error, [b] Cross-correlation, [c] Mean ± 2 standard deviations, [d] relative to the estimated parameter value, [e] percentual decrease of parameter ucertainty

Table 2 shows that the uncertainty range associated with the specific yield drops from 0.022 to 0.016 when TL-RG observations are incorporated. *Blainey et al.* [2007] reported values of respectively 0.020 and 0.012 with and without the use of TL-RG measurements. Parameter uncertainties listed in Table 2 are slightly higher due to the larger amount of measurement errors added to the drawdown (0.05 m instead of 0.045 m) and TL-RG observations (2 μGal instead of 1 μGal). Table 2 shows the same potential, if not more, for the inclusion of TL-MRS observations in reducing parameter uncertainty for this setup of aquifer testing. Parameter uncertainty for the specific yield dropped to 0.014. Therefore a last

inversion exercise was conducted in which drawdown, TL-RG and TL-MRS observations were included. This yielded an accuracy of 0.013 in determining the value for the specific yield, which is a reduction of approximately 50% of the original uncertainty range (when only head data comprises the calibration dataset). Similar values apply for the estimation of the hydraulic conductivity. As Table 2 shows, improvements are small relative to the estimated parameter values.

4.2 Partially Penetrating Well in an Anisotropic Aquifer, Measurement Error & Delayed Yield

Based on our experience, 2 μGal and 10 nV are very optimistic estimates for the data errors encountered during field surveys with MRS and RG. For this purpose we investigate the effect for measurement errors of respectively 4 μGal and 20 nV on the parameter estimation results in scenario 'High Noise'. Table 2 shows a smaller decrease in parameter correlation and parameter uncertainty reduction, especially for the TL-RG observations. Only 12 % of improvement can be made in terms of parameter uncertainty reduction, which is small assuming the highly idealized conditions associated with this synthetic study. The MRS-data suffers less from the increased data errors and results in a ca. 30% uncertainty reduction.

When a partially penetrating well is considered under anisotropic aquifer conditions, water table drawdown and geophysical signals are considerably smaller (Figure 4). When compared to the previous pumping scenario, the cross-correlation between the specific yield and hydraulic conductivity changes from -0.86 to -0.97 if aquifer properties are estimated with water table drawdown data only. When TL-RG and TL-MRS measurements are introduced, with a measurement error of respectively 2 μGal and 10 nV, specific yield uncertainty ranges are reduced with ca. 40%, being more effective compared to a fully penetrating well. This can be explained by the lower information content of the drawdown data. Average parameter estimates for S_y and K_h deviate more from the true values when including the geophysical data, although the "true" aquifer properties are captured within two standard deviations of the estimated parameter values.

The inclusion of delayed yield does not have a large influence on the inversion results, considering the fact we use a rather large time delay index $1/a_d$ of 2 days. This can be explained by the fact that we use drawdown, TL-MRS and TL-RG data obtained after 7 days of pumping; indicating the soil above the water table

had enough time to release the drainable water. Inversion results are roughly the same compared to the fully penetrating well assuming instantaneous drainage.

In scenario 5, we see an improvement in parameter estimates of 15 % for the TL-RG data. For the TL-MRS observations this value was around 30%. However parameter cross-correlation only decreased slightly for the inclusion of both data types. Including both TL-RG and TL-MRS data yielded similar results compared with the inclusion of TL-MRS and drawdown data only.

In the final scenario 'Correlated Noise Gravity' we analyze the impact of correlated measurement errors for TL-RG. Comparing with the scenario "High noise', there is no significant difference in the results. Parameter estimates are perfect and uncertainty ranges are comparable. While we could fit the data with a RMSE of 0.93 in the 'High Noise' – scenario, now this value is 0.84. Also the gravity component of the objective function remains unchanged. This could be explained by the smaller standard deviation of the added data error (for generating the correlated noise we assumed 4 μGal for the measurement error on the gravimeter readings, after which we performed the network adjustment). Obviously the correlated component of the TL-RG measurement error has no significant impact, as its component could be well captured assuming a linear drift in the timeframe in which we assume the TL-RG data to be collected.

4.3 Sensitivity Analysis for Pumping Test Design and Aquifer Properties

The previous section showed that the effectiveness in reducing parameter uncertainty by including TL-MRS and/or TL-RG data strongly depends on the pumping test design and configuration. To explore the additional value of TL-MRS and TL-RG data for aquifer testing in a more general way, we conducted a local sensitivity analysis for parameters governing the pumping test design and aquifer properties with respect to the observed water table drawdown and geophysical signal changes. This sensitivity analysis was performed for the drawdown, TL-RG and TL-MRS observations with respect to the seven different pumping test design and configuration variables that were used in the scenario "Partially Penetrating" (Q, K_h, hi, K_h/K_z, D_s, D, S_y, which are defined in Table 1 except for D_s which represents the depth to the top of the well-screen with respect to the initial water table). These sensitivities are calculated using [*Hill*, 1998]

$$ss_h = \frac{\Delta h / h}{\Delta p / p} \quad (15) \qquad ss_{GRAV} = \frac{\Delta GRAV / GRAV}{\Delta p / p} \quad (16) \qquad ss_{MRS} = \frac{\Delta MRS / MRS}{\Delta p / p} \quad (17)$$

where ss_h, ss_{GRAV}, ss_{MRS} are the scaled sensitivities for the individual drawdown, TL-RG and TL-MRS observations. p is the parameter value for the reference run (partially penetrating well, Table 1), Δp the parameter change. h, $GRAV$ and MRS represent the simulated drawdown, TL-RG and TL-MRS signals for the reference run and Δh, $\Delta GRAV$ and ΔMRS symbolize their change compared to the reference run. As the sign of the sensitivities for each data type was constant with respect to the different pumping test design parameters, we then calculate the sum of these scaled sensitivities (S_j) for each separate observation group according to

$$S_j = \sum_{i=1}^{N_j} ss_j \text{ with } j = HEADS, GRAV, MRS \quad (18)$$

where N_j represents the number of observations associated with every observation group (drawdown, TL-RG and TL-MRS).

Figure 6 shows the calculated sensitivities for the seven pumping test configuration parameters with respect to the total sum of water table drawdown observations (HEADS) and the geophysical signal changes (TL-RG, TL-MRS). Larger values for the hydraulic conductivity, anisotropy, aquifer depth and depth to the pumping well screen will cause a smaller drawdown, which results in a smaller TL-RG and TL-MRS signal. When the pumping rate is increased, more water mass is withdrawn resulting in larger drawdown and larger TL-RG and TL-MRS signals. Water table drawdown does not depend on the initial water table. However, both geophysical methods are sensitive for this characteristic, as stronger signal changes are observed, when mass and water content changes occur closer to the instrument. The TL-RG signal is shown to be more sensitive to the initial water table in comparison with the TL-MRS signal. Figure 6 shows an opposite sensitivity for the specific yield with respect to water table drawdown and the observed geophysical signal changes. Obviously, the higher water content that is released per volume of the subsurface outweighs the smaller drawdown that occurs. This opposite sign of the sensitivity causes the decrease in cross-correlation during the previously executed calibration exercises. According to Figure 6, the most dominant or sensitive pumping test variables are the extraction rate, anisotropy, hydraulic conductivity and the specific yield.

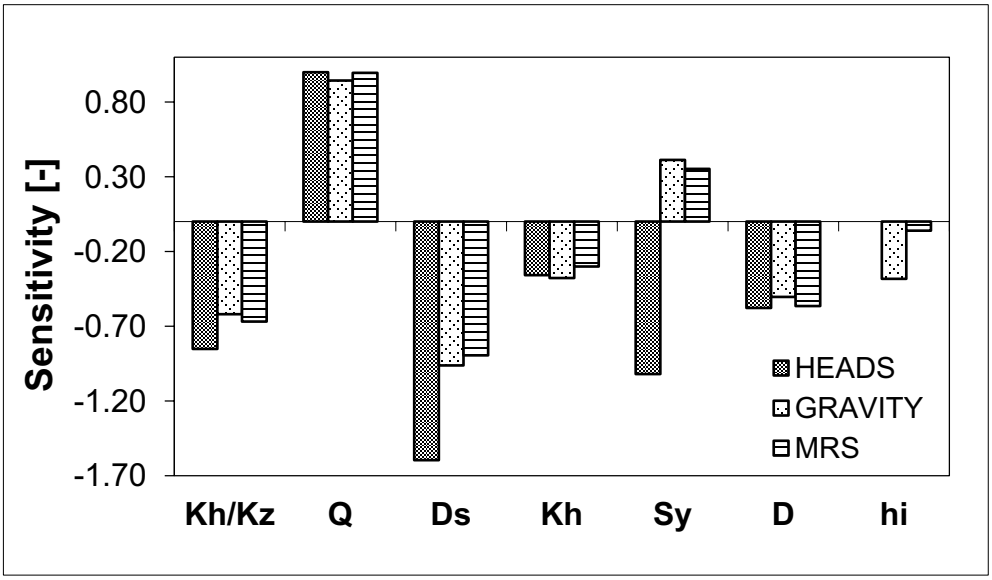

Figure 6 Sensitivity of drawdown, TL-MRS and TL-RG data pumping test design and configuration variables. The original parameter values are those pertaining to the partially penetrating well, listed in Table 1.

5. Discussion and conclusions

For a pumping test, we have evaluated the inclusion of TL-RG and TL-MRS data to improve parameter estimates during unconfined aquifer testing using a coupled hydrogeophysical inversion approach. This was done by generating synthetic observations of drawdown, TL-RG and TL-MRS data, to be used for parameter estimation. In response to the optimistic conclusions and intentions in *Blainey et al.* [2007] and *Damiata and Lee* [2007], we first investigated the impact of three issues that will reduce the signal-to-noise ratio for TL-RG and TL-MRS measurements that could limit their additional value in the inversion process. These are (1) a partially penetrating well in an anisotropic aquifer, (2) typical data errors for TL-RG and (3) delayed yield. Furthermore, we applied the same coupled hydrogeophysical inversion framework for data acquired with TL-MRS, which was subjected to the same analysis used for TL-RG.

Simulated forward responses and objective function plots showed small signal-to-noise ratios for both TL-RG and TL-MRS data for different pumping test configurations. For a fully penetrating well, considering instantaneous drainage and minimum geophysical data errors, parameter uncertainty could be reduced successfully with the incorporation of TL-RG and TL-MRS measurements, although these reductions are small relative to the parameter estimates. Incorporation of more conservative data error estimates for the TL-MRS and TL-RG observations, respectively 20 nV and 4 μGal, resulted in a significant decrease of the additional value of TL-RG data. When analyzing a partially

penetrating well, parameter uncertainty could be reduced more effectively with the inclusion of TL-MRS and TL-RG data when compared to a fully penetrating well. Inclusion of delayed yield did not influence the parameter estimation results significantly; however, this is also an effect of the specific setup of the synthetic study as we used measurements at a time interval where delayed yield effects are small. A scenario including a combination of the three signal-to-noise ratio reducing issues, showed only a marginal improvement in parameter estimates for TL-RG. The informative value of the TL-MRS data was less affected by these. Finally, we show that typical correlated measurement errors associated with TL-RG data are not likely to influence its potential to improve the estimation of aquifer parameters. In contrast to TL-RG, we have not conducted simulations for TL-MRS data with correlated measurement errors. A local sensitivity analysis indicated that the hydraulic conductivity, thickness and specific yield of the aquifer are the most sensitive factors, together with the extraction rate.

The findings of this study suggest a limited applicability of a coupled hydrogeophysical inversion with TL-RG data for practical pumping tests, but inversion results proved to be more optimistic than we expected beforehand, especially for the partially penetrating well. The inclusion of TL-MRS data appears more promising compared to the TL-RG data, as parameter uncertainty could be reduced by ca. 30 % for most of the investigated scenarios in this work. Due to consistency reasons with *Blainey et al.* [2007] and *Damiata and Lee* [2007], we did not account for one major characteristic of practical pumping tests in our simulations, which is the fact that drawdown data often comprises a few time series rather than several drawdown measurements in space. Another important issue that was not included in this study are structural model errors, such as those due to a heterogeneous aquifer, a slightly variable pumping rate and the estimation of other aquifer parameters that are unknown (e.g. delay index, anisotropy, aquifer thickness).

As the TL-RG and TL-MRS signals observed during a pumping test will be small in terms of signal-to-noise ratio, a model study as presented in this paper is a necessity to assess the potential for additional TL-MRS and TL-RG observations to improve the estimates of aquifer parameters for a real-world pumping test using the coupled inversion procedure described here. This should be combined with accurate noise measurements for both techniques at the location were the pumping test is conducted. When these tests indicate whether acceptable sensitivities can be obtained for the geophysical data with respect to the aquifer parameters that are estimated, this could yield a great benefit as TL-RG and TL-

MRS surveys are often much cheaper to conduct compared with the installation of a monitoring well and no drilling is involved with these type of measurements. Another advantage of including the geophysical data, in addition to the existing drawdown observation locations, would be the reduction of the required accuracy for the drawdown measurements, which allows for a greater flexibility of picking the monitoring well locations and the use of monitoring wells that already exist at the site. As the geophysical data can yield a high spatial resolution dataset, this information would not only be suited to constrain the parameter estimation process, but can also provide much more information about the shape of the water table depression around the pumping well due to the spatial variability of the aquifer properties.

Acknowledgements

This work was supported by the Danish Agency for Science Technology and Innovation funded project RiskPoint - Assessing the risks posed by point source contamination to groundwater and surface water resources under grant number 09-063216.

References

Archie, G. E., The electrical resistivity log as an aid in determining some reservoir characteristics, *Transactions of the American Institute of Mining and Metallurgical Engineers, 146*, 54-61, 1942.

Barlow, P. M. and A. F. Moench, *WTAQ:* A Computer Program for Calculating Drawdowns and Estimating Hydraulic Properties for Confined and Water-Table Aquifers, 99-4225, 1-84. 1999. Northborough, Massachusetts, U.S. Geological Survey.

Binley, A., P. Winship, R. Middleton, M. Pokar, and J. West, High resolution characterization of vadose zone dynamics using crossborehole radar, *Water Resour. Res., 37(11)*, 2639–2652, 2001.

Blainey, J. B., T. P. A. Ferré and J. T. Cordova, Assessing the likely value of gravity and drawdown measurements to constrain estimates of hydraulic conductivity and specific yield during unconfined aquifer testing, *Water Resour. Res., 43*(12), 2007.

Boucher, M., G. Favreau, M. Descloitres, J. M. Vouillamoz, S. Massuel, Y. Nazoumou, B. Cappelaere and A. Legchenko, Contribution of geophysical surveys to groundwater modelling of a porous aquifer in semiarid Niger: An overview, *Comptes Rendus Geoscience, 341(10-11),* 800-809, 2009.

Boulton, Analysis of data from pumping tests in unconfined anisotropic aquifers, *Journal of Hydrology*, *10*(4), 369-378, 1970.

Braun, M. and U. Yaramanci, Inversion of resistivity in Magnetic Resonance Sounding, *Journal of Applied Geophysics, 66(3-4)*, 151-164, 2008.

Bushong, S.C., Magnetic resonance imaging: physical and biological principles, Mosby, 528 pp, 2003.

Carmichael, R.S., Henry Jr., G., Gravity exploration for groundwater and bedrock topography, *Geophysics, 42*, 850–859, 1977.

Cassiani, G., G. Böhm, A. Vesnaver, and R. Nicolich, A geostatistical framework for incorporating seismic tomography auxiliary data into hydraulic conductivity estimation, *Journal of Hydrology, 206*, 58–74, 1998.

Cassiani, G., V. Bruno, A. Villa, N. Fusi, and A. Binley , A saline trace test monitored via time-lapse surface electrical resistivity tomography, *Journal of Applied Geophysics*, *59*, 244–256, 2006.

Chalikakis, K., M. R. Nielsen and A. Legchenko, MRS applicability for a study of glacial sedimentary aquifers in Central Jutland, Denmark, *Journal of Applied Geophysics, 66(3-4),* 176-187, 2008.

Chen, J. S., S. Hubbard, Y. Rubin, C. Murray, E. Roden, and E. Majer, Geochemical characterization using geophysical data and Markov chain Monte Carlo methods: A case study at the South Oyster bacterial transport site in Virginia, *Water Resour. Res., 40*, 2004.

Chen, J., S. Hubbard, J. Peterson, K. Williams, M. Fienen, P. Jardine, and D. Watson , Development of a joint hydrogeophysical inversion approach and application to a contaminated fractured aquifer, *Water Resour. Res., 42*, 2006.

Christiansen, L., S. Lund, O.B. Andersen, P.J. Binning, D. Rosbjerg and P. Bauer-Gottwein, Measuring gravity change caused by water storage variations: Performance assessment under controlled conditions, *Journal of Hydrology*, *402(1-2), 60-70*, 2011a.

Christiansen, L., Binning, P. J., Rosbjerg, D., Andersen, O.B. and P. Bauer-Gottwein, Using time-lapse gravity for groundwater model calibration: An application to alluvial aquifer storage, *Water Resour. Res.*, *47*, 2011b.

Coates, G.R., Xiao, L., Prammer, M.G., NMR logging principles and applications, Halliburton, 233 pp., 1999.

Day-Lewis, F. D., J. W. Lane Jr., J. M. Harris, and S. M. Gorelick, Time lapse imaging of saline tracer transport in fractured rock using difference attenuation radar tomography, *Water Resour. Res., 39(10)*, 1290, 2003.

Damiata, B. N. and T. C. Lee, Simulated gravitational response to hydraulic testing of unconfined aquifers, *Journal of Hydrology, 318*(1-4), 348-359, 2006.

Descloitres, M., L. Ruiz, M. Sekhar, A. Legchenko, J. J. Braun, M. S. M. Kumar and S. Subramanian, Characterization of seasonal local recharge using electrical resistivity tomography and magnetic resonance sounding, *Hydrological Processes, 22(3)*, 384-394, 2008.

Doherty, J., PEST: Model-independent parameter estimation, *Watermark Numer. Comput.*, Brisbane, Queensl., Australia [Available at http:/www.pesthomepage.org.

Duffield, G. M., AQTESOLV for Windows, Version 3.5, HydroSOLVE, 2002.

Dunn, K.-J., Bergman, D.J., Latorraca, G.A., Nuclear Magnetic Resonance Petrophysical and Logging Applications. Pergamon. 293 pp., 2002.

Ezersky, M., A. Legchenko, C. Camerlynck, A. Al-Zoubi, L. Eppelbaum, S. Keydar, M. Boucher and K. Chalikakis, The Dead Sea sinkhole hazard - new findings based on a multidisciplinary geophysical study, *Zeitschrift fur Geomorphologie, 54*, 69-90, 2010.

Ferré, T. P. A. and M. J. Thomasson, Understanding the Impacts of Anisotropy on the Extent of Drawdown, *Ground Water, 48*, 478-479, 2010.

Ferré, T., L. Bentley, A. Binley, N. Linde, A. Kemna, K. Singha, K. Holliger, J. A., Huisman, B. Minsley, Critical steps for the continuing advancement of hydrogeophysics. *EOS*, *90* (23), 200–201, 2009.

Gehman, C.L., Harry, D.L., Sanford, W.E., Stednick, J.D., Beckman, N.A., Estimating specific yield and storage change in an unconfined aquifer using temporal gravity surveys, *Water Resour. Res., 45*, 2009.

Guerin, R., J. M. Baltassat, M. Boucher, K. Chalikakis, P. Y. Galibert, J. F. Girard, V. Plalgnes and R. Valois, Geophysical characterisation of karstic networks - Application to the Ouysse system (Poumeyssen, France), *Comptes Rendus Geoscience, 341(10-11)*, 810-817, 2009.

Hill, M. C., Methods and guidelines for effective model calibration, US Geological Survey water resources investigations report 98-4005, 1998.

Hinnell, A. C., T. P. A. Ferré, J. A. Vrugt, J. A. Huisman, S. Moysey, J. Rings and M. B. Kowalsky, Improved extraction of hydrologic information from geophysical data through coupled hydrogeophysical inversion, *Water Resour. Res., 46*, 2010.

Hubbard, S. S., Y. Rubin, and E. Majer, Spatial correlation structure estimation using geophysical and hydrogeological data, *Water Resour. Res., 35(6)*, 1809–1825, 1999.

Huisman, J., S. Hubbard, J., Redman, A., Annan, Measuring soil water content with ground penetrating radar: A review, *Vadose Zone Journal, 2(4)*, 476–491, 2003.

Hunt, T.M., Gravity changes at Wairakei geothermal field, New Zealand, *Geological Society of America Bulletin, 81*, 529–535, 1970.

Hunt, T.M., Recharge of water in Wairakei geothermal field determined from repeat gravity measurements, *New Zealand Journal of Geology and Geophysics, 20*, 303–317, 1977.

Hyndman, D. W., and S. M. Gorelick, Estimating lithologic and transport properties in three dimensions using seismic and tracer data: The Kesterson aquifer, *Water Resour. Res., 32(9)*, 2659–2670, 1996.

IRIS Instruments, NUMIS Poly: Multi-Channel MRS System Magnetic Resonance System – User's Manual, 32 pp., 2010.

Jacob, T., J. Chery, R. Bayer, N. Le Moigne, J.-P. Boy, P. Vernant and F. Boudin, Time-lapse surface to depth gravity measurements on a karst system reveal the dominant role of the epikarst as a water storage entity, *Geophysical Journal International 177 (2),* 347–360, 2009.

Jacob, T., Bayer, R., Chery, J. and N. Le Moigne, Time-lapse microgravity surveys reveal water storage heterogeneity of a karst aquifer, *Journal of Geophysical Research-Solid Earth, 115*, 2010.

Knight, R., Ground penetrating radar for environmental applications, *Annual Review Of Earth And Planetary Sciences*, 29, 229–255, 2001.

Kemna, A., J. Vanderborght, B. Kulessa, and H. Vereecken, Imaging and characterization of subsurface solute transport using electrical resistivity tomography (ERT) and equivalent transport models, *Journal of Hydrology, 267*, 125–146, 2002.

Körver, R. J. P., P. H. M. H. Theunissen, W. T. van de Kreeke, M. J. A. van der Linde and I. C. Heyligers, Juxta-articular myxoma of the knee in a 5-year-old boy: a case report and review of the literature (2009: 12b), *European Radiology, 20*, 764-768, 2010.

Kowalsky, M. B., Finsterle, S., Peterson, J., Hubbard, S., Rubin, Y., Majer, E., Ward, A. and G. Gee, Estimation of field-scale soil hydraulic and dielectric parameters through joint inversion of GPR and hydrological data, *Water Resour. Res., 41,* 2005.

Lachassagne, P., Baltassat, J.M., Legchenko, A., Machard de Gramont, H., The links between MRS parameters and the hydrogeological parameters, *Near Surface Geophysics, 3(4)*, 259–265, 2005.

Lambot, S., M. Antoine, I. van den Bosch, E. C. Slob, and M. Vanclooster (2004), Electromagnetic inversion of GPR signals and subsequent hydrodynamic inversion, *Vadose Zone Journal, 3*, 1072–1081, 2004.

Lambot, S., Slob, E. C., Vanclooster, M. and H. Vereecken, Closed loop GPR data inversion for soil hydraulic and electric property determination, *Geophysical Research Letters, 33*, 2006.

Lambot, S., Slob, E., Rhebergen, J., Lopera, O., Jadoon, K. Z. and H. Vereecken, Remote Estimation of the Hydraulic Properties of a Sand Using Full-Waveform Integrated Hydrogeophysical Inversion of Time-Lapse, Off-Ground GPR Data, *Vadose Zone Journal, 8*, 743-754, 2009.

Legchenko, A. and O. Shushakov, Inversion of surface NMR data, *Geophysics, 63(1)*, 75-84,1998.

Legchenko, A. and P. Valla, A review of the basic principles for proton magnetic resonance sounding measurements, *Journal of Applied Geophysics, 50*(1-2), 3-19, 2002.

Legchenko, A., J. M. Baltassat, A. Beauce and J. Bernard, Nuclear magnetic resonance as a geophysical tool for hydrogeologists, *Journal of Applied Geophysics, 50*(1-2), 21-46, 2002.

Legchenko, A., Magnetic resonance sounding: Enhanced modeling of a phase shift, *Applied Magnetic Resonance, 25(3-4)*, 621-636, 2004.

Leirião, S., X. He, L. Christiansen, O. B. Andersen and P. Bauer-Gottwein, Calculation of the temporal gravity variation from spatially variable water storage change in soils and aquifers, *Journal of Hydrology, 365*(3-4), 302-309, 2009.

Lubczynski, M. and J. Roy, Hydrogeological interpretation and potential of the new magnetic resonance sounding (MRS) method, *Journal of Hydrology, 283(1-4)*, 19-40, 2003.

Linde, N., S. Finsterle, and S. Hubbard, Inversion of tracer test data using tomographic constraints, *Water Resour. Res., 42*, 2006.

Looms, M. C., K. H. Jensen, A. Binley, and L. Nielsen, Monitoring unsaturated flow and transport using cross-borehole geophysical methods, *Vadose Zone Journal, 7*, 227–237, 2008.

Merlet, S., A. Kopaev, M. Diament, G. Geneves, A. Landragin and F. P. Dos Santos, Micro-gravity investigations for the LNE watt balance project, *Metrologia 45(3)*, 265–274, 2008.

Moench, A. F., Flow to a well of finite diameter in a homogeneous, anisotropic water table aquifer, *Water Resour. Res., 33*, 1397–1407, 593-596, 1997.

Mueller-Petke, M. and Yaramanci, U., QT inversion – Comprehensive use of the complete surface NMR data set, *Geophysics, 75*, WA199-WA209, 2010.

Montgomery, E.L., Determination of specific yield using gravity measurements, *EOS, Transactions, American Geophysical Union: Annual Meeting, 52*, 205, 1971.

Moore, C., T. Wohling and J. Doherty, Efficient regularization and uncertainty analysis using a global optimization methodology, *Water Resour. Res., 46*, 2010.

Narasimhan, T.N. and M. Zhu, Transient flow of water to a well in an unconfined aquifer – Applicability of some conceptual models, *Water Resour. Res, 29 (1)*, 179-191, 1993

Neuman, S. P. Theory of flow in unconfined aquifers considering delayed response of the water table, *Water Resour. Res.*, *8*, 1031-1045, 1972.

Neuman, S.P. Supplementary comments on "Theory of flow in unconfined aquifers considering delayed response of the water table", *Water Resour. Res.*, *9*, 1102-1103, 1973.

Plata, J. L. and F. M. Rubio, The use of MRS in the determination of hydraulic transmissivity: The case of alluvial aquifers, *Journal of Applied Geophysics, 66*(3-4), 128-139, 2008.

Poeter, E. P., A New Tool: Delineation of Textural Heterogeneities in Unconfined Aquifers, Using Microgravity Surveys During Pumping, *Bulletin of the Association of Engineering Geologists, 27*(3), 315-325, 1990.

Pollock, D. and O. A. Cirpka, Fully coupled hydrogeophysical inversion of synthetic salt tracer experiments, *Water Resour. Res., 46*, 2010.

Pool, D.R., Eychaner, J.H., Measurements of aquifer-storage change and specific yield using gravity surveys, *Ground Water, 33*, 425–432, 1995.

Pool, D., The utility of gravity and water-level monitoring at alluvial aquifer wells in southern Arizona, *Geophysics 73 (6)*, WA49–WA59, 2008.

Rajesh, M., Kashyap, D. and K.S.H. Prasad, Estimation of unconfined aquifer parameters by genetic algorithms, *Hydrological Sciences Journal-Journal des Sciences Hydroliques, 55(3*), 403-413, 2010.

Scintrex Limited, CG-5 Scintrex Autograv System Operation Manual rev. 4, URL www.scintrexltd.com/gravity.html, 2009.

Topp, G. C., J. L. Davis, and A. P. Annan, Electromagnetic determination of soil water content: Measurements in coaxial transmission lines, *Water Resour. Res.*, *16(3)*, 574–582, 1980.

Vanderborght, J., A. Kemna, H. Hardelauf, and H. Vereecken , Potential of electrical resistivity tomography to infer aquifer transport characteristics from tracer studies: A synthetic case study, *Water Resour. Res., 41*, 2005.

van Gelderen, M., Haagmans, R., Bilker, M., Gravity changes and natural gas extraction in Groningen, *Geophysical Prospecting, 47*, 979–993, 1999.

Vereecken, H., A. Binley, G. Cassiani, A. Revil and K. Titov, Applied Hydrogeophysics, Springer Verlag, Dordrecht, 2006.

Vouillamoz, J.M., M. Descloitres, J. Bernard, P. Fourcassié, L. Romagny, Application of integrated magnetic resonance sounding and resistivity methods for borehole implementation, a case study in Cambodia, *Journal of Applied Geophysics, 50*, 67–81, 2002.

Wessells, C.W. and W.E. Strange, Results of repeat gravity measurements in areas of ground water withdrawal, EOS, *American Geophysical Union, Spring Meeting, 66*, 364, 1985.

Wyns, R., J.M. Baltassat, P. Lachassagne, A. Legtchenko, J. Vairon, Application of proton magnetic resonance soundings to groundwater reservemapping in weathered basement rocks (Brittany, France), *Bulletin de la Société géologique de France, 175(1)*, 21–34, 2004.

Yeh, T., C. J., S. Liu, R. J. Glass, K. Baker, J. R. Brainard, D. Alumbaugh, and D. LaBrecque, A geostatistically based inverse model for electrical resistivity surveys and its applications to vadose zone hydrology, *Water Resour. Res., 38(12)*, 1278, 2002.

Zawila, J.S., B.N. Damiata, S.C. Biehler, T.C. Lee, Gravity mapping of subsurface structures in batholithic terrain, *Symposium on the Application of Geophysics to Engineering and Environmental Problems*, 801–810, Reno, 1997.

The Department of Environmental Engineering (DTU Environment) conducts science-based engineering research within four themes:
Water Resource Engineering, Urban Water Engineering,
Residual Resource Engineering and Environmental Chemistry & Microbiology.
Each theme hosts two to four research groups.

The department dates back to 1865, when Ludvig August Colding, the founder of the department, gave the first lecture on sanitary engineering as response to the cholera epidemics in Copenhagen in the late 1800s.

DTU Environment
Department of Environmental Engineering
Technical University of Denmark

Miljoevej, building 113
DK-2800 Kgs. Lyngby
Denmark

Phone: +45 4525 1600
Fax: +45 4593 2850
e-mail: reception@env.dtu.dk
www.env.dtu.dk

ISBN 978-87-92654-53-3